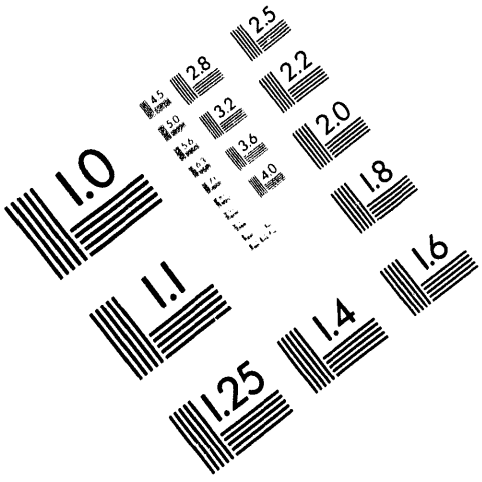

Association for Information and Image Management

1100 Wayne Avenue, Suite 1100
Silver Spring, Maryland 20910

301/587-8202

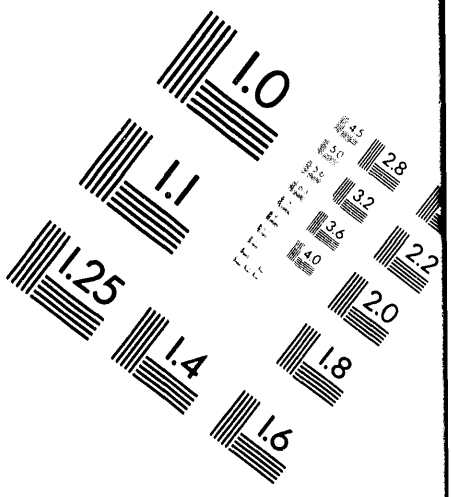

Centimeter

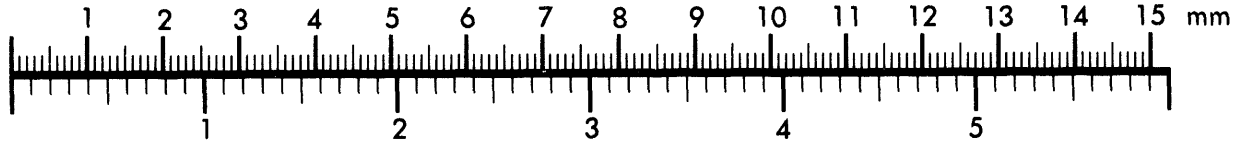

Inches

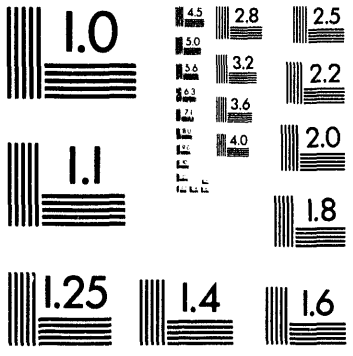

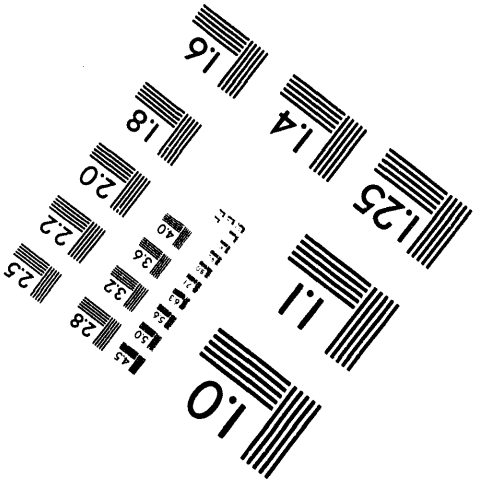

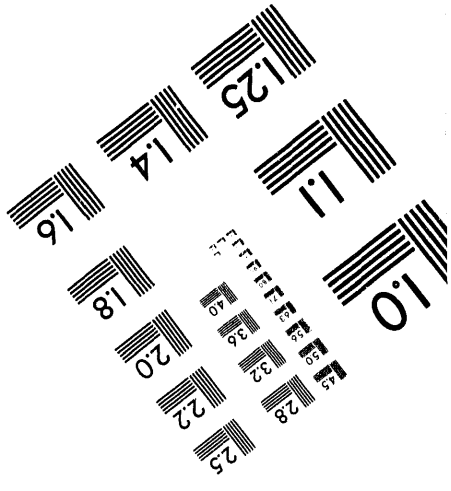

MANUFACTURED TO AIIM STANDARDS
BY APPLIED IMAGE, INC.

1 of 2

DOE/MC/24207-3322
(DE94004090)

An Experimental Study of the Hydrodynamics and Cluster Formation in a Circulating Fluidized Bed

Topical Report
January 1, 1991 - June 30, 1992

M. Gautam
J. Jurewicz
Y. Heping
K. Clifton

July 1992

Work Performed Under Contract No.: DE-FC21-87MC24207

For
U.S. Department of Energy
Office of Fossil Energy
Morgantown Energy Technology Center
Morgantown, West Virginia

By
West Virginia University
Department of Mechanical and Aerospace Engineering
Morgantown, West Virginia

DISCLAIMER

An Experimental Study of the Hydrodynamics and Cluster Formation in a Circulating Fluidized Bed

DOE/MC/24207-3322
(DE94004090)
Distribution Category UC-103

An Experimental Study of the Hydrodynamics and Cluster Formation in a Circulating Fluidized Bed

Topical Report
January 1, 1991 - June 30, 1992

M. Gautam
J. Jurewicz
Y. Heping
K. Clifton

Work Performed Under Contract No.: DE-FC21-87MC24207

For
U.S. Department of Energy
Office of Fossil Energy
Morgantown Energy Technology Center
P.O. Box 880
Morgantown, West Virginia 26507-0880

By
West Virginia University
Department of Mechanical and Aerospace Engineering
P.O. Box 6064
Morgantown, West Virginia 26506-6064

July 1992

SUMMARY

This research program involves two major aspects. First, to evaluate techniques to effectively probe the polydisperse gas-solid flows and second, to apply these techniques to study the gas-solid flow structure and clusters in the riser of a circulating fluidized bed riser. Amongst the non-intrusive techniques a modified laser Doppler technique based on the fluorescence-emission concept has been adopted and the other techniques involve pitot-static pressure probes.

A circulating fluidized bed (CFB) facility has been designed, built and is currently operational at West Virginia University. The design provides for maximum versatility in investigating the hydrodynamics of the CFB riser. The cold-flow CFB model is made out of Plexiglas and has a 200 mm diameter and 5.5 m height. Two stage cyclones are employed to capture the particles exhausted from the riser. Measurements of gas velocity distribution were carried out in the circulating fluidized bed riser with particles having a mean diameter of 112 μm and a density of 2305 kg/m^3 and another set of particles with a mean diameter of 145 μm and a density of 2245 kg/m^3. The experimental results showed that the local gas velocity varied with the radial position, elevation, solids circulation rate, superficial velocity and particle size. A general formula for gas velocity distribution in the circulating fluidized bed riser was obtained based on the particle ciriculation, superficial velocity and particle diameter. The pressure drops across the L-

valve were also studied for different particle sizes, L-valve diameters and aeration. The solids flowrate was found to be a function of the L-valve geometry, operating parameters and solids properties. Pressure drop of L-valve increases with increasing solids diameter and decreasing diameter of the L-valve. Pressure drop across standpipe increases as the solids diameter and diameter of the standpipe decrease.

Table of Contents

Chapter 1 Introduction 1

Chapter 2 Literature Review 5

2.1 Circulating Fluidized Bed Hydrodynamics 5

2.2 Velocity Measurement Techniques in Two-Phase flow 15

Chapter 3 Experimental Equipment and Procedure 23

3.1 Experiment for Laser Anemometry 23

3.1.1 Horizontal Test Section 23

3.1.2 Laser Doppler Anemometer 27

3.1.3 Laser-Induced Fluorescence Emission Based LDA 32

3.1.4 Flow Seeding 34

3.1.5 Data Acquisition System (for Laser Anemometer) 38

3.2 Experimental Procedure (for Laser Anemometry) 40

3.2.1 LDA Velocity Measurements 40

3.2.2 Uncertainties in LDA Measurements 46

3.2.3 Dye Optimization 49

3.2.4 Particle Dying Procedure 50

3.2.5 Calibration 52

3.3 Circulating Fluidized Bed Facility 54

3.3.1 Design of the Distributor 57

3.3.2 Design of the Riser 57

3.3.3 Design of the Cyclones 59

3.3.4 Design of the Hopper 63

3.3.5 Design of the L-valve 63

3.4 Instrumentation and Procedures (Gas Velocity Profile and Pressure Drop) 66

3.4.1 Design of Experiments 71

3.5 Experimental procedures for Solids Flow through the L-valve 73

Chapter 4 Results and Discussion 78

4.1 Fluorescence-Emission Based Laser Anemometery 78

4.2 Gas Velocity Profile in the Riser 80

4.3 Solids Flow through the L-valve 97

Appendix 118

Bibliography 133

List of Figures

Figure 2.1	Typical Signal (a) from Solid Phase Particle and (b) from Seeding Particle	16
Figure 3.1	Schematic of the test Section for Technique Optimization	25
Figure 3.2	Schematic of the Test Loop Support	26
Figure 3.3	Schematic of One_Component LDA System without Frequency Shift	30
Figure 3.4	Ray Diagram for the Axial velocity Component Measurement	31
Figure 3.5	Laser Doppler Measuring Volume	33
Figure 3.6	Fluidized Feeder	37
Figure 3.7	Schematic of Data Acquisition System	39
Figure 3.8	Logic Print of the Master Computer Interface Unit	41
Figure 3.9	Absorption and Emission Spectra of Rhodamine 6-G	44
Figure 3.10	Circulating Fluidized Bed	55
Figure 3.11	Distributor plate Flow Characteristics (MOTT POROUS MEDIA)	58
Figure 3.12	Schematic of Cyclone	61
Figure 3.13	Schematic of Solids Hopper	64
Figure 3.14	Schematic of the L-valve	65
Figure 3.15	The Pitot-static Probe	68
Figure 3.16	The Block Diagram of Measurement System	70
Figure 4.1	The Gas Velocity Distribution in Circulating Fluidized Bed Riser	82
Figure 4.2	Power-Law Velocity Profiles in CFB	83
Figure 4.3	Exponent for Power-Law Profile	84

Figure 4.4	Gas Velocity Profile	86
Figure 4.5	Gas velocity Profile	87
Figure 4.6	Gas velocity Profile	88
Figure 4.7	Gas velocity Profile	90
Figure 4.8	Gas velocity Profile	91
Figure 4.9	Gas velocity Profile	92
Figure 4.10	Gas velocity Profile along with Elevation of Riser	94
Figure 4.11	Schematic Representation of Gas Flow Up and Down Relative to the Standpipe Wall(Geldart,1986)	99
Figure 4.12	Types of Flow Relative Velocity, and Pressure Gradient in Flowing Gas-solids Mixture with High Bulk Density of Solids (Kunii & Levenspiel,1962)	101
Figure 4.13a	Solid Flowrate versus Aeration Rate with Different Solids Using Smaller L-valve	107
Figure 4.13b	Solid Flowrate versus Aeration Rate with Different Solids Using Bigger L-valve	108
Figure 4.13c	Solid Flowrate versus Aeration Rate with Different L-valve Using Smaller Solids	109
Figure 4.13d	Solid Flowrate versus Aeration Rate with Different L-valve Using Bigger Solids	110
Figure 4.14	Pressure Drop of L-valve versus Aeration Rate at Different Diameter of L-valve	113
Figure 4.15	Pressure Drop across Standpipe versus Aeration Rate at Different Diameter of L-valve	114
Figure 4.16	Pressure Drop of L-valve versus Aeration Rate at Different Solids Diameter	115
Figure 4.17	Pressure Drop across Standpipe versus Aeration Rate at Different Solids Diameter	116

LIST OF SYMBOLS

A	cross-section area of L-valve, m^2
b	number of blocks
c	solids circulation rate
d_p	mean solids diameter, μm
d_t	diameter of L-vale, m
G_s	solids mass flowrate kg/s
k	number of factors per block
l	length of L-valve, m
L	length of standpipe, m
Δp	pressure drop, mm H_2O
Δp_f	Pressure drop in horizontal section of L-valve, mm H_2O
ΔP	pressure difference between stagnation and static points
r	number of replication of each factor
R	diameter of the CFB riser (mm)
t	number of factors
u_g	gas velocity m/s
u_s	solids velocity, m/s
u_r	relative velocity between gas and solids (m/s)
V_{max}	gas velocity at the centerline (m/s)
V_{local}	local gas velocity (m/s)
$\bar{U}$	mean gas velocity (m/s)
ϵ	voidage in the standpipe
μ	viscosity of gas, kg/m.s
ρ_g	gas density, kg/m^3
ρ	mean solids density, kg/m^3

CHAPTER 1

INTRODUCTION

There is increasing interest in operating fluidized beds at high gas velocities where gas-solids contacting may be much improved. In the form of a circulating fluidized bed, it has been recognized as a key to efficient gas-solid processing. The several advantages offered by CFB's over the conventional fluidized bed systems such as uniform bed temperature, reduced aggregation and agglomeration have resulted in a recent vote of confidence by the U.S. utility companies.

To date, the understanding of the CFB's and fundamental research into the underlying phenomena of high-velocity fluid beds and systematic compilation of design data is at best sketchy and even the most rudimentary model and correlation which would permit design are lacking. There are three different flow regimes: bubbling, turbulent, and fast fluidization. In the bubbling regime, gas crosses a horizontal section through a fluidized bed by the following mechanisms:

(i) translation of bubble voids, often called visible bubble flow;

(ii) flow through the bubbles relative to them, often called the through flow component;

(iii) interstitial flow relative to the particles in the dense phase;

(iv) net flux of interstitial voids moving with particles.

Lanneau (1960) was the first to recognize the transition from bubbling to turbulent fluidization and the potential advantages of operating in the turbulent regime. What Kehoe and Davidson (1971) saw as the velocity of the gas flowing through narrow beds of fine powders was a breakdown of the slugging regime into a state of continuous coalescence - virtually a channelling state with "tongues" of fluid darting in zigzag fashion through the bed. Kehoe and Davidson (1971) coined the word "turbulent" to describe this state. They reported that this transition to the turbulent fluidization occurred at a velocity equal to three times the terminal velocity of particles belonging to the smallest cut. The transition from bubbling to turbulent fluidization is gradual and spans a range of gas velocities. Clusters also exist in this stage.

The transport velocity may be regarded as the boundary which divides vertical gas-solid flow into two groups of states. Below it lie the bubbling and the turbulent fluid beds. The bed in general experiences no net flow and remains at the bottom of the holding vessel. Above, lie the transport regimes which encompass a wide range of states from dilute-phase flow to the fast bed condition. This occurs at twenty times the terminal velocity.

The fast bed condition is marked by relatively high solid concentrations, aggregation of the particles in clusters and strands which break apart and reform in rapid succession, extensive backmixing of solid, and slip velocities of the individual particles. A way to create the dense suspension is to circulate the very solid emerging from the top of the reactor to its bottom.

Currently, the published work in circulating fluidized beds falls short of answering the questions on the intimately interacting gas-solid flow fields and their influence on each other at a localized level in the riser. Therefore, there is little information available to design engineers for use in optimizing fuels, improving reaction rates of increasing combustion efficiencies. The object of the study of the air-solid two-phase flow is to clarify the flow mechanism resulting from interaction between gaseous and solid phases in the riser.

To study the hydrodynamics and cluster formations in a circulating fluidized bed riser, non-invasive measurement of the gas-solid flow is one of the techniques that has been adopted. This technique utilizes a Laser Doppler Anemometer (LDA) system and is based upon the fluorescence-emission from doped particles which allow differentiation between particle size and obtain velocity measurements. Additionally, gas velocity profiles have been determined using a custom built pitot static probe. Presented in this report is a collection of time averaged local gas velocity profiles covering a range of solids circulation ratesm, superficial velocities and bed material which provide insight into the gas flow behavior in relatively dilute gas-solids riser flow. Detailed measurements of gas and solid flows in the riser of a cold CFB are being taken at different operating parameters to study the phenomena of clusters and streamers.

A detailed literature review in Chapter 2 is followed by a chapter on the experimental equipment, procedures and various analyses of the techniques adopted for the project. Chapter 4

describes the design of the components of the cold CFB model. The results are discussed in a Chapter 4.

CHAPTER 2

LITERATURE REVIEW

A review of the published literature has revealed several works on the flow behavior in circulating fluidized beds. Presented here are only the recent investigations into the hydrodynamics of CFB's and the cluster phenomena in the risers.

2.1 Circulating Fluidized Bed Hydrodynamics

Despite intensive experimental and theoretical study over the last four decades, there are still many aspects of fluidized beds and related fluid-particle systems that remain obscure (Homsy, Jackson, Grace, 1992). Homsy, Jackson and Grace strongly recommended that further work is needed to understand interactions between the particles, influence of particle physical properties, development of non-obtrusive experimental techniques, and study of high-velocity beds and of novel-geometry beds that promote gas-solids interaction.

Arena et al. (1992) studied the hydrodynamics of CFB risers by using one rectangular cross-section and two cylindrical columns. The bed meterials ranged in sizes from 48 μm to 300 μm and ranged in density from 1330 kg/m^3 to 2600 kg/m^3. The instantaneous and time averaged voidage profiles were obtained from the instantaneous pressures pressure data. A model based on Taylor instability at the interface between 'plugs' and their upstream 'slugs' was proposed to estimate the length of the dense and transition regions

in terms of the riser's design and operating variables. They detected unit flow structures made of 'plugs' and 'slugs' in dense and transition regions of the risers, regardless of the size and the shape of the column and the type of solids. It was reported that the dense and transition regions as a whole formed the inlet section of the riser.

Wang et al. (1992) experimentally studied the hydrodynamics of cocurrent downflow gas-solid sspension in a CFB reactor. The influence of gas velocity and solid circulating rate on axial pressure drop, radial profiles of solid concentration and particle velocity were studied in their CDCFB (cocurrent downflow CFB). They have shown that radial solid concentrations, are relatively low in the center region and near the bed wall. An annular region of high solid concentration was shown to exist between the core and the bed wall. The radial solid concentration profile is mainly dependent on the cross-sectional average voidage, irrespective of the actual operating conditions and axial positions. The radial profiles of particle velocity and solid concentration in CDCFB were whown to be more uniform than those in the riser, and a maximum particle velocity was sometimes observed in the region where the solid concentration was at a peak.

Gas and solid hydrodynamics were studied by Martin et al. (1992) in dilute circulating fluidized beds under conditions occurring in catalytic cracking risers. Gas radial velocity profiles and dispersions were established by a tracer technique in a cold CFB model. The local solids concentrations were measured by a tomographic technique. The core-annulus structure of the bed was

examined and the solid radial and axial dispersions were determined. The researchers concluded that the gas flow can be considered to be plug flow with a radial velocity profile and a radial dispersion while the solid flow is more dispersed due to the core-annulus structure and a high radial mixing.

Werther (1991) presented data showing solids flux measurements obtained using a sampling probe. The probe could be aimed upwards or downwards to gather data on upwards or downwards solids fluxes. Results from a 200 mm diameter riser not only confirmed the findings from smaller diameter beds that the wall layer thickness is proportional to the diameter or width of the unit. Despite high gas velocity (8 m/s) and high net solids flux (15 kg/m^2s) the particle flow near the wall is predominantly downwards and this downward flow of solids occupies a substantial region near the wall. Using gas (carbon dioxide) tracer technique he found that the thickness of the wall layer is typically 10 - 15% of the column radius. The radial; mixing in the dilute core was found to be insensitive to the concentration of the particles in that region.

Wirth (1991) has presented a model to describe the hydrodynamic behaviors of the CFB's. He suggested that a series of dense cylindrical strands or clusters extend over the entire height of the riser, with transfer of momentum by impaction of solid particles such that each collision dislodges another particle. The relative velocity of the particles in the dilute phase is equal to the terminal setting velocity of single particles. Their model predicts coexistence of a denser lower region at higher flows.

Yoshioka et al. (1987) found that the velocity of the fluidized particles could be determined by measuring the deflection of a spring plate inserted into the bed. The bubbles were detected with the aid of a light transmitting probe. The probe detected bubbles by the intensity of the light being transmitted between the two elements of the probe. Yoshioka developed profiles of the velocity ratio of the fluidized particles, of the bubble fraction, and of the ratio of tracer concentration. He found that the bubbles moved upward away from the center of the bed whereas the particles move upward along the center of the bed but downward near the wall with a circulatory motion.

Drahos et al. (1988) identified three basic flow regimes when the gas velocity was decreased at the given solid feed rate, namely: uniform dilute flow, with particles flowing upwards in a uniform dispersion; dense flow, characterized by the presence of clouds of particles and voids free of solids; and bubbling dense bed, with the accumulation of solids in the bottom part of the column, forming there a dense bed with the distinct upper surface level. These regimes were found by introducing pressure fluctuations.

Berruti and Kalogerakis (1989) developed a mathematical model capable of predicting the two-phase flow characteristics and required only the experimental average voidage profile along the riser and the net solids circulation rate. The model has been tested in different regimes, and the model predictions compared well with experimental results.

Rhodes and Geldart (1989) formulated pressure losses in the

riser, primary cyclone, solids control valve, and slow bed. Their model enabled axial density profiles to be predicted. The terms of entrainment from bubbling beds and choking in pneumatic conveying were the basis for this mathematical model.

Kato et al. (1989) measured the axial particle holdup and the axial pressure drop in a fast fluidized bed. They concluded that the superficial circulation rate of particles, tube diameter, particle Reynolds number, and axial distance from distributor affected the particle holdup. An empirical equation for the location of the inflection point between the dense and dilute region of particles and an empirical equation for particle holdup in a fast fluidized bed were obtained.

Biswas et al. (1987) checked the validity of published choking correlations. By controlling and measuring gas and solid flowrates independently, it was shown that it was possible to delineate the limiting operating flowrates for the fast-fluid bed regime and to obtain a quantitative flow regime defining the limits of fast fluidization. The transition gas velocity was defined as the upper critical gas velocity. For a given solid flux, the upper critical gas velocity represents the highest gas velocity for operation in the fast fluidization mode. The Yousfi and Gau (1974) correlation underpredicts the upper critical velocity by between 15 and 25%, depending on the magnitude of the solid gas flux. The transition from lean-phase conveying to fast fluidization was found to be analogous to the so-called choking transition in pneumatic conveying.

Carey (1987) goes over the early work of Richardson and Zaki

(1954) which gave a relation between concentration and the settling velocity of suspended spherical particles. He also derived equations to define the n term in the Richardson and Zaki equation.

Dry (1986) developed an experimental technique to examine radial gas concentration profiles. Solids were found to appear to congregate on the outside of the lift pipe - fast bed bend. He found the distance above the grid the gas-only radial profile is fairly flat. He also found that at gas velocities between 2 m/s and 4 m/s, the core/annulus distribution is maintained, but at 6 m/s the lean core migrates across the tube to the outer wall. Also, Dry (1987) found that at higher velocities, the course particles tend to concentrate along the wall region. The course particles were observed to move from the top of the bed toward the bottom.

Horio et al. (1989) developed scaling laws for circulating fluidized beds. His theory was based on the clustering annular flow model. Experiments were performed using two geometrically similar CFB cold models. Similarity was assumed since the voidage distributions and the annular flow structures were similar and so were the cluster voidages.

Salem and Gibbs (1987) investigated the feasibility of a circulating system, where the driving force for transporting particles is provided by jet pumps. The jets would enable an even distribution of the circulating solids and could also be used to provide a multi-location feeding and withdrawal system. The jets could also be computer controlled to compensate for changes. Salem and Gibbs found that large particles were easier to circulate with

jets.

Fox et al. (1989) studied the circulation of particles between two fluidized beds for an open-loop circulation. They developed equations to calculate the driving and resisting forces. The authors found that the most efficient way to control the circulation rate of solids was by varying the valve of the vertical resisting force in the downflowing compartment. This adjusts the state of de-fluidization.

Knowlton et al. (1986) discussed the design of lockhoppers which transfer solids from a high-pressure vessel to atmospheric pressure. They found that a restricted pipe discharge system can lower capital cost, giving continuous discharge of solids, and result in a much lower valve maintenance cost. Additionally, the gas requirements were found to be less.

Mountzaris and Jackson (1986) investigated the effects of aeration in standpipes. Their model was based on differential continuity and momentum balances for a system which consisted of a mass flow hopper, a vertical aerated standpipe and a flow restricting device at its lower end. The authors developed equations for the design of each of the above components. With one aeration point, they obtained and discussed twelve flow regimes.

Shingles and Silverman (1986) studied the pressure profile in a stand pipe. Their results showed that the gas compression effect going down the standpipe of the reactor is limited. Sufficient entrapped aeration from the hopper entered the top of the standpipes to enable a fluidized dense-flow regime to exist over the entire length of the standpipe.

Extensive reviews of circulating fluidized bed research are presented by Yerushalmi et al. (1979). They concluded that the transition from bubbling to turbulent fluidization is represented by the fluctuations of dynamic pressure at any point across the bed and the pressure drop across the bed. This transition is characterized by velocities U_c and U_k. U_c is the velocity at the peak pressure fluctuations and U_k is the velocity at which pressure fluctuations level off marking the turbulent regime. Both velocities increase with particle size and density.

The turbulent regime has two interacting phases, dense phase and lean phase, which result in the bed having properties of both individual particles and clusters. Dense phase consists of closely packed clusters and streamers of particles with downward motion. Lean phase is characterized by individual particles and small clusters with upward motion. Yerushalmi et al. (1978) also concluded that the fast bed condition is characterized by high solid concentration, large cluster formations, backmixing of solids, and slip velocities greater than freefall velocities of individual particles by an order of magnitude.

Bader et al. (1989) conducted tests in the riser of a CFB with FCC catalyst'to determine the degree of gas/solid contacting the fast fluidized bed regime using an intrusive sampling probe and helium tracer technique. They concluded that the solid distribution in the riser is of a core-annulus flow type which high velocity dilute phase core is surrounded by slower, denser solid annulus. The solids flux profile in the riser was determined to be parabolic. The solids flux core was 3 to 5 times the average

solids flux and the wall flux flows downward 6 to 8 times the average flux in the riser. The radial particle velocity distribution in the riser was found to also be parabolic through the use of a pitot tube. The application of a pitot tube for this purpose is open to question. It was also concluded that there was substantial backmixing of solids in the riser.

A quantitative discussion and comparison was done by Neale et al. (1972) exploring possible solutions to the problem of creeping flow relative to an isolated permeable sphere. They suggested the most satisfactory solution is based upon a generalized Brinkman's extension of Darcy's Law. It was concluded that internal permeation within a high porosity permeable particle usually cannot be neglected.

Jackson's (1963) linear stability analysis of dense beds of solid particles operating near minimum fluidization was extended by Grace and Tuot (1979) to apply to more dilute systems. They postulate the origins of particle clusters which occur due to the instability of uniform dispersions of particles in a gas.

Guilin et al. (1984) studied the characteristics of gas mixing a fast fluidized bed which was 8 m high, 115 mm inside diameter, and had a 100 mm inside diameter downcomer. The bed material was spherical silica-gel particles with a diameter of 0.22 mm. They concluded that the bed could be divided into two regions; the variable voidage zone (4 m from the bottom) and the constant voidage zone. The constant voidage zone is characterized by a constant pressure drop and a uniform axial average voidage. It was revealed that the axial mixing could be neglected.

Yerushalmi et al. (1978) studied the extent of gas backmixing in a catalyst fluidized bed at gas velocities spanning the bubbling, turbulent, and fast bed regimes. The regimes were characterized with high backmixing in bubbling, diminishing backmixing in the turbulent regime, and plug flow in the fast regime.

Lean phase properties were explained with equations for cluster size and terminal velocity by Subbarao (1986). Slack (1963) studied the sedimentation of clusters composed of a few particles in a viscous medium.

The effects of hydrodynamic aggregate size, shape, and porosity have upon settling velocity was analyzed by Hamdullahpur et al. (1989). The slip velocity ratio (U_a/U_p) was found to increase as more particles were incorporated within the aggregate. Hydrodynamic aggregates undergo internal circulation since there are no forces holding particles in position. The forces holding the aggregate together are small and therefore making deformation and disruption easy. They concluded that the relative motion between the aggregate and the fluid results in the fluid passing through of around the aggregate; however, this does not affect the drag coefficient except at high porosities (> 0.85).

Knowlton and Hirsan (1977) investigated the solids flow control using a nonmechanical L-valve. Their study explored the effect of geometrical (pipe length and diameter) and particle parameters (particle size and density) on solids flow rate and pressure drop through the L-valve. The effect of aeration location on L-valve performance was also determined.

Sutherland and Tan (1970) applied Stoke's solution for flow around a solid sphere to creeping flow outside a permeable sphere and applied Darcy's Law to describe the internal flow. This was in an attempt to obtain limits on permeability for any size aggregate beyond which internal flows may be neglected.

The concept of continuity wave and cluster formation was used to derive a relationship for choking in vertical pneumatic flow by Yang (1983). These relationships were used by Yang (1984) to develop mechanistic models to predict the transitions between the different regimes of fluidization for fine particles. The continuity wave equation was used to predict the transition between bubbling and turbulent regimes. The transition between dilute phase and fast fluidization regimes was approximated using the choking correlations (Yang, 1984).

The computation of bed-solid circulation rates and patterns induced by a central jet and slug motion was performed by Kececioglu (1989). The experiment measured profiles of tracer particles concentrated inside a fluidized bed.

2.2 Velocity Measurement Techniques in Two-Phase Flows

Yianneskis (1987) and Gautam et al. (1987) have reviewed recent developments in optical and unobtrusive techniques based on laser Doppler anemometry that permit the measurement of the velocities and/or of the sizes of particles.

Durst (1982) reported on some techniques in laser Doppler anemometry with emphasis on combined systems which permit simultaneous measurements of particle velocities, size

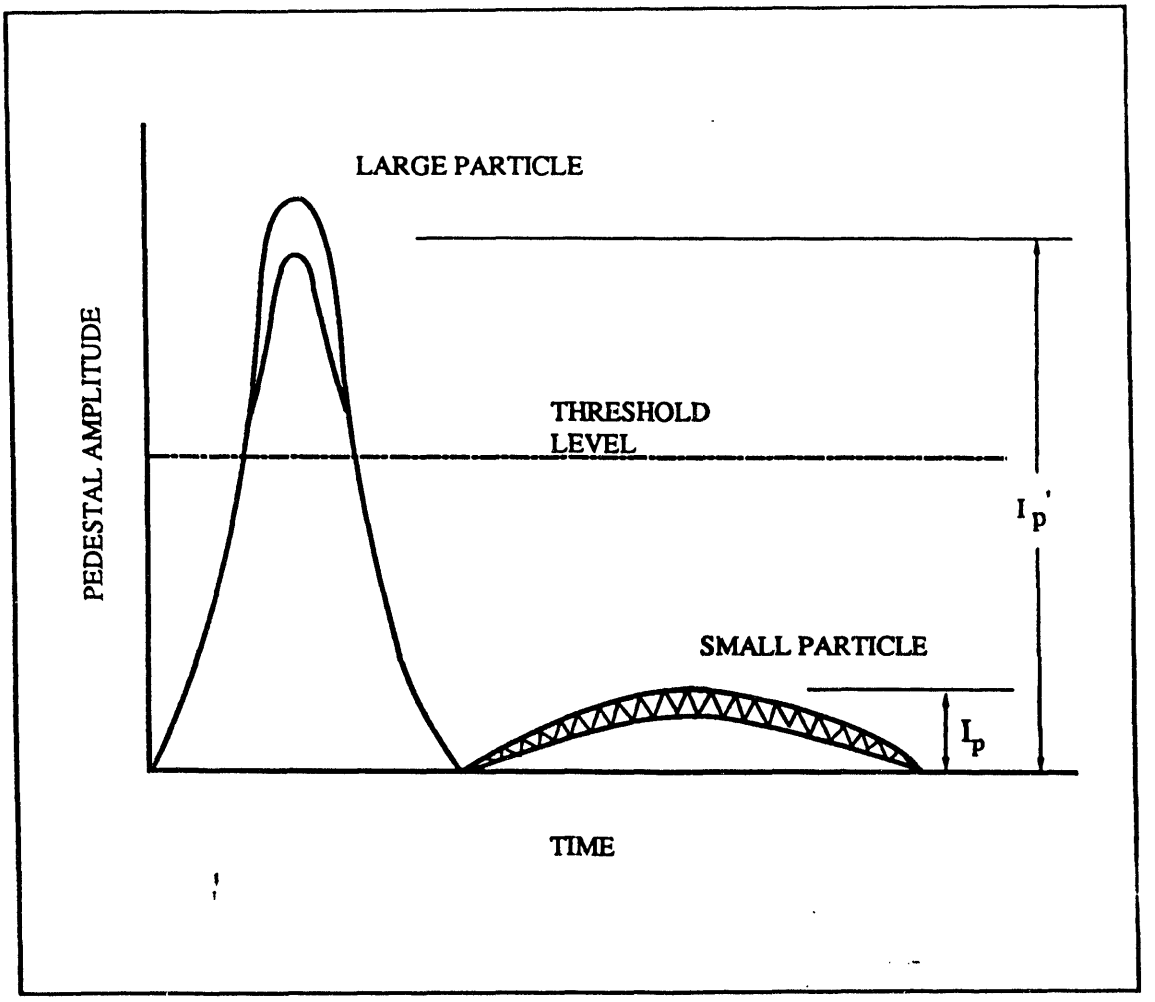

Figure 2.1 Typical Signals from (a) Solid Phase Particle and (b) from a Seeding Particle

distributions and concentrations. The blocking of the incident and the scattered light by the suspensions in two-phase flows along with the complexities involved in separating the information from the two-phase remains a major research area.

Several researchers have used LDA in two-phase flows for making velocity, concentration and particle size measurements (Durst and Zare, 1975; Durst and Umhauer, 1975; Birchenough and Mason, 1976; Yule et al., 1977). Levy and Lockwood (1983), Modaress et al. (1982) and Yianneskis and Whitelaw (1984) measured both the gas and the solid phase velocities. Figure 2.1 shows a typical output signal from the photomultiplier tube and I_p and I_p' are the pedestal amplitudes of the dispersed and the continuous phases, respectively. Discrimination between the light scattered by large particles (mainly from the solid phase) and from the small particles (mainly from the gas phase) was accomplished by setting a variable threshold level on the photomultiplier output. However, they did not account for the trajectory ambiguity which originates from the inherent non-uniformity of illumination in optical measuring volume (Farmer, 1972). Durst and Umhauer (1975) attempted to by-pass this problem by employing a second optical system, designed for particle sizing, which was focused around the same measuring volume. Lee and Srinivasan (1978) suppressed the ambiguity due to non-uniform distribution of incident light inside the measuring volume by electronically isolating the effective measuring volume to the central core portion of the original measuring volume. Lee and Durst (1982) employed a technique reported by Durst (1975) to carry out local velocity measurements

in particulate two-phase flows. By combining the use of automatic filterbanks with amplitude discriminators and photodiodes, they were able to minimize the trajectory ambiguity and record signals from the two-phases. Maeda et al. (1980) separated the signals by taking the wave number into account in addition to the pedestal amplitude, and measured and gas-solid two-phase flow in a vertical pipe. Tsuji and Morikawa (1982) employed and amplitude validation circuit and set threshold values for the pedestal and Doppler components of the Doppler signal by which simultaneous measurements of the gas and solid phases could be made. Modaress and Tan (1983) employed a two color LDA with two overlapping measuring volumes of different diameters. The Doppler signals from the smaller volume yielded the velocity information of the gas phase and the discrimination between the two-phases was effected on the basis of the pedestal amplitudes of the signals from the larger volume. The velocity of the particles was obtained by reducing the photomultiplier sensitivity. Stevenson et al. (1975,1977) investigated the concept of laser-induced fluorescence coupled with an LDV system for particle size and discrimination in aerosol droplets and velocity measurements. Their "fringe mode" fluorescence velocimetry concept was investigated by adding fluorescent dyes to various solvents. The scope traces of the fluorescence signals showed that the quantum yield and the attainable dye concentration are strongly dependent on the solvent. Particle fluorescence was induced with 0.01 molar solution of Rhodamine 6-G in ethanol (Stevenson et al., 1975) and Rhodamine 6-G in a 50-50 volumetric mixture of benzyl alcohol and ethylene glycol

(1977). They suggested that further studies were required to determine the optimum dye-solvent combinations that will permit high dye concentrations to be attained without reducing the quantum yield.

Hamdullahpur et al. (1987) modified the laser-fluorescence technique of Stevenson et al. (1975, 1977) to determine gas and particle velocities in a turbulent two-phase flow field. The technique is based on the discrimination between the scattered light from particles and the fluorescence emission from particles coated with a fluorescent dye. A high powered argon-ion laser-Doppler velocimeter was used in single channel, on-axis backscatter mode. Wood particles were dyed with Rhodamine 6G in a 50:50 (% by volume) mixture of benzyl alcohol and ethylene glycol. Their optimized dye solution constituted 13.4 g of Rhodamine 6G per liter of solution. The solid-gas two-phase flow behavior in the freeboard of a cold gas-fluidized bed was done implementing this fluorescence emission technique. They have reported axial velocity and turbulence intensity distributions of the gas and solid phases. However, the technique used by Hamdullahpur et al. (1987) could not be reproduced by the authors despite following the instructions very closely and conducting the experiments with meticulous care. A closer analysis of the procedure has led to the conclusion that the size of the scattering particle is of prime importance in fluorescence emission based laser anemometery.

Patrose and Caram (1982) made measurements of particle velocities in a transparent two-dimensional bed. The transit timing type optical consisted of five fibers located inside a

hypodermic needle which in turn, was introduced into the bed from the top. They used and LDA system also to make particle velocity measurements. They observed good agreement between the two techniques leading them to conclude that their probe could be used for particle velocity measurements in fluidized beds. All of these measurements were made at the distribution grid orifices and they have mapped the particle flow field for bed heights of 43.2 mm and 184 mm. However, they did not measure the fluid velocities.

Johnston et al. (1975) used an LDA in a fixed bed of transparent spheres to measure the local velocity of liquid whose refractive index matched liquid-solid fluidized bed flow system and made detailed LDA measurements of particle velocity in its interior. But, the refractive index matchin~ requirement limits the use of this technique to a few liquid-solid systems. They did not make any fluid velocity measurements inside the bubbles. Durrett et al. (1985) designed a corrective lens for use with an LDV system. The lens negates many of the aberrations caused by the cylindrical wall when LDV measurements are made off the plane of symmetry. Durrett et al. (1988) experimentally mapped the flow field of an axi-symmetric sudden expansion air flow using an LDV with a correction lens system. The implementation of the correction lens eliminated the optical aberrations thus allowing measurement of the axial and radial velocity components. The mean velocities, turbulence intensities, turbulent kinetic energy, and Reynolds stresses were measured and/or derived.

Lai and Faeth (1987) describe a combined LDA and LIF system to simultaneously measure gas velocities and concentrations at a

point. Turbulent mixing between two streams and turbulent transport from surfaces can be studied using this system. The extremely expensive LDA/LIF system has good spatial resolution and frequency response, operated in particle-containing environments and near surfaces, and performs acceptably at high turbulence intensities.

Lourenco et al. (1986) presented a new technique for two-dimensional flow visualization and measurement of instantaneous velocity and vorticity fields. The Particle Image Displacement Velocimetry (PIDV) involves taking multiple photographs of an illuminated plane (created with a ruby or a NdYg laser or a continuous wave laser with shutter device) while the seeded particles pass through. A moving pattern is created by the light scattered form the seeded plane. The relative information is then obtained from an analysis of the photograph. It is well suited for the study of unsteady or complex flowfields.

A laser velocimeter based on a combination of a crossed beam laser velocimeter (LDV) and laser-induced fluorescence is proposed by Keefer (1987). The system, laser fluorescence velocimeter (LFV), utilizes the temporal and spatial characteristics of the fluorescence induced by a crossed-beam interference region to determine flow velocity. The advantages of the system are: applications to both strong and weak accelerated flows, no particles are required, discrimination against undesirable particle scattering and background radiation due to the spectral shift of fluorescence, and the continuous LFV signal has its own advantages in signal processing.

LDA based diagnostics have been employed by some investigators to measure the elutriation rates in the freeboard region where the particle loading is low, thus producing less interference. Levy and Lockwood (1983) used an LDA to measure gas-phase velocities above a bed in which 400 to 1000 micron sand was fluidized. They used a rectangular channel 0.6 m x 0.3 m x 2.4 m (height) with 19 mm thick float glass to enable clear passage to the laser beams.

Kale and Eaton (1985) used a single component LDA to make gas phase velocity measurements in the freeboard region. Using a fluidized bed with a 150 mm square cross section and a variable-angle diffuser in the freeboard region, they showed that a particle loading of as low as 2% by weight significantly alters the freeboard fluid mechanics.

The literature review shows several pioneering works on the hydrodynamics of circulating fluidized beds but experimental studies have been performed only under limited conditions. Specifically, there is no detailed experimental data available on the flow field inside the riser in circulating fluidized beds. The gas-solid flow structure is of paramount importance in reactor modelling. The absence of experimental data is due partly to the lack of appropriate experimental techniques. Therefore, a test facility was constructed and a non-intrusive technique was developed for measuring the velocity of fluid and particles flowing through the riser. Details of the experimental apparatus and the procedures adopted are given in the following chapter.

CHAPTER 3

EXPERIMENTAL EQUIPMENT AND PROCEDURE

The research program involves two major aspects. First, is to develop techniques to effectively probe the polydisperse gas-solid flows and the second aspect is to apply these techniques to study the gas-solid flow structure and clusters in the riser of a circulating fluidized bed riser. The non-intrusive technique involved modification of the conventional laser Doppler anemometry technique by employing the fluorescence emissions phenomena. Other techniques such as customized pitot-static pressure probes, gas tracer techniques and flow visualization are also applied.

The equipment and procedures adopted in this research program are described in the following order:

i) Laser anemometery

ii) Circulating Fluidized Bed

3.1 Equipment for Laser Anemometery

Under the category of laser anemometery the equipment is described as follows:

a) Horizontal Test Section for Fluorescence-emission work

b) Laser Doppler Anemometer

c) Flow Seeding (for fluorescence-emission work)

d) Data Acquisition System (for laser anemometry)

3.1.1 Horizontal Test Section

The 13 ft. horizontal section consists of two pieces of 5 ft. long clear, cast acrylic tubing and a clear 4 foot long Pyrex

glass section (see Figure 3.1.). Both the acrylic and glass sections have an outer diameter of 2 in. and an inner diameter of 1.95 in. The sections of tubing are fastened together using a rubber coupling which provides an airtight seal at the joint. The test section is made of clear Pyrex because, unlike Plexiglas, it is resistant to scratches and surface marring caused by the abrasive seeding particles thus providing unrestricted optical access to the internal pipe flow. The condition of transparency is necessary when using the LDA system to ensure reliable measurements.

The lightweight supports for the tubing are 8 in. lengths of angle iron welded to a stand (see Figure 3.2). The stand is bolted to a wooden support which is in turn clamped to the table. The tubing rests on the supports and is secured with ring clamps. The set up has been aligned and leveled. Particles exit the glass section and are fed to the pre-filter and HEPA filter via a flexible driver hose 3 in. in diameter. The HEPA filter is a Flanders double nipple HEPA filter (part 007-4-03-02-IU-N2N2) capable of handling 35 cfm with an efficiency of 99.9% of 0.3 μm particles. The pre-filter (Flanders # BFDL2) is constructed of a polyester media and is supported by a lightweight frame.

Downstream from the filters is the 2 Hp Baldor centrifugal air blower (Model VM3155). The flow rate through the system is controlled using a Reliance AC motor controller connected to the blower. The flowrate is checked against readings from a pitot-static tube installed in the system. The exhaust from the blower flows to a hood through flexible hose.

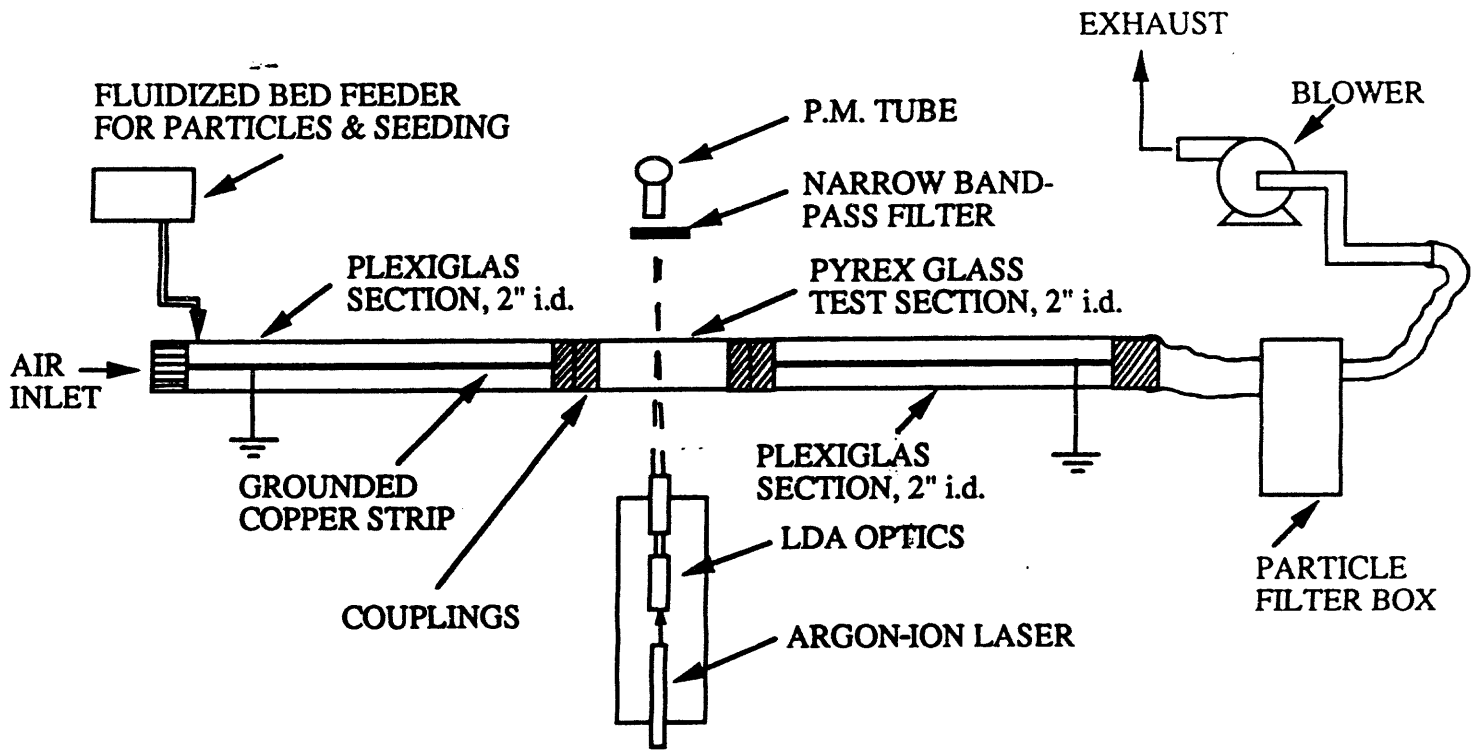

Figure 3.1 Schematic of the Test Section for Technique Optimization

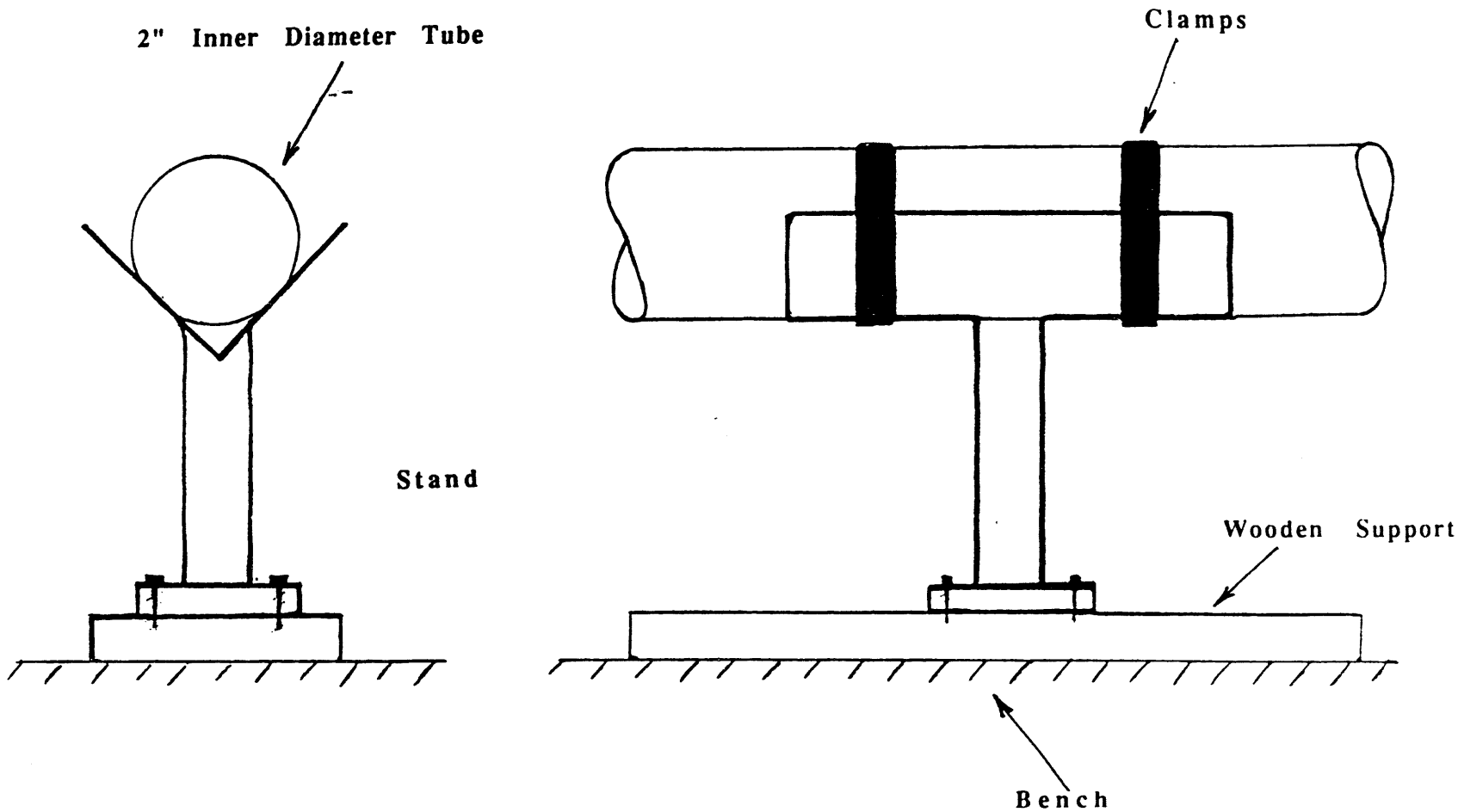

Figure 3.2 Schematic of the Test Loop Support

3.1.2 Laser Doppler Anemometer

Pointwise measurements of the gas-solid flow are being made using an Argon-Ion (514.5nm) gased laser Doppler anemometer (LDA). The objectives of this program demand the use of a non-intrusive fluorescence-emission based LDA technique. The unique advantages offered by LDA's over other fluid flow instrumentation are listed below:

a. The measurement is non-invasive in nature hence it retains all the flow field characteristics.

b. No calibration is required. It has a linear response to fluid velocity.

c. Measures the desired component of velocity directly in any complex flow field. The quantity measured by the LDA is the projection of the velocity vector on the measuring direction defined by the optical system.

d. A very high dynamic range--can measure velocities ranging from microns/sec to hypersonic speeds.

e. In addition the high spatial and temporal resolution, combined acousto-optical and electronic shifting allows measurement of reversing flows (flows which change direction).

The only requirements for LDA application are (i) the fluid must be reasonably transparent to the laser light and that there must be a clear optical access through a window to the measuring point, and (ii) presence of seed particles (light scattering sources) in the field.

The performance of the LDA is described by some important

parameters. They relate the calibration constant, the dimensions of the measuring volume and the number and separation of interference fringe lines in the measuring volume to input parameters such as laser wavelength, beam waist parameters, LDA beam separation, beam expansion and measuring distance. The important parameters are:

Doppler Frequency $$f_d = \frac{2u}{\lambda} \sin\left\{\frac{\theta}{2}\right\}$$

Fringe Spacing $$\delta_f = \frac{\lambda}{2\sin\left\{\frac{\theta}{2}\right\}}$$

Diameter of Focused Laser Beam $$d_f = \frac{4 f \lambda}{\pi E d_i}$$

Measuring Volume Dimensions $$d_x = \frac{d_f}{\cos\left\{\frac{\theta}{2}\right\}} \qquad d_y = d_f$$

$$d_z = \frac{d_f}{\sin\left\{\frac{\theta}{2}\right\}}$$

Calibration Factor $$C = \frac{\lambda}{2\sin\left\{\frac{\theta}{2}\right\}}$$

where:

λ ..... Laser wavelength

E ..... Beam expansion factor

d ..... Diameter of laser beam waist before expansion

d ..... Diameter of focused laser beam

D ..... Beam separation before expansion

θ ..... Beam intersection angle

f ..... Focal length of optics

$\tilde{u}$ ..... Velocity component in measuring direction

A block diagram of the system with and without frequency shift is shown in Figure 3.3. Currently, no frequency shift is being employed. The light source is a 2 watt LEXEL Argon-Ion laser emitting a single line at 514.5 nm. The laser can emit only a single laser line as a result of the insertion of a second cavity, etalon, in the laser cavity. This adds to the stability of the laser and reduces the noise. The system is configured in a dual beam forward-scatter mode. A DANTEC type 55x190a Counter Processor is being used and the future tasks in this year's work plan will involve use of DANTEC type 55n10 Frequency Shifter along with a Bragg Cell (acousto-optic cell) will be used. The system is interfaced with a dedicated PDP-11 laboratory computer which is used for acquiring and analyzing the data. A ray diagram of the optical set-up is shown in Figure 3.4.

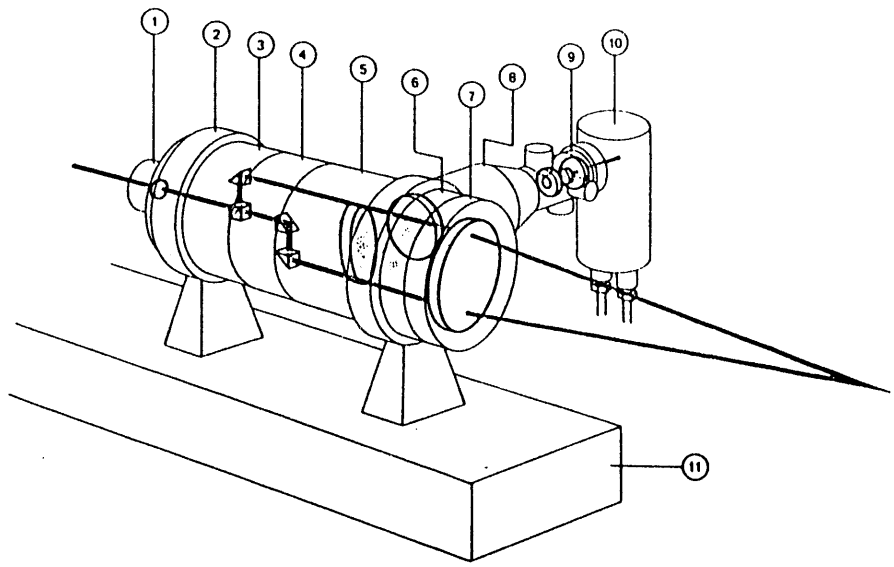

1	Cover and Retarder
2	Support
3	Beamsplitter Neutral
4	Beam Displacer
5	Backscatter Section
6	Lens Mounting Ring
7	Front Lens Achromatic (600 mm)
8	PM Optics
9	Interference Filter 514.5 nm
10	PM Section
11	Mounting Bench

Figure 3.3 Schematic of One-Component LDA System Without Frequency Shift

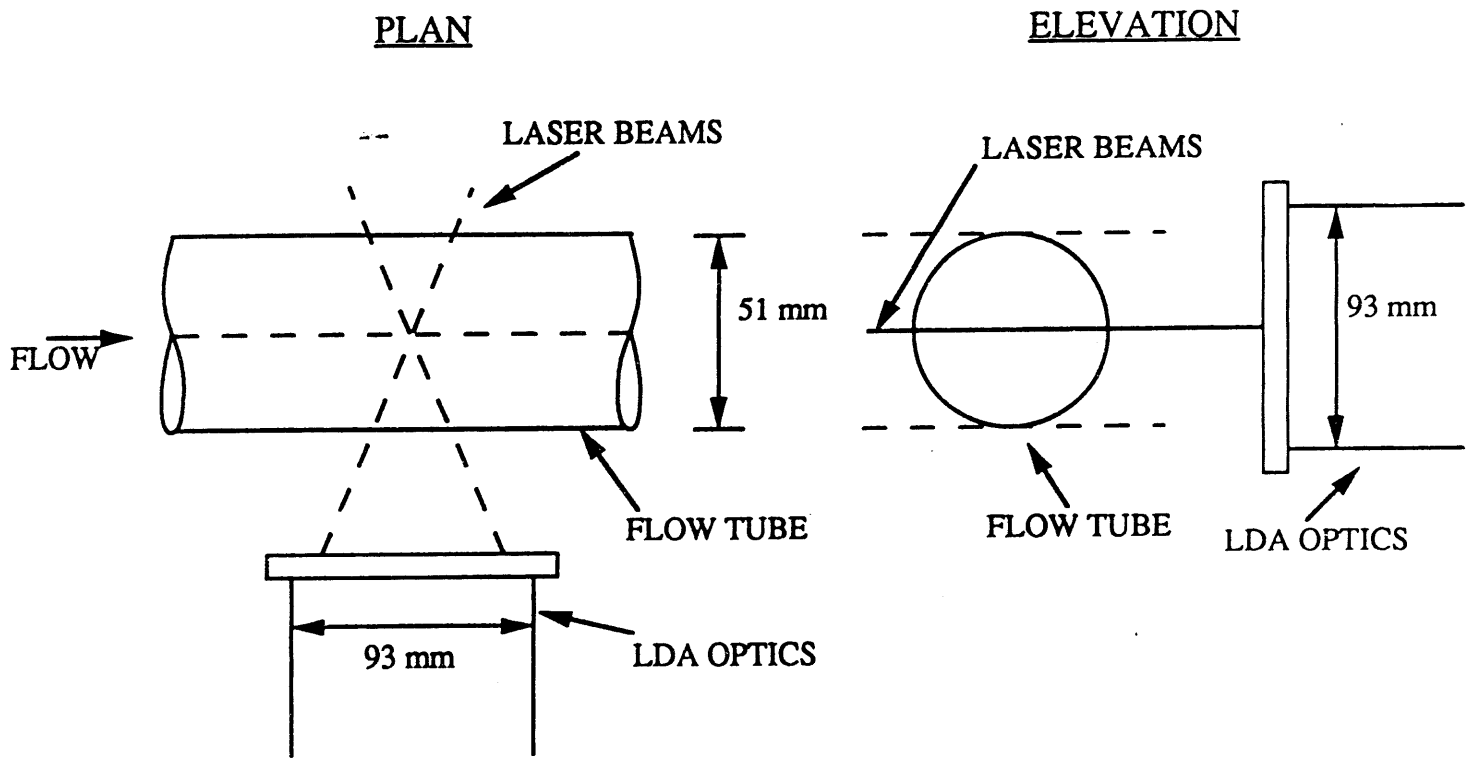

Figure 3.4 Ray Diagram for the Axial Velocity Component Measurements

3.1.3 Laser-Induced Fluorescence Emission Based LDA

Conventional LDA systems are generally operated in the fringe mode as shown in Figure 3.5. Two coherent, monochromatic equal-intensity Gaussian beams intersect at their waists and form a standing electromagnetic wave distribution in the intersection zone, the measuring volume, which may be visualized as a set of planar fringes perpendicular to the plane of the two beams and parallel to their bisector. The generation of Doppler signals is explained by the time-varying intensity of the light scattered by a particle passing through the fringe pattern. The modulation frequency under the Gaussian envelope is the Doppler frequency as given above.

The detection process is basically incoherent, since the intensity fluctuation is the measured quantity. This allows for modification of the conventional LDA in which the standing electromagnetic field induces a time-varying fluorescent emission from particles treated with a dye. The wavelength difference between the incident beams and the detected fluorescent emission resulting from the use of fluorescence emission based LDA system. Fluorescent emission, being spatially isotropic and unpolarized eliminates any reduction in signal modulation due to light of unequal amplitude and polarization interfering at the photo-tube (Durst et al., 1973). Thus large aperture receiving optics will be very effective especially when large input beam angles are used. The fluorescence emission based LDA permits discrimination between different sized particles as well as between phases in multiphase flows.

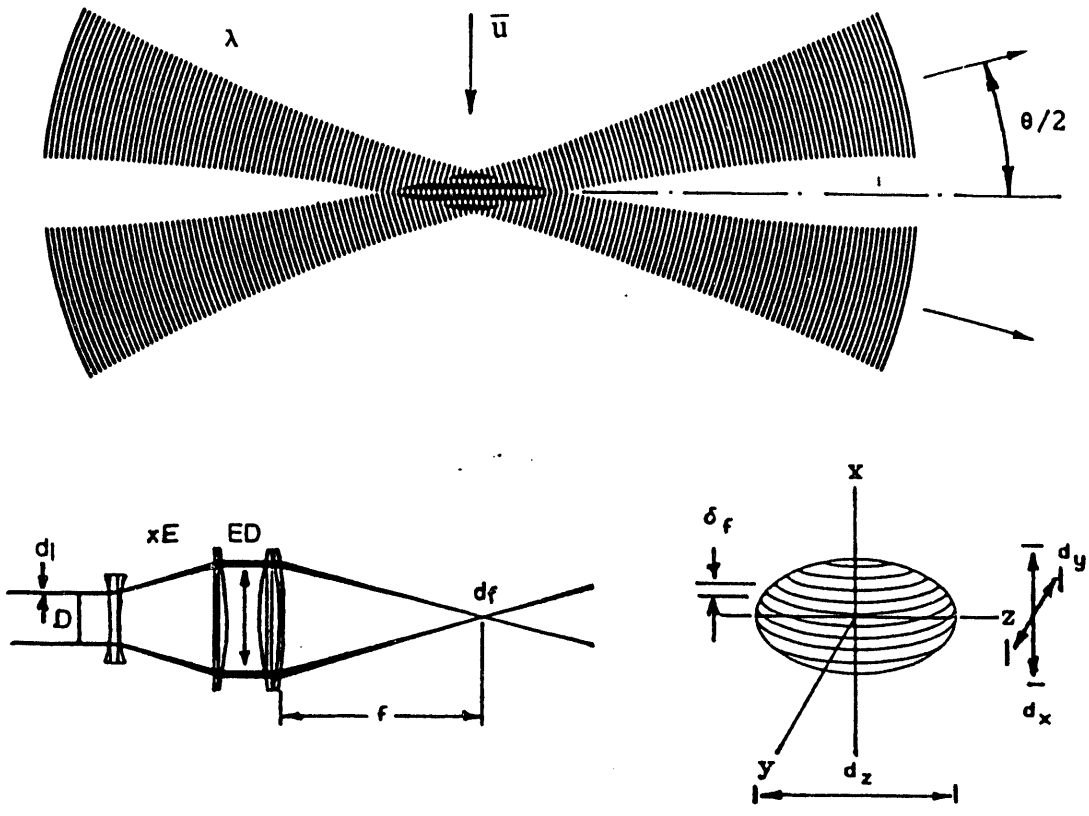

NOMENCLATURE

λ	.....	LASER WAVELENGTH
E	.....	BEAM EXPANSION FACTOR
d_1	.....	DIAMETER OF LASER BEAM WAIST BEFORE EXPANSION
d_f	.....	DIAMETER OF FOCUSED LASER BEAM
D	.....	BEAM SEPARATION BEFORE EXPANSION
θ	.....	BEAM SEPARATION ANGLE
λ	.....	FOCAL LENGTH OF FRONT LENS
$\bar{u}$	.....	VELOCITY VECTOR MEASURED

Figure 3.5 Laser Doppler Anemometer Measuring Volume

3.1.4 Flow Seeding

Investigations of the permissible size of a single seeding particle have been carried out by Melling and Whitelaw (1973). In this investigation, titanium dioxide powder was used as seeding material for gas phase measurements. However, the titanium dioxide particles are not spherical enough to impart a high scattered light intensity which is necessary to obtain the best LDA signal. Titanium dioxide particles also performed poorly in the fluorescent dying procedure. The adsorption of the dye solution proved to be somewhat less than expected.

The behavior of dilute concentrations of particles in a turbulent fluid has been investigated (Tchen, 1947) by considering the equation of motion, the Basset-Boussinesq-Oseen equation, for a spherical particle in a fluid:

$$\frac{\pi}{6} d_p^3 \rho_p \frac{du_p}{dt} = 3\pi\mu d_p(u_f - u_p) + \pi d_p \rho_f \frac{du_f}{dt} + \frac{1}{2}\cdot\frac{\pi}{6} d_p^3 \rho f \left[\frac{du_f}{dt} - \frac{du_f}{dt}\right] +$$

$$+ \frac{3}{2} d_p^3 \rho_f \sqrt{\pi\nu} \int_{\xi} d\xi \left[\frac{du_f}{d\xi} - \frac{du_p}{d\xi}\right] / \sqrt{t - \xi} \qquad (3.1.1)$$

where, the origin and meaning of individual terms of the equation is described in detail elsewhere (Hinze, 1959; Hjelmfelt and Mokros, 1966).

Equation 3.1.1 may be divided by the particle mass and

rewritten as:

$$\frac{du_p}{dt} = 36\,\frac{\nu}{d_p^2\,(2\rho_p/\rho_f + 1)}\,(u'_f - u_p) + \frac{3}{(2\rho_p/\rho_f + 1)}\,\frac{du_f}{dt} +$$

$$+ \frac{18}{d_p(2\rho_p/\rho_f + 1)}\,\sqrt{\nu/\pi}\int_0^t \frac{(du'_f/dt - du_p/dt)}{t - \xi}\,d\xi \qquad (3.1.2)$$

Neglecting the history and added mass terms in addition to the pressure gradient effect gives:

$$\frac{du_p}{dt} = \frac{36\nu}{d_p^2(2\rho_p/\rho_f + 1)}\,(u'_f - u_p) \qquad (3.1.3)$$

Particle relaxation time is defined as:

$$\tau_p = \frac{d_p^2(2\rho_p/\rho_f + 1)}{36\nu} \qquad (3.1.4)$$

Substituting Equation 3.1.4 in Equation 3.1.3 gives:

$$\frac{du_p}{dt} = \frac{1}{\tau_p} (u_p - u'_f) \qquad (3.1.5)$$

Equation 3.1.5 indicates that the system behaves as a first order system with a relaxation time, τ_p. The amplitude response of such a system is given by:

$$A_p(\omega) = \frac{1}{\sqrt{1 + (\tau_p \omega)^2}} \qquad (3.1.6)$$

Applying Equation 3.1.6 to seed particles (typically less than 2 microns) yields a frequency response of 430 Hz at an amplitude ratio (A_p/A_f) = 99% and a response of 6030 Hz at an amplitude ratio 50%.

Fine powders and glass beads mixed with larger beads in fluidized bed feeders have been successfully used by several investigators (Jurewicz et al., 1975; Durst, 1982; Kale and Eaton, 1985; Gautam, 1989) and have not had problems with smaller particles agglomerating on the glass beads such as to remove all of them from the flow.

The seeding material is provided by a fluidized bed feeder (See Figure 3.6) consisting of a cylindrical tube, 43 cm long and 3.5 cm in diameter with a cone shaped distributor for uniform supply of compressed air. To enhance uniform fluidization 1 mm to 1.5 mm glass beads were introduced in the vessel. The vessel walls were periodically tapped to prevent particles from clinging to it.

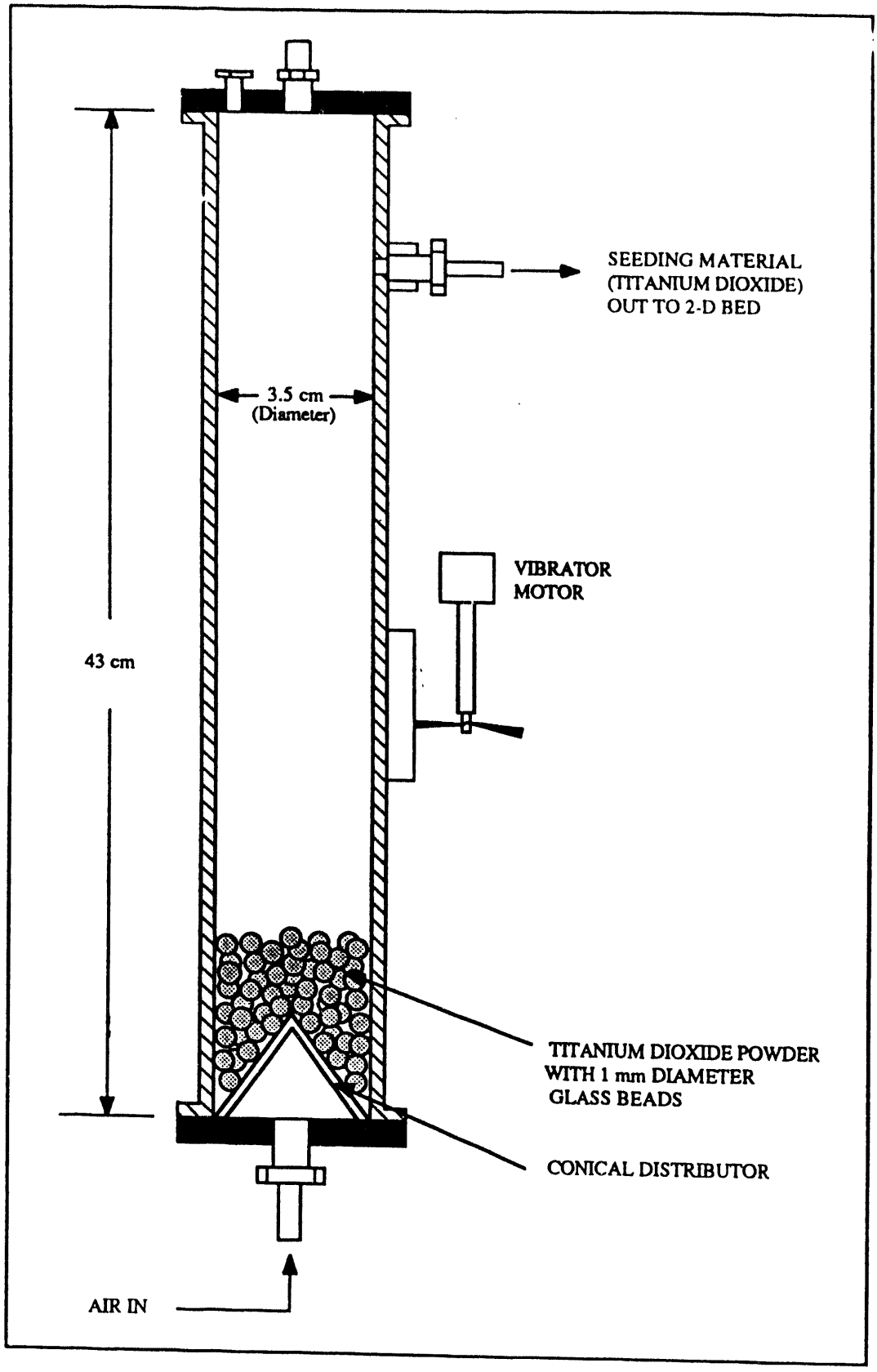

Figure 3.6 Fluidized Bed Feeder

The fluorescent dyed polystyrene latex particles (PSL) have also been used. The uniform PSL dyed particles, 1.212 μm in diameter (Polymer: S/V-COOH.Rhodamine B; 10% solids) with pink fluorescence were obtained from Bangs Laboratories, Carmel, IN. The other set of PSL particles that have been used in the development work were the Fluoresbrite Carboxylate Microspheres (1.0 μm in diameter, 2.5% solids) with Rhodamine dye. Additionally, procedures developed by NASA (Nichols, 1987) were followed and apparatus to produce PSL particles was set-up in the LDA lab. PSL particles with a diameter of 0.6 μm have been grown in the lab.

3.1.5 Data Acquisition System (for Laser Anemometery)

The data acquisition system for this investigation is controlled by PDP-11 microcomputer manufactured by Digital Electronics Corporation. The DANTEC type 55x190a LDA Counter Processor is interfaced to the computer. The schematic of the entire data acquisition system for velocity measurements is shown in Figure 3.7.

Software was developed in FORTRAN and PDP-11 MACRO Assembly Language to sequentially start the data acquisition via the LDA system and reduce the data. The software developed for this purpose is user friendly and provides complete automation. PDP-11 micro is able to accept data at a maximum rate of 10 Khz while the LDA Counter Processor is able to give data at a rate of up to 1 Mhz. In the absence of a Direct Memory Access (DMA) link, data recording at a rate fast enough so as not to affect the operation of the experiment is not possible. During the bed operation, the

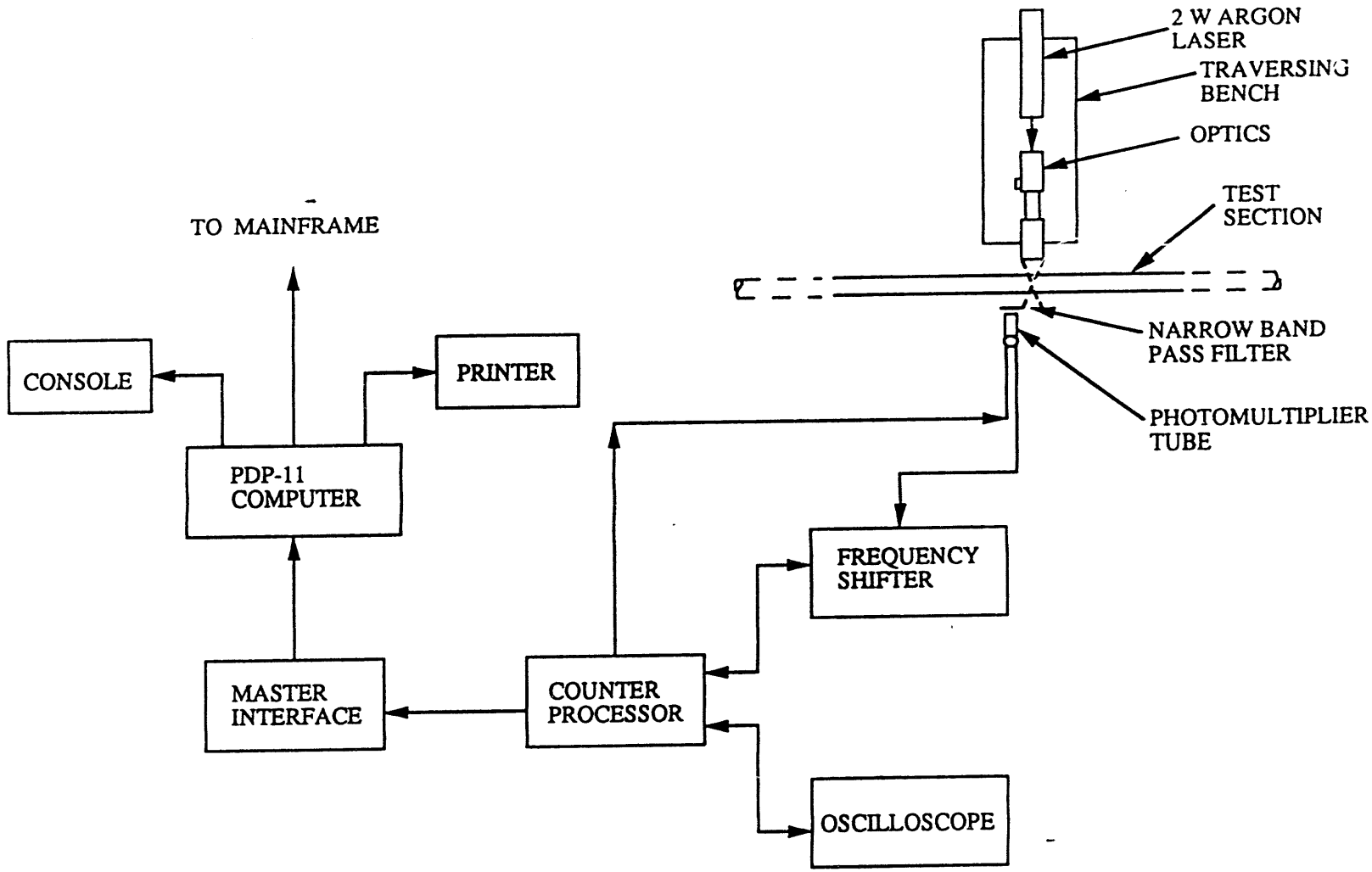

Figure 3.7 Schematic of the Data Acquisition System

data is stored in arrays in the memory and processed at the end of each run. At the end of each run, the raw data (on velocity and sample interval time) is analyzed and stored on the 20 MB hard disk. The post-test data from the PDP-11 computer is uploaded to the mainframe computer systems for further reduction and analysis. The data is plotted using SAS and the downloaded to a MacIntosh computer to obtain a hard copy of the graph. The custom built interface unit (Gautam, 1989) services the test facility during the flow field measurements with the LDA. The logic diagram is shown in Fig. 3.8.

3.2 Experimental Procedures (for Laser Anemometery)

A description of the experimental procedures, for laser anemometery, adopted is given in this section. The major tasks have been divided as follows:

i) LDA signals
ii) uncertainty in LDA measurements
iii) optimization of the dye strength
iv) particle dying procedure, and
v) calibration technique.

3.2.1 LDA Velocity Measurements

The utility of LDA in measurement of single phase flows has been demonstrated beyond question. However, the use of LDA in gas-solid multiphase flows is still in a developmental stage. New instrumentation such as the Phase Doppler Particle Analyzer and the transit-time type of devices from INSITEC are now on the market but

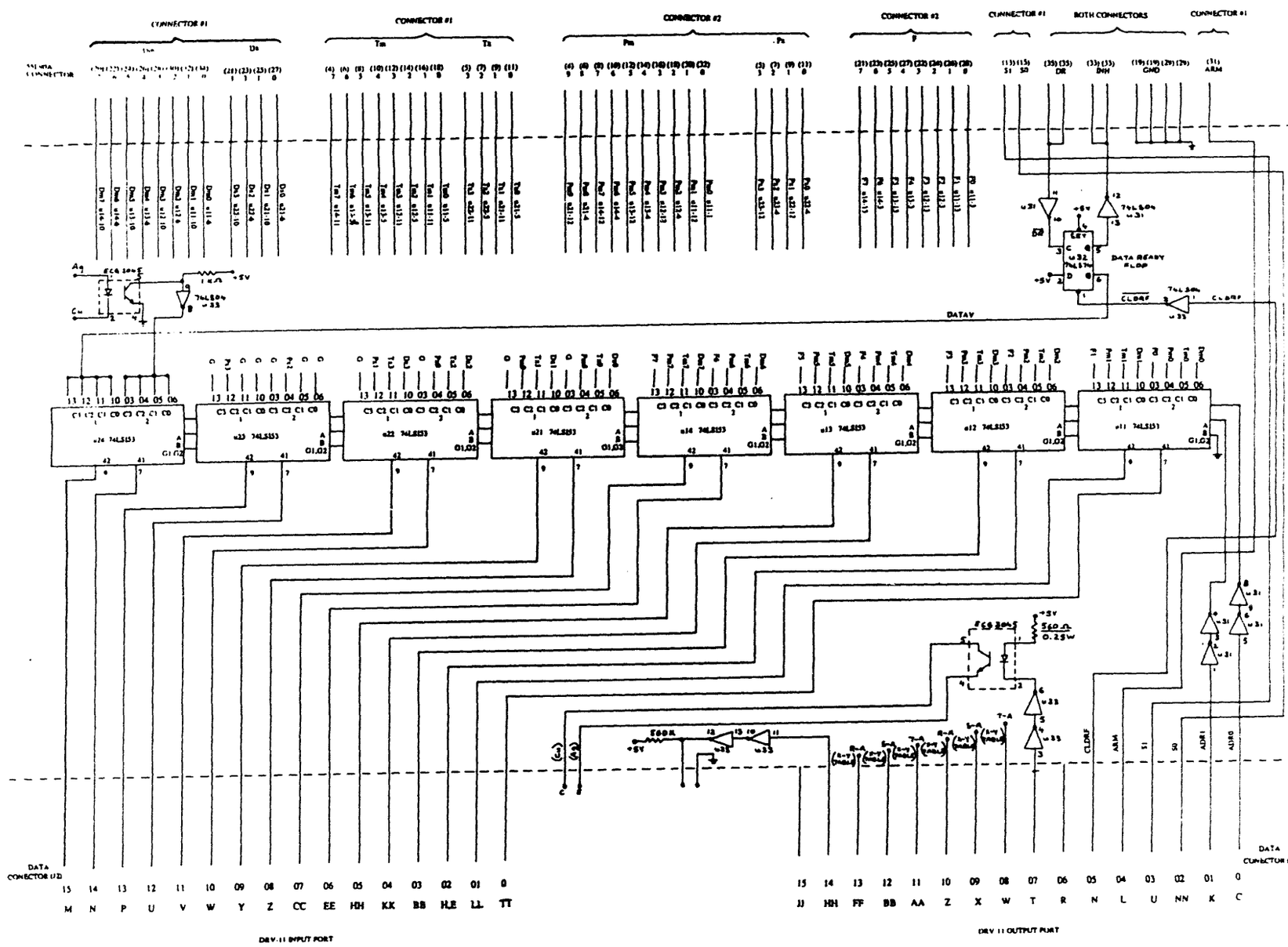

Figure 3.8 Logic Print of the Master Computer Interface Unit

they are severely limited in their capabilities and yet very expensive. For monodispersed and lightly loaded flows, the light scattered from seed particles small enough to follow complex fluid motions, including turbulence, is converted into velocity information. For flows with higher particulate loading or with polydispersed flows, other LDA techniques using amplitude and frequency discrimination are required to distinguish between fluid and particle velocity fields. However, these techniques have severe limitations of their own (Gautam et al., 1987). The velocity measurements were carried out using the LDA in the forward scatter mode. The receiving optics were placed at an angle of 30 degrees off of the central axis of the transmitting optics to avoid the light reflected from the glass faces from entering the receiving optics and with consequent improvement in the signal-to-noise ratio. All of the axial component measurements were made along the horizontal plane at three radial locations. However, passage of the laser beams through the media of different indices of refraction, air-glass-air, resulted in spatial displacement of the measuring volume. This displacement of the measuring volume was calculated and the necessary corrections were made. Lee and Srinivasan (1978) and Gautam (1989) employed amplitude discrimination to distinguish between gas phase and particle phase velocity information. The laser-induced fluorescence emission based LDA technique in combination with amplitude discrimination yields velocity information in a multisolid flow. Seed particles or any one particular group of solids coated with a fluorescent dye, such as the Rhodamine 6-G

(Stevenson et al., 1977) scatter light at wavelengths in the range 520 nm-660 nm (see Figure 3.9). Weak scattered light at 514.5 nm wavelength is also present. Initially a narrow band pass filter with a central wavelength of 560 nm (Andover FS-10-50), as dictated by the spectrum in Figure 3.9, was used. Scattered light (the strong scatter from undyed particles and the weak scattered light from the coated particles) at 514.5 nm wavelength was prevented from entering the photomultiplier tube. Later, a transparent amber acrylic sheet (AIN Plastics Acrylite 408-5) with a wavelength of 535 nm was used instead of the Andover filter. The dyed PSL particles provide the information on the gas phase velocity. By coating the larger sized bed material (glass beads of 300 micron mean diameter) it was expected that information on the particulate velocity flow field could be obtained. Exhaustive testing with dyed 300 μm glass beads was conducted but very noisy signals were obtained. This aspect is discussed later in this report.

In the absence of DMA link, data recording is slow; hence, an alternate software based system of storing the incoming data had to be employed given the limitations of the PDP-11 such as data acceptance and storage. The incoming data is reduced and stored in arrays while velocity and sample interval time data are stored on the hard disk.

Fluid velocity data is obtained from light scattered by the seed particles. Amplitude discrimination is being employed in addition to the fluorescence-emission to discriminate signals originating from larger particles and the seeding material. Hence, the large particles selected had a mean diameter greater that 300

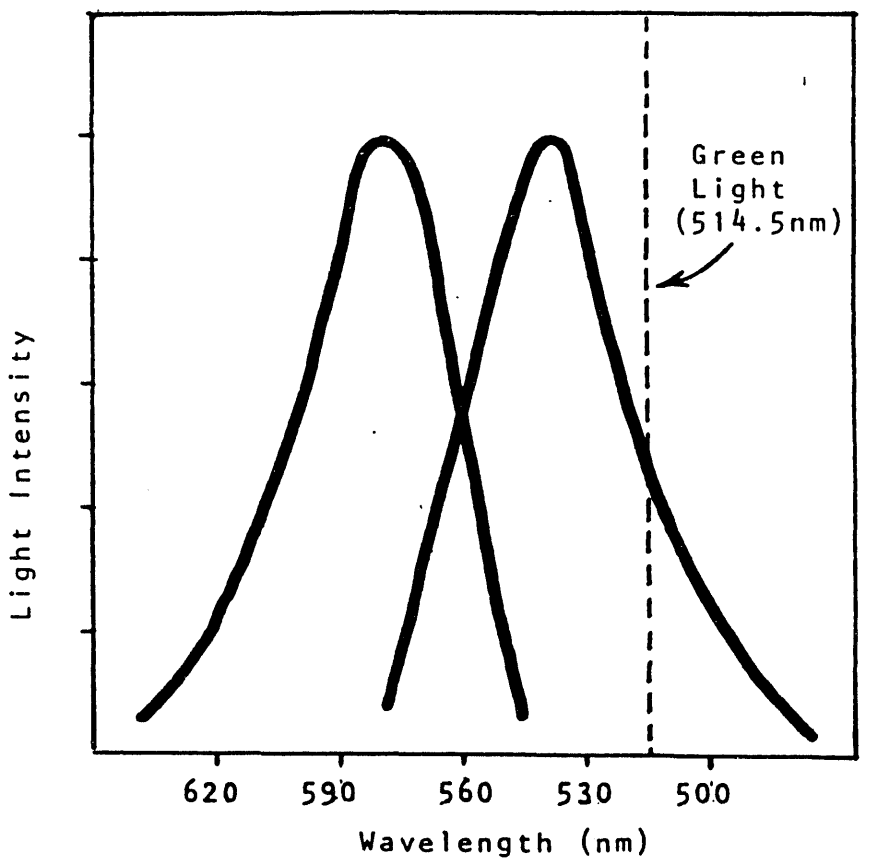

Figure 3.9 Absorption and Emission Spectra of Rhodamine 6G

micron rendering signal discrimination tractable. The threshold settings on the counter processor are set to discard signals from larger particles, i.e. signals with a larger pedestal or the larger d.c. component. The threshold settings were determined prior to running the experiments. Larger particles passing through the measuring volume scatter more light and produce a larger intensity response from the PM tube (called the pedestal) than the smaller particles. Thus, when the threshold level of the signal is set above that for the smaller particle signal only small or large particle signals are processed, and the velocity of the two phases could be separated. The difficulty encountered with this approach lies in the inability to accurately distinguish between the signals from small particles passing through the center of the measuring volume and the signals of large particles crossing near the edges of the measuring volume. Since laser beams have Gaussian light intensities both signals may have similar pedestals. This inability to separate large and small particle signals is referred to as trajectory ambiguity.

Typically, one thousand data points were required at each location to obtain statistically accurate velocity information. The standard derivation and ninety-five percent confidence interval, based on Student-t distribution, was calculated. Velocity bias was eliminated using the incremental times and weighing each sample. The mean velocity and turbulent intensity at each data location was determined.

3.2.2 Uncertainties in LDA Measurements

The procedure outlined by Kline and McClintock (1953) has been used to calculate the uncertainty of a given parameter in the current study. The uncertainty interval of a measurement is generally stated at specified odds; typically, odds of 20 to 1 (corresponding to 95% level of confidence) are used.

The uncertainty of a measured quantity is expressed as:

$$R \pm u_R \qquad (20 \text{ to } 1)$$

where, R is the mean value of the variable and u_R the uncertainty interval.

Consider a variable, N which is a function of n independent variables,

$$N = f(u_1, u_2, u_3, \ldots\ldots u_n)$$

Then the uncertainty in N is given by:

$$u_R = \left[\left(\frac{\partial N}{\partial u_1} \Delta u_1 \right)^2 + \left(\frac{\partial N}{\partial u_2} \Delta u^2 \right)_2 + \ldots + \left(\frac{\partial N}{\partial u_n} \Delta u_n \right)^2 \right]^{1/2}$$

In a dual beam fringe mode LDA system the particle velocity is given by the following relation:

$$\bar{u} = \delta_f . f_d$$

where,

$\bar{u}$ = Particle velocity

δ_f = Fringe spacing

f_D = Doppler frequency

The fringe spacing is a function of the laser light wavelength and the beam intersection angle:

$$\delta_f = \frac{\lambda}{2\sin(\alpha)}$$

where,

λ = Laser wavelength (514.5 nm)

α = Half of the intersection angle (= $\theta/2$)

For small value of θ, $\sin\theta = \tan\theta = a/F$, where 2a is the beam spacing at beam splitter and F is the focal length of transmitting lens:

$$\alpha_f = \frac{\lambda \cdot F}{2 \cdot a}$$

Using uncertainty estimates (Kline and McClintock, 1953) :

$$\delta\left(\delta_f^2\right) = \left[\frac{\partial \delta_f}{\partial F}\ \delta F\right]^2 + \left[\frac{\partial \delta_f}{\partial a}\ \delta a\right]^2$$

$$\delta(\delta_f) = \frac{\lambda}{2}\left[\left(\frac{1}{a}\,\delta F\right)^2 + \left(\frac{F}{a^2}\,\delta a\right)^2\right]^{1/2}$$

$$\delta(\delta_f) = \frac{\lambda}{2a}\left[(\delta F)^2 + \left(\frac{F}{a}\,\delta a\right)^2\right]^{1/2}$$

$$= \frac{\lambda}{2a}\left[\left(\frac{\delta F}{F}\right)^2 + \left(\frac{\delta a}{a}\right)^2\right]^{1/2} \cdot \frac{2a.d_{fr}}{\lambda}$$

where,

$$F = \frac{2a\delta_f}{\lambda}$$

$$\frac{\delta(\delta_f)}{\delta_f} = \left[\left(\frac{\delta F}{F}\right)^2 + \left(\frac{\delta a}{a}\right)^2\right]^{1/2}$$

The uncertainty is a function of $\delta F/F$ and $\delta a/a$ only. By allowing the beams to hit a distant screen, the relative magnitudes of these uncertainties can be reduced. Here, $\delta F/F$ is denoted by $\delta F'/F'$ and $\delta a/a$ by $\delta a'/a'$, where $2a'$ is the beam separation at a plane distance F' from the measuring volume. The corresponding uncertainties were $\delta F' = 0.2$ cm and $\delta a' = 0.1$ cm thus, yielding $\delta(\delta_f)/\delta f = 0.50\%$ as the uncertainty in the calibration constant, the fringe spacing, δ_f.

However, data show that scatter in the measurements is larger than the uncertainty calculated above. The observed variations are dominated by statistical uncertainties in the measurement process.

3.2.3 Dye Optimization

The fluorescent dye consists of Rhodamine 6-G in a solution of 50-50% by volume of ethylene glycol and benzyl alcohol. Several solution strengths were tested for the optimum LDA signal. Solutions with molar concentrations ranging from 0.0200 M to 0.0292 M (approximately 10 - 14 g. of Rhodamine 6-G per liter of solution) were prepared. The solutions were then tested to select the dye strengths that provided the best signals.

Strands of 38 gage (100 microns) Nichrome wire were immersed in solution for a period of 24 hours in an attempt to attain a fluorescent coating. When removed from the solution, they were allowed to dry for approximately 1.5 hours. When removed from the solution, the wires had an oxidized film and did not retain the fluorescent coating of the dye. Signal quality was very poor from the dyed wire. Human hairs seemed to be better suited to the dying procedure and were substituted for the wires.

Once the hairs were dyed, each was attached to a calibration wheel and tested with the LDA system. The calibration wheel consists of a Plexiglas disc attached to a variable DC motor. The speed of the wheel is verified using a strobe. A hair is attached to the outer edge of the wheel so that it passes through the measuring volume once per revolution of the wheel; thereby simulating a particle crossing the fringes. The speed of the wheel was measured using both the LDA and a strobe. Those solutions providing the best signals were chosen for the particle dying procedure. However, this method of optimizing the dye was considered inappropriate. The alternative method adopted to

optimize the dye was to use an air brush and atomizing the dye solution. The dye solution was atomized immediately upstream of the horizontal section through which the air was sucked by the blower. The signal quality was very good and the signal amplitude was chosen as the criteria from choosing the optimum solution strength.

3.2.4 Particle Dying Procedure

In the particle dying procedure, the optimum dye solution was prepared as mentioned previously. Particles of titanium dioxide were mixed with the solution. The mixture was then agitated for several hours using a wrist-action shaker. Several methods for removing the dyed particles from solution were employed.

First, the unseparated mixture was heated in a drying oven in an attempt to drive off the excess moisture. After the particles were in the oven an appropriate amount of time, they were placed in a desiccator to prevent the further absorption of moisture from the air. The time necessary for the evaporation of the excess dye took as long as four days. This process was too slow and the particles emerged from the oven caked together.

The second method attempted to separate the dyed particles from the excess solution before placing it in the drying oven. This was done by filtration, centrifuging, and decanting. The particles formed a "colloid-like" suspension which did not filter well. This process was also slow and messy and proved to be inefficient due to the small amount of particles retrieved from the solution.

The third method increased the amount of particles mixed per milliliter of dye solution. Since less dye was used, the excess was small and the time needed for drying decreased to one day. This method was the most effective and is used in all further dying procedures.

Because titanium dioxide particles emerged from the oven caked together, running them through a grinder and then through a ultrasonic separator was required to ensure the retention of the 2 micron sizing. Also, the absorption of the fluorescent dye by the titanium dioxide was poor. The particles did not retain the fluorescent orange color of the dye. Instead, they were purple when removed from the drying oven. Due to these problems and that of particle sphericity mentioned earlier, glass shot was substituted. Initially, it appeared that the fluorescent dye solution coated the glass shot relatively well but when dry showed a slight shift in the dye's original orange color. The glass shot did not dry in "cakes" and retained its size and shape.

The ability of the Rhodamine solution to adhere to the glass beads was thoroughly investigated. Several authors (Liang et al., 1984, 1985; Reisfeld et al., 1988) have conducted research involving the application of a Rhodamine solution onto glass plates. Liang et al. (1984) cleaned glass surfaces with an ultrasonic cleaner, first with ethanol then with distilled water. Rhodamine B was recrystalized from ethanol and then dissolved in distilled water to make solutions with concentrations between 10^{-4} and 10^{-6} M. The glass was placed in the dye solution for 15 minutes. When removed from solution the solution, two plates were

put together to form a "sandwich" with a layer of dye trapped between them. Dry samples were also prepared where the dye solution film evaporate. Reisfeld et al. (1988) used the sol-gel method to incorporate a Rhodamine 6G dye into glass.

By working closely with a company named Exciton, 50 μm to 100 μm glass beads as well as silica gel were dyed with Rhodamine 640 (with methanol as the solvent). Using a polymer substrate Exciton coated the glass beads and silica gel with the dye. However, the signal quality was very poor. The investigators also used a commercially available 5 μm (bore) capillary and injected the fluorescent dye in it. Additionally, fine capillaries (< 5μm bore) were drawn at WVU glass shop. Even though the bore was less than or equal to 5 μm the O.D. of the capillaries were about 100 μm to 150 μm. The diameters of the capillaries were measured under a microscope. The experience gained in this study showed that even though the bore size was less than 5 μm (and the dye was injected in the capillary) the outer dimension of the capillary was much larger that what is required for fluorescence work. The poor signal quality was attributed to the glass walls acting as lenses and their contribution to the refraction of light.

3.2.5 Calibration

A series of calibration tests were conducted in the horizontal test section using 2 micron undyed titanium dioxide as the seeding particle. The velocity measurements were taken at several different flowrates and at several positions along the center axis using the LDA with the PM optics in forward scatter mode. The data taken by the LDA was then compared to the velocity calculated from

the pressure differential measured using a pitot tube upstream from the LDA apparatus. These results were in good agreement.

The calibration wheel, as mentioned earlier, was then used to test the dyed and undyed glass shot and the 560 nm narrow bandwidth filter. The first test used 500 micron undyed glass shot attached to the Plexiglas disc on the calibration wheel so that the particles passed through the measuring volume with each revolution of the disc. The PM optics were placed in backscatter mode and no optical filter was used. Velocity measurements were taken and compared to those calculated from rpm measured by the strobe. The data was in good agreement with the calculated values.

Next, 500 micron glass shot coated with the fluorescent dye was placed on the calibration wheel. Data was taken and was in good agreement with the calculated values. The 560 nm bandwidth filter was then placed on the PM optics and this yielded a a very noisy signal was obtained.

The undyed glass shot was again placed on the calibration wheel and the 560 nm optical filter was placed on the PM optics. Because the glass shot was undyed, the 560 nm filter prevented the 514.4 nm scattered light from passing.

Tests were conducted to measure the instrumentation's sensitivity to gain, PM tube voltage, and threshold by varying only one quantity at a time. Tolerance levels for signal to noise ratio were established. The range of gain necessary to obtain a good signal and accurate velocity measurements was found.

Velocity measurements were made with undyed glass shot (300 μm) in the horizontal test section and the 514.4 nm optical filter

was placed on the PM optics which operated in forward scatter mode. Measurements were taken at three different flowrates and at five different locations along the center axis. The velocity measurements were comparable to calculated values using the measured pressure differential upstream.

The 560 nm optical filter was then added to the PM optics and 300 micron glass shot coated with the fluorescent dye was used. Velocity measurements, initially, were taken at the same three flowrates and at the same five positions along the center axis. The velocity measurements appeared to be in good agreement (as reported in the previous report) with those taken with the undyed glass shot and the 514.4 nm optical filter. However, upon closer scrutiny of the raw data, significant noise was observed. The velocity measured with the dyed particles was 10.5 m/s and this was in agreement with the velocities of undyed particles. However, measurements at different flowrates revealed that there existed a persisting noise at 10.5 m/s for all cases. Atomizing the Rhodamine dye solution with an airbrush (as described in section 3.2.3) yielded an excellent signal. The dyed PSL particles were not as effective as the spray but the signals were still very satisfactory.

3.3 Circulating Fluidized Bed Facility

A Circulating Fluidized Bed (CFB) experimental set-up was designed (see Figure 3.10) to provide maximum versatility in investigating particle cluster formation in the CFB riser using LDA, optic fiber probes, and other probes. The cold-flow CFB

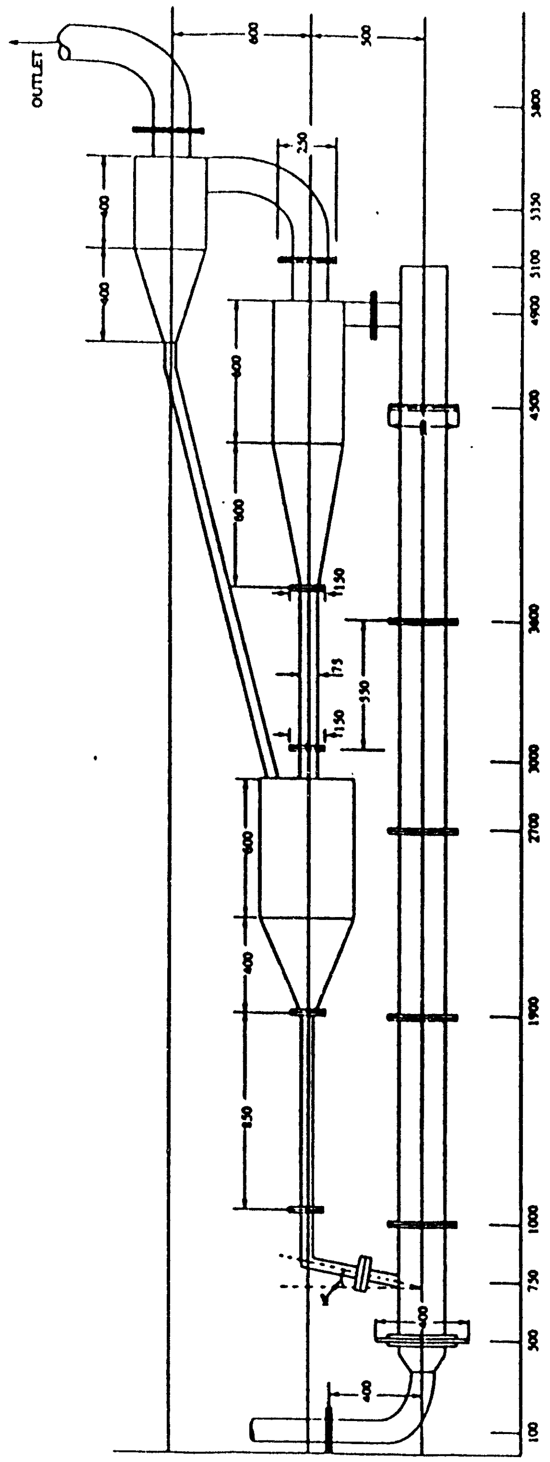

Figure 3.10 Circulating Fluidized Bed

facility has been set-up in the Fluidization Center and is currently fully operational. The cold-flow CFB model is 6 m high and constructed mainly out Plexiglas. Two stage cyclones are employed to capture the particles exhausted from the riser. The baghouse connected to the outlet of the secondary cyclone prevents fines from being exhausted to the atmosphere. The riser is made of Plexiglas tube with an inside diameter of 200 mm, wall thickness of 8 mm, and consists of 6 jointed sections in order to enhance the versatility of the experimental set-up.

Under normal operating conditions the fluidizing velocity in the CFB varies from 8 m/s to a maximum of 12 m/s. Design air flowrate is 0.25 m^3/s. Circulation of particles varies from 50 kg/m^2s to 200 kg/m^2s. At maximum fluidizing velocity, the entrainment capacity of air is 138 kg/m^3, and the mean voidage at outlet of riser is 0.94.

In order to observe the quality of fluidization and the flow patterns, the riser is made of Plexiglas. Transparent bed wall provides clear access for observing and videotaping gas bubbles, particle clusters, etc., and help in the adjustment of parameters controlling the flow patterns and fluidization.

The CFB experimental set-up was designed as a cold-flow model; however, studies at temperatures above ambient can be performed. The fluidizing air can be heated with electrical heaters up to 100 degrees Celsius. This will be very helpful in studying the formation of clusters as a function of temperature.

Design details of each component of the cold-flow CFB system are given below:

3.3.1 Design of the Distributor

Published literature has presented ample evidence showing that the quality of fluidization is strongly influenced by the type of gas distributor used. For few air inlet openings the bed density fluctuates appreciably at all flow rates, though more severely at higher flow rates. For more air inlet openings the fluctuation in bed density is negligible at low air flow rate. Bed density is more uniform throughout. Since the mean diameters of particle is 50 μm, the orifice of the distributor must be small enough to maintain the particle. Considering the distributor size, the pressure drop and fluidizing velocity, a sintered stainless steel porous plate manufactured by MOTT POROUS MEDIA will be used as the distributor. The distributor plate flow characteristics are shown in Figure 3.11 At the operating condition the pressure drop across the distributor is 4.2 KPa.

3.3.2 Design of the Riser

The Diameter of the Riser

Most of the previous investigations (van Zoonen, 1962; Hartage et al. 1986) with a few exceptions (Bader, Findlay, and Knowlton, 1989) employed a small diameter riser (50 mm to 100 mm). Experimental results obtained from both the large and the small diameter test units have shown that the flow in the riser of circulating fluidized beds is of a core-annulus type.

The solid and gas interaction between the core and the annulus is an important consideration in the evaluation of risers since the amount of interaction affects the solid and gas residence times.

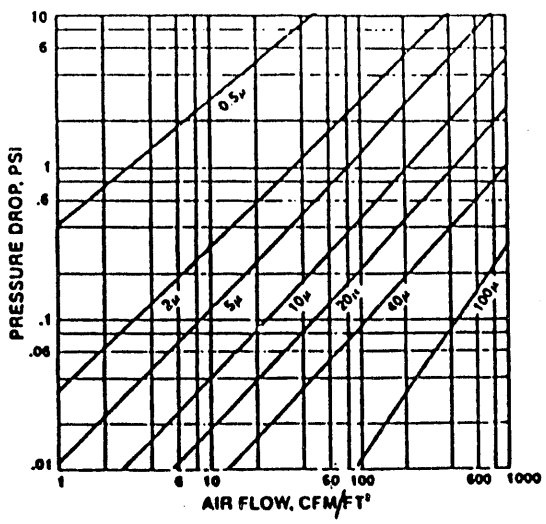

Figure 3.11 Distributor plate Flow Characteristics
(MOTT POROUS MEDIA)

Therefore, tests should be conducted in a unit with suitable size riser in order to determine the mass flux and particle velocity distributions as a function of riser radius and also axial riser position.

The results of experiments conducted by Bader, Findlay, and Knowlton (1989) have shown that the radial solids flux profile in the riser is parabolic. At a location 9.1 m above the solids entry point, the net mass flux rate decreased with riser radial position to a value of zero at about 25 mm from the wall, and the particle velocity profile is also similar to the mass flux profile. Voidage profile is smoother than both the mass flux and particle velocity profiles. Taking the wall effects and particle-particle interaction into consideration, a riser with a diameter of 200 mm was selected which 2 times the width of the particle flux region.

Height of the Riser

Bader, Findlay, and Knowlton (1989) have shown that, the mass flux and voidage profiles at positions of 9.1 and 4.0 m are nearly the same except for the quantity of mass flux and voidage. So, the height of the riser was selected as 4.5 m and divided into 6 sections. From bottom to top, the various sections are 700 mm, 800 mm, 800 mm, 800 mm. and 600 mm, respectively in length.

3.3.3 Design of the Cyclones

Circulating fluidized beds are characterized by particle circulation. The circulation of particles depends mainly on the fluidizing velocity and the quantity of particles captured from

exhausted gas. If the particles captured from the exhaust gas are much smaller than those in the exhaust gas then a stable circulation cannot be maintained. Hence, provisions are made to improve the collection of exhausted particles using a multistage cyclone, baghouse, electrical filters and so on. Considering the actual situation, two stage cyclones are inserted in the experimental set-up and the design details are given below:

Dimensions of the Cyclones

Two similar cyclones are employed in the test unit in order to capture the particles exhausted from the riser as shown in Figure 3.12 The outside diameters of both the cyclones are 300 mm. Diameter of the outlet is 150 mm. Height of the primary cyclone is 600 mm and that of the secondary cyclone is 400 mm. Other dimensions of both of the cyclones are as follows:

Primary Cyclone	Secondary Cyclone
D = 300 mm, A = 1200 mm	D = 300 mm, A = 1200 mm
B = 600 mm, C = 600 mm	B = 600 mm, C = 600 mm
E = 75 mm, F = 188 mm	E = 75 mm, F = 188 mm
L = 75 mm, K = 150 mm	L = 75 mm, K = 150 mm
M = 150 mm, N = 38 mm	M = 150 mm, N = 38 mm

The inlet velocity of both cyclones is 18.8 m/s and the outlet velocity of both is 11.9 m/s.

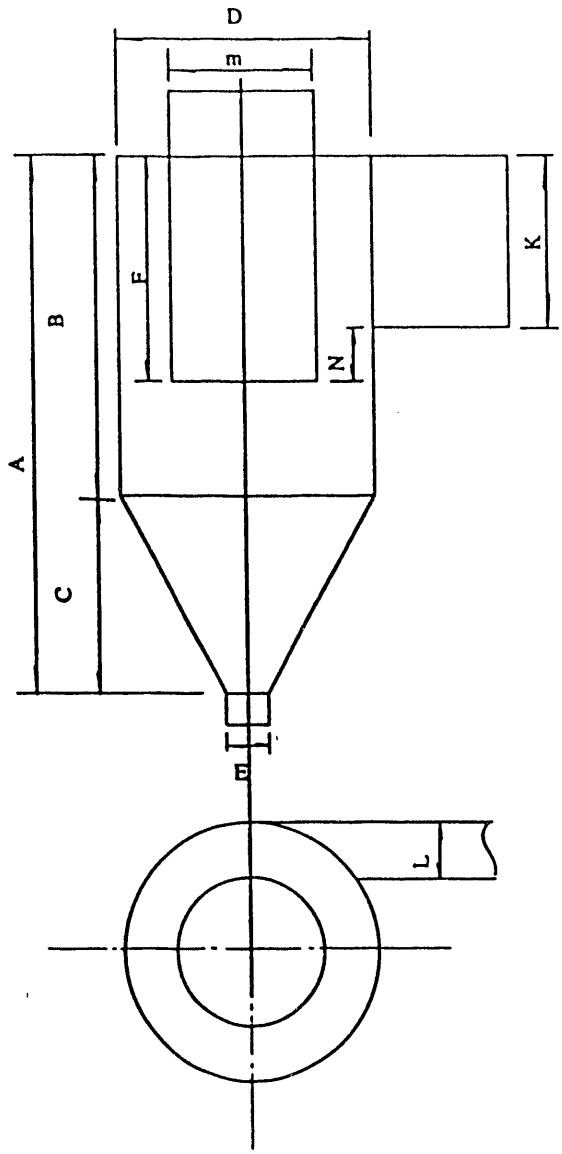

Figure 3.12 Schematic of Cyclones

Calculation of Pressure Drop

The air flowrate is 2.5 m^3/s and the inlet velocity V_c of the cyclone is 18.8 m/s. The number of cyclone inlet heads p_c:

$$P_c = k_o KL/M^2 = 16.0 \times 150 \times 75/150^2$$

$$= 8.0$$

here k_o is a constant, for the following conditions, $k_o = 16.0$

L/D = 1/12 - 1/4
K/D = 1/4 - 1/2
M/D = 1/4 - 1/2

The velocity head (in H_2O):

$$h_{vi} = 0.05 \times \rho v_c^2 = 0.05 \times 1.2 \times 18.8^2 = 21.2 \text{ mm } H_2O$$

The total pressure drop across cyclone:

$$p = p_c \times h_{vi} = 8.0 \times 21.2 \text{ mm } H_2O = 169.6 \text{ mm } H_2O$$

The minimum particle size:

$$D_{p\,min} = \left[\frac{9\mu D}{\pi N V_c(\rho_s - \rho)}\right]^{1/2} = \sqrt{\frac{9 \times 1.2 \times 10^{-5} \times 0.3}{3.14 \times 5 \times 18.8\ (2000-1.2)}} = 7.6 \times 10^{-6} m$$

Here V_c is the inlet velocity, μ is the viscosity, N is the number of turns, N=5

The cut size:

$$D_{pc} = \sqrt{\frac{9\,\mu\,D}{2\,\pi\,N\,V_c(\rho_s - \rho_g)}} = \sqrt{\frac{9 \times 1.2 \times 0.3 \times 10^{-5}}{2 \times 3.14 \times 5\ 18.8\ (2000 - 1.2)}} = 5.2\ \mu m$$

The separation efficiencies are:

d_p	3 μm	10 μm	15 μm	20 μm
efficiency	22%	80%	90.5%	99.5%

3.3.4 Design of the Hopper

A schematic of the particle hopper employed in the experiment unit is shown in Figure 3.13. Since the maximum mass flux rate is 25 kg/s in the test unit, there should be enough room to store the circulating particles in the loop to maintain a stable circulation.

Considering the particle circulation to be stable and the time required for each complete circulation in the CFB to be 5 seconds, the quantity of particles passing a given section in the stand pipe, W, is 125 kg per circulation. The hopper was designed to store at least twice this amount. The volume of the hopper, V is $V = 2W/\rho_s = 2 \times 125 / 2500 = 0.1\ m^3$, at least assuming the density of particles, ρ_s, is 2500 kg/m^3.

3.3.5 Design of the L-Valve

Several types of non-mechanical valves are in use today to transfer the particles from the standpipe to the riser. Notable amongst them are L-valves and U-valves. Importance of a well designed L-valve cannot be overstressed. Depending on the particle characteristics, two types of flows can exist in the non-mechanical valves, namely aerated flow and stick-slip flow. If stick-slip

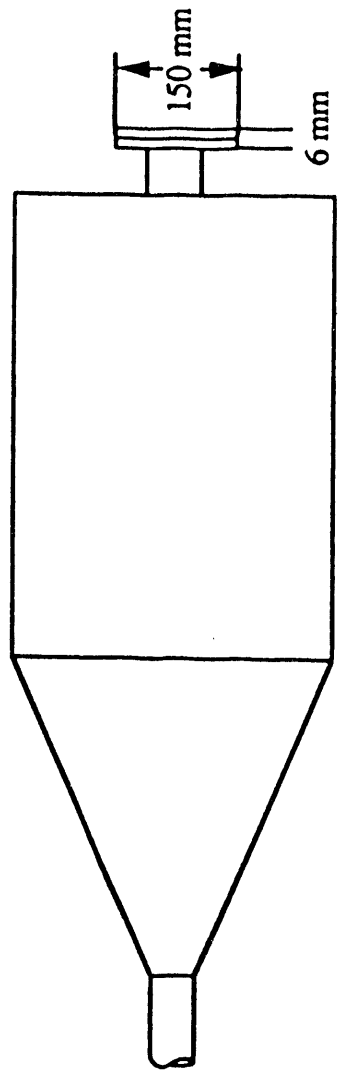

Figure 3.13 Schematic of Solids Hopper

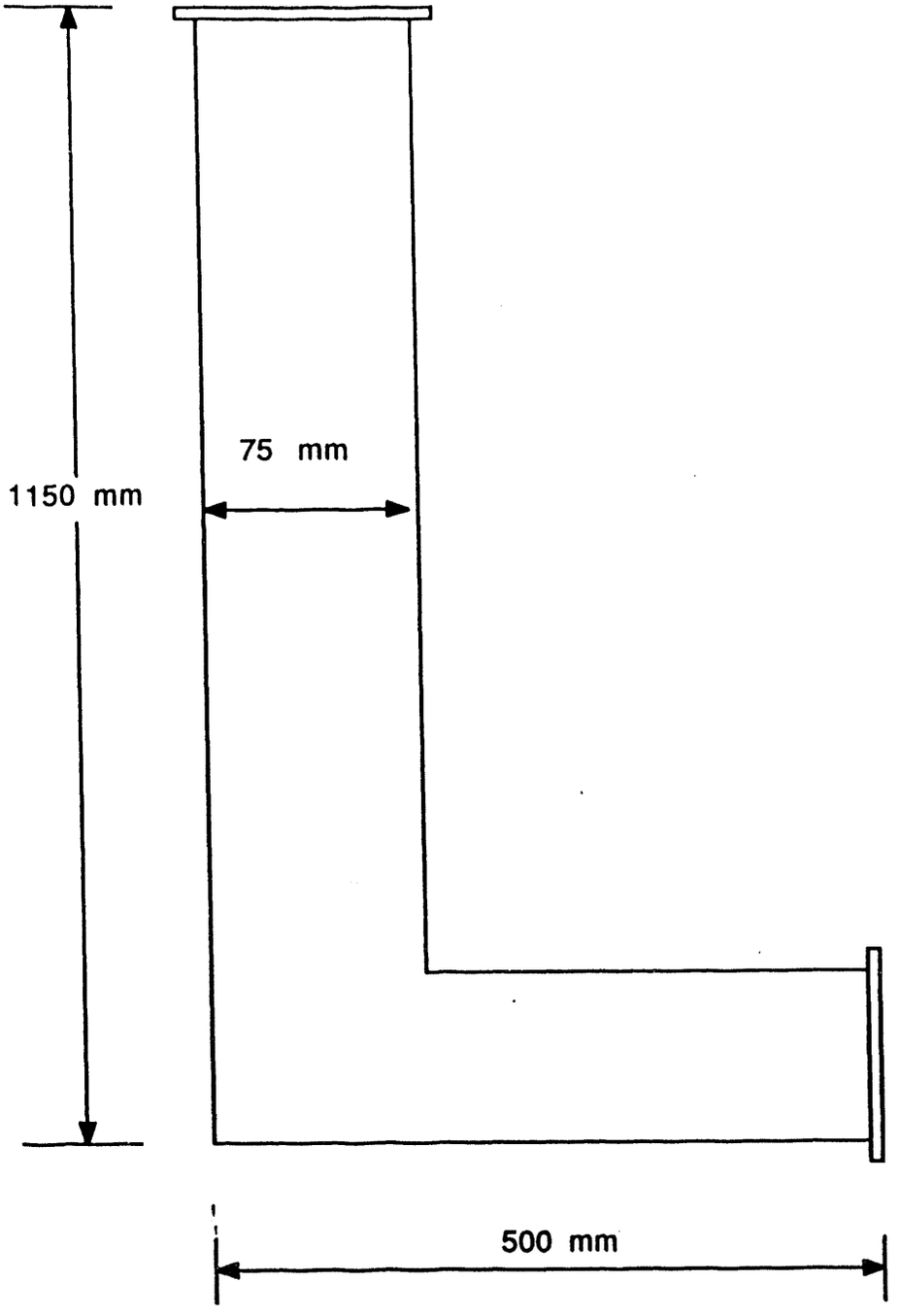

Figure 3.14 Schematic of the L-valve

flow exists, it is necessary to determine whether there exists a positive pressure difference (pressure at the top is lower than the pressure at the bottom).

From the operating conditions and the particles employed in the test, it is apparent that a stick-slip flow exists in this test. The ideal seal height (where there is a net zero gas flow rate) and the height (where the solids in the leg flow continuously downward) are determined. In the experimental unit, an L-valve is employed and its dimensions are shown in Figure 3.14.

3.4 Instrumentation and Procedures (Gas Velocity Profiles and Pressure Drops)

Experiments to determine the gas velocity distribution in the riser were carried out in the circulating fluidized bed. Two kinds of glass beads with mean diameter of 112 μm, density of 2305 kg/m^3 and mean diameter of 145 μm density of 2245 kg/m^3 respectively were employed in the experiments. Gas velocity distributions were obtained as a function of radial position, elevation, solids circulations rate, superficial velocity and particle size. A circulating fluidized bed runs at relatively high mass flow flowrate and at superficial velocity above particle terminal velocity.

Experiments were carried in a lab-scale circulating fluidized bed with a 200 mm diameter riser and the height of the riser is 5.5 meter. As shown in Figure 3.15, the air supply was provided by a compressor with total pressure of 0.1 bar and flowrate of 1370 m^3/hr. The primary air and the aeration air were introduced below

the distributor and L-valve. The orifice distributor was employed with a very fine screen to prevent particle falling through the orifices. The particles entrained by fluidized air and captured by primary and secondary cyclones return to a particle storage hopper via a measuring vessel which provides means for determining the solids circulation rates. The returned particles enter the riser through L-valve and begin another circulation

In the experiments, the superficial velocity was adjusted by primary and aeration air. The solids flowrate discharged into the riser was set by the aeration rate. The solids circulation rate was measured by closing the slide valve under the measuring vessel and recording the time it took for the transparent measuring vessel to fill up with solids. The volume of measuring vessel is 0.00228 m^3. The apparent packed density of the solids was measured for the calculation of the solids circulation rates. The flowrate of aeration was measured by a rotary flowmeter and the primary air flowrate was measured by a DS-200 Flow Sensor produced by Dwyer Instruments,INC.

The probe used in this work to measure the pressures is a Pitot-static tube probe, and its design is shown in Figure 3.15. The probe consist of two hypodermic stainless steel tubes with 0.7 mm I.D. and 1 mm O.D., fixed together by nickrome wire and encased in a 5 mm O.D. steel pipe for reinforcement. The tubes are aligned parallel to each other and separated by a distance of 0.5 mm (between the axes). One of the tubes was sealed at the tip, and at 10 mm from the tip, one of 0.5 mm hole was drilled perpendicular to the plane of the tubes. The hole are flush with the surface, and it

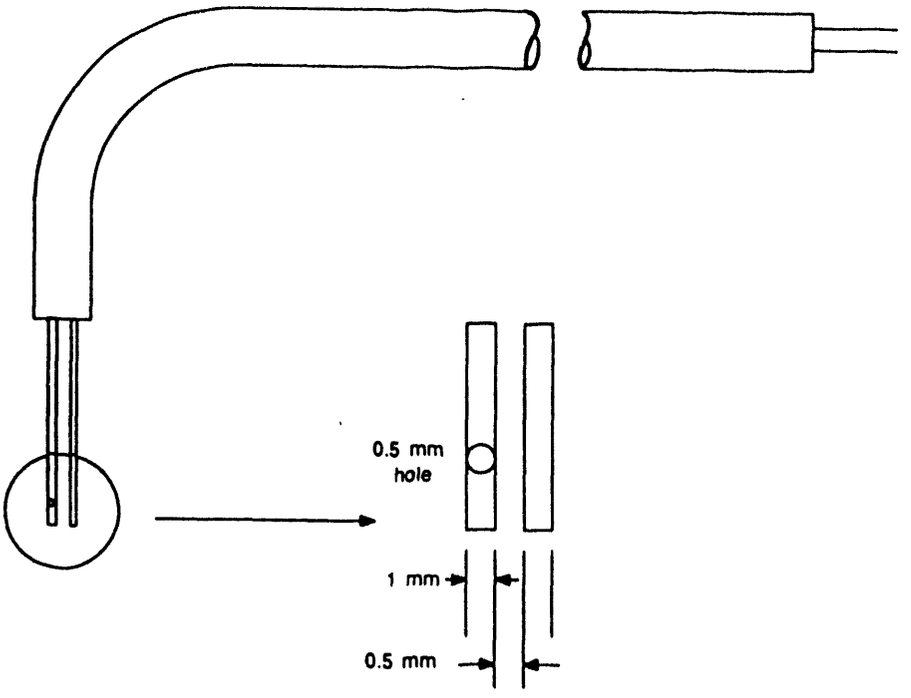

Figure 3.15 The Pitot-static Probe

is round off. This is the static tube. The other tube has the open, circular end flattened. This is the impact tube. The surface of the tubes are made as smooth as possible.

Figure 3.16 shows the schematic of the measuring system. The two three way valves may be used in two ways: one way is to clean the pressure tap line when the valves are switched to the pressurized air line and other one to measure the differential pressures between dynamic and static pressures which come from the probe. With the three way valves in clean position, a stream of air flows from the pressurized air line to the probe tip to prevent particle entering probe. A differential pressure transducer range of 0 - 124 mm H_2O was employed to measure the differential pressure. The pressure transducer produce 0 to 5 DC volt. And a RTI-815 ADC board was used to condition and to convert the DC volts signal produced by the pressure transducer into digital signal for processing by computer. The acquisition frequency was 10 Hz.

For Pitot-tube static probe, the local gas velocity can be got by using a standard Pitot-tube static probe equation:

$$V_{local}=C(2\Delta P/\rho_f)^{1/2}$$

Where V_{local} is the local gas velocity, ΔP is the pressure difference between stagnation pressure and static pressure, ρ_f is the fluid density, C is a dimensionless constant. For this probe we got C=0.97 after calibration in the wind tunnel.

In the experiments, superficial velocities ranged from 3.50

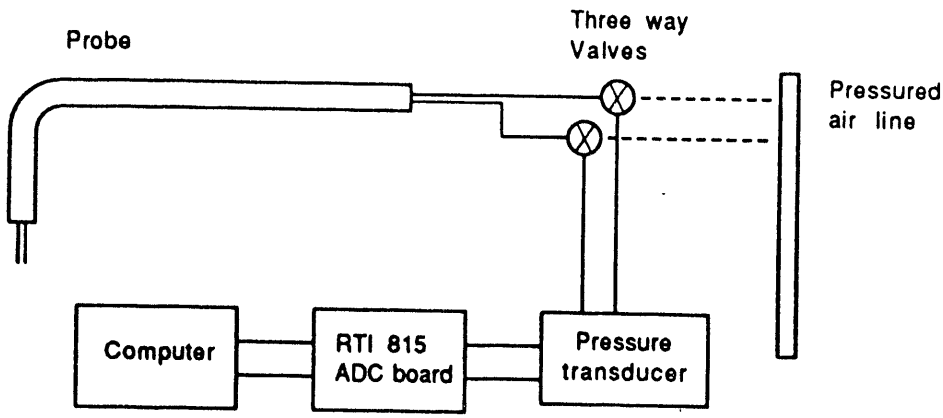

Figure 3.16 The Block Diagram of Measurement System

m/s to 7.33 m/s. The solids circulation rates are between 10 kg.m^{-2}.s^{-1} and 25 kg.m^{-2}.s^{-1}. Two kinds of glass beads with mean diameter of 112 μm, density of 2305 kg/m^3 and mean diameter of 145 μm density of 2245 kg/m^3 respectively were employed in the experiments. Experiments were conducted at two elevations, 2108 mm and 2743 mm above the distributor respectively.

3.4.1 Design of Experiments

There are many factors effecting gas velocity profile in circulating fluidized bed such like superficial velocity, solids circulation rate, solids properties and the height above distributor etc.. And each factor varies at different levels. It will take too much time and power to have tests for every parameter at every level. It is necessary to use analysis of variance technique in experiments improving accuracy and reducing cost of experiment.

In applying the analysis of variance we must first construct an appropriate statistical model, and frame the question we wish to investigate in terms of this model. In these experiments, there are more than 2 factors, we can not use a simple analysis method to deal with this matter. Many of modifications of pure completely balance designs have been developed to suit frequently occurring practical problems. One of them is balanced incomplete blocks. In this design, each block does not contain a representative of each level of each factor but subset of these levels. By appropriate choice of these subsets considerable simplification of analysis is made possible, while the reduction of block size increases

Table 1. Balanced Incomplete Block Design

Factors	Blocks					
	I	II	III	IV	V	VI
A	×				×	×
B	×	×		×		
C		×	×		×	
D			×	×		×

flexibility and may well reduce residual variation.

In experiment of gas velocity profile, there are four factors(mean gas velocity, solids circulation rate, the height above bed and the solids mean diameter) were considered. If the balanced incomplete blocks design is employed in the experiment, the following formula for the experiment design is obtained:

$$kr=r+(t-1)\lambda \tag{2}$$

$$r(k-1)=(t-1)\lambda \tag{3}$$

where t is the number of factors, b is the number of blocks, k is the number of factors per block, r is the number of replication of each factor and λ is the number of blocks in which any given pair of factors appear together.

By choosing b = 6, k = 2, and r = 3, a value of $\lambda = 1$ is obtained. A table of balanced incomplete blocks design was obtained in the experiment. In the experiments, all the factors are not changed for a change in one particular factor. Only some of the factors are varied and this significantly reduces the size of experiments. In Table 1, only those factors corresponding to the cross marks are changed and not the other factors.

3.5 Experimental Procedures for Solids Flow through the L-Valve

The three most commonly used types of non-mechanical valves are L-valve, J-valve, and the reverse seal. In the study an L-valve

was used and several parameters, such as geometry, aeration and particle size that influence the performance characteristics were varied.

In the experiments, two kinds of the solids were employed. The solids circulation rate was from 0 to 3,200 kg/hr. Mean gas velocity in the riser of circulating fluidized bed is 5.5 m/s. The riser height is 4.5 m/s with a diameter of 200 mm. The riser and L-valves were made of Plexiglas in order to have visual access of solids flow pattern. The system pressure was kept at 0.0017 bar. As shown in Fig. 3.10, the air supply was provided by a compressor with a total pressure of 0.1 bar and flowrate of 1370 m^3/hr. The primary air and the aeration air were introduced below the distributor and L-valve. The aeration tap is located just above the right angle bend in the L-valve. The orifice distributor was employed with a very fine-mesh screen to prevent particles from falling through the orifices. The particles entrained by fluidized air and captured by primary and secondary cyclones return to a particle storage hopper by passing through a measuring vessel which provides means to measure the solids circulation rates. The returned particles re-enter the riser through L-valve and begin another circulation. The pressure measurements in the L-valve related study were made with water manometers. The data was collected before the data acquisition system with the electronic pressure sensors was installed.

TABLE 3.2 Signal Range, LSB Values, and Sample Throughput for each Gain Setting

Gain	+/- 10 V Unipolar		
	Signal Range	LSB values	Sample Throughput
1	+/- 10 V	4.88 mV	31.2 kHz
10	+/- 1 V	488 uV	31.2 kHz
100	+/- 100 mV	48.8 uV	25.0 kHz
500	+/- 20 mV	9.76 uV	12.5 kHz

Table 3-1

Analog Input Range Configure	Gain	The Low-level signals can be measured
0 to 10 V (unipolar)	1	0 to 10 v
	10	0 to 1 v
	100	0 to 100 mv
	500	0 to 20 mv
- 5 v to + 5 v	1	- 5 v to + 5 v
	10	-500 mv to +500 mv
	100	-50 mv to +50 mv
	500	-5 mv to +5 mv
- 10 v to + 10 v	1	- 10 v to + 10 v
	10	- 1 v to + 1 v
	100	- 100 mv to + 100 mv
	500	- 10 mv to + 10 mv

THIS PAGE IS INTENTIONALLY LEFT BLANK

CHAPTER 4

RESULTS AND DISCUSSION

Measurements of gas velocity distribution were carried out in the circulating fluidized bed riser with a diameter of 200 mm and height of 5.5 m using a custom built pitot static tube. Two kinds of glass beads with mean diameter of 112 μm, density of 2305 kg/m^3 and mean diameter of 145 μm density of 2245 kg/m^3 respectively were employed in the experiments. The experimental results showed that the local gas velocity varied with the radial position, elevation, solids circulation rate, superficial velocity and particle size. And the particle circulation rate influences the gas velocity profile most. A general formula for gas velocity distribution in the circulating fluidized bed riser was obtained based on the particle circulation, superficial velocity, and particle diameter.

4.1 Fluorescence-Emission Based Laser Anemometery

Exhaustive tests with the dye strengths yielded an optimum strength of 0.02 M (Rhodamine 6G in a 50:50 vol.% solution of benzyl alcohol and ethylene glycol. Excellent results were obtained when the solution was atomized and injected into an air stream. Additionally, the fluorescent dye polystyrene latex particles also yielded very satisfactory results. Tenite Propionate (Formula 360A 19312 H2) from Kodak has very good fluorescent properties but it comes in 3 mm diameter granules which had to be further ground on a mill to a smaller size. The grinding resulted in a fibrous mass

that had to be classified to obtain 50 μm particles. These particles had very satisfactory laser fluorescence properties but were rather large for fluorescence-emission based anemometery.

A significant finding of this effort has been that even though large particles (greater than 3 μm diameter) emit fluorescence and yield a burst signal in a dual beam fringe mode of the LDA there is no signal modulation. Hence, the data obtained is not representative of the velocity of the flow stream. It is imperative that for fluorescence emission based laser anemometry the diameter of the particles has to comparable with the fringe spacing in the measuring volume. The experiments with the glass capillary tubes had the drawback that the walls were acting as a lense and the refracted light was resulting in a noisy signal. Hence, the success with the atomized dye solution and the polystyrene latex particles could be explained.

The optical filter should allow the fluorescence emission to reach the PM tube and block out the scattered light. Fluorescence emission eliminates the dependence of the signal modulator on the aperture geometry of the PM receiving optics primarily because fluorescence is spatially isotropic and unpolarized (Stevenson et al.,1975). The adopted technique permitted optical discrimination between the scattered light and fluorescence emission. The Laser Doppler Anemometer used in this effort was configured in the differential Doppler or fringe mode. This utilizes the scattered light when a particle passes through the point of intersection of the Gaussian beams. The scattered intensity varies with time and the modulation frequency under the Gaussian envelope is given by

$$f_d = \frac{2\ U_x}{\lambda} \sin\frac{\theta}{2}$$

The detection process, being essentially incoherent permitted the introduction of fluorescent particles in the flow such that the standing electromagnetic field, in the intersection region, could induce a time varying fluorescent emission (Stevenson et al., 1975). Hence, by using a narrow band pass filter in the receiving optics, signals from the two classes of particles (dyed and undyed) were effectively discriminated. The investigation into the filters has resulted in use of a customized filter from DANTEC that fits in-line between the P.M. optics and the photomultiplier tube. The low-fluorescence filter has a cut-off at 525 nm wavelength and transmission at 514.5 nm.

4.2 Gas Velocity Profiles in the Riser

Information regarding the gas velocity profile in circulating fluidized bed riser is required while designing and operating the circulating fluidized bed systems. The gas velocity distribution plays very important role in gas-particle back mixing and influences the solids concentration profiles, solids velocity profiles and voidage distribution. These parameters have a direct impact on the gas-solids reactions and heat and mass transfer rates.

A new collection of time averaged local gas velocity distribution covering a range of solids circulation rates, superficial velocity and solids properties, and provides insight of

gas flow behaviors in a relatively dilute gas-solids two phase flow.

1. Gas velocity profile in Circulating Fluidized Bed.

The gas velocity profile was obtained by time averaged local gas velocities at 10 radial locations at a given operating condition and probe elevation.

Figure 4.1 shows nondimensional gas velocity distribution (V/V_{max}) versus nondimensional radial position(y/R) in the riser. The profile was measured at 2743 mm above the distributor. The circulation rate for the 116 μm glass beads was 11.38 $kg.m^{-2}.s^{-1}$. The maximum velocity ($V = V_{max}$) is at the centerline (y/R = 1) of the pipe and the minimum velocity (V= 0 m/s) at the wall (y/R = 0). The gas velocity profile is parabolic. Since the flow is fully developed and turbulent, the gas velocity profile in circulating fluidized bed may be represented by the empirical "power law" equation where the exponent, n, varies with the mean gas velocity, solids circulation rates, and elevation. In Figure 4.2 a set of data obtained in the experiments are shown on a plot of ln(y/R) versus $\ln(V/V_{max})$; the slop of the straight line through the data gives the values of n. Even the power law profile is not applicable close to the wall and the profile gives an infinite velocity gradient at the wall and fails to give a zero slope at the centerline, it fits the experimental data in most of the pipe.

2. Variation of the Velocity Profile with Mean Gas Velocity

The most important factor in power law profile is the exponent

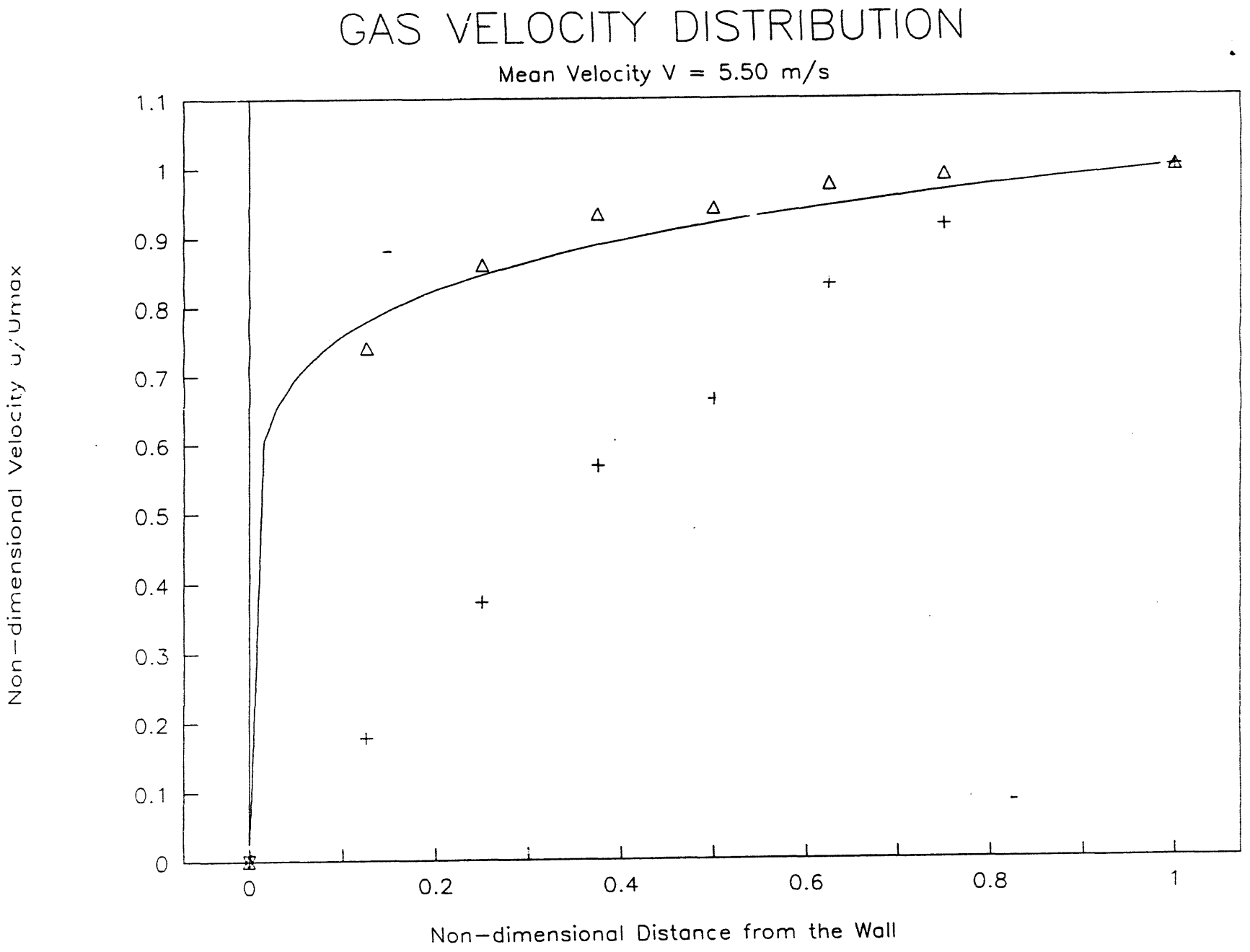

Figure 4.1 The Gas Velocity Distribution in Circulating Fluidized Bed Riser

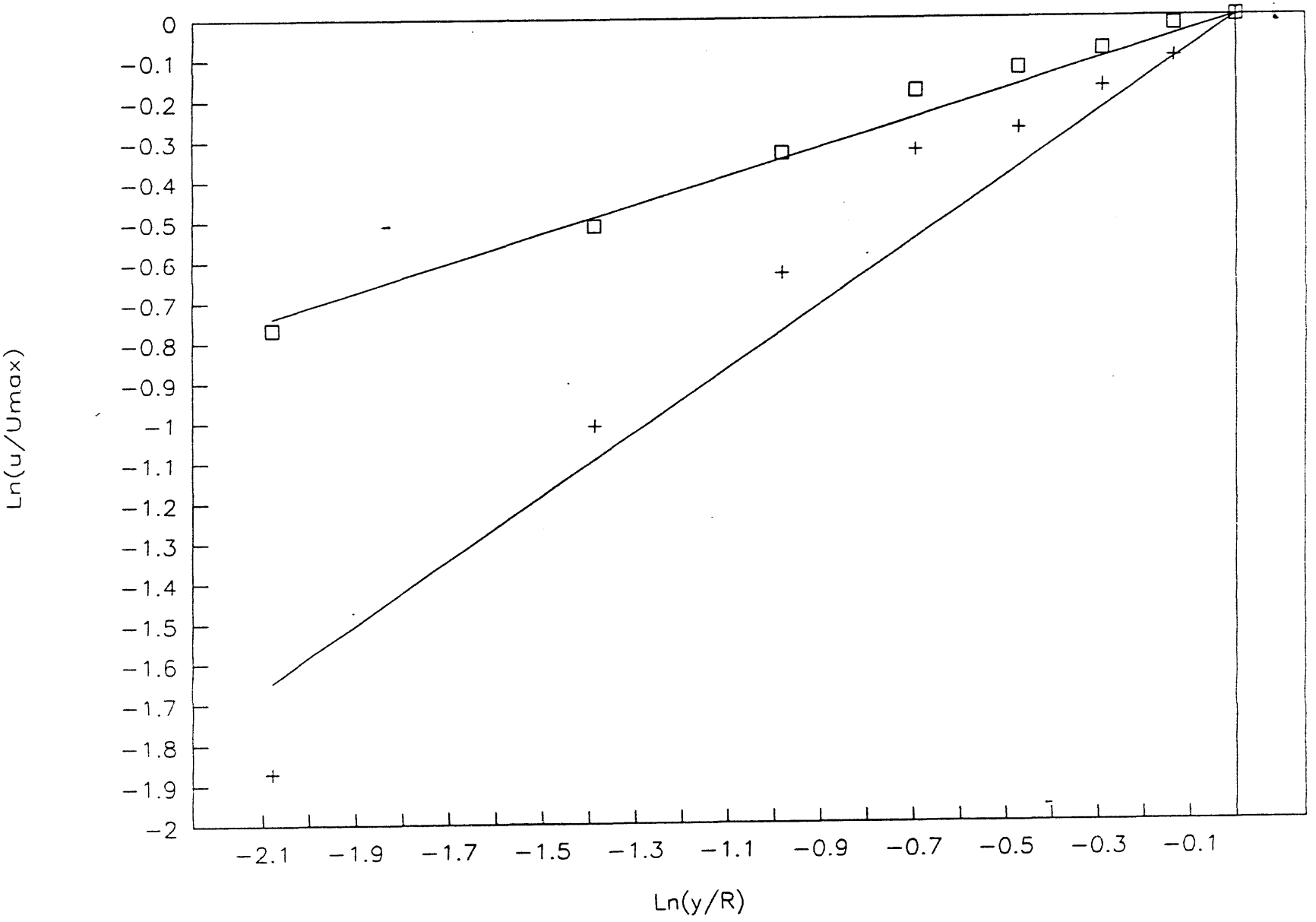

Figure 4.2 Power-Law Velocity Profiles in CFB

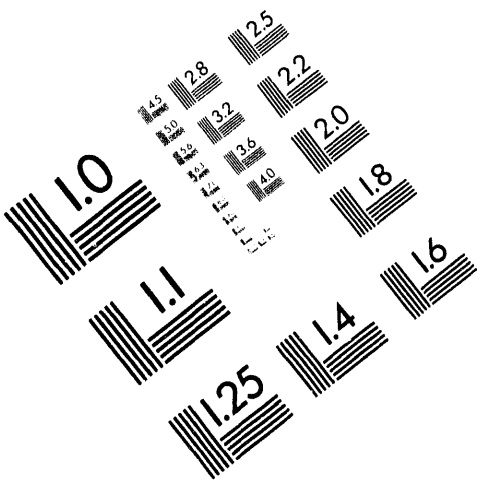

Association for Information and Image Management

1100 Wayne Avenue, Suite 1100
Silver Spring, Maryland 20910

301/587-8202

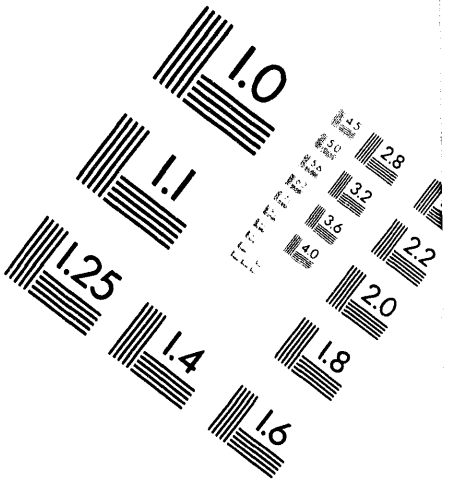

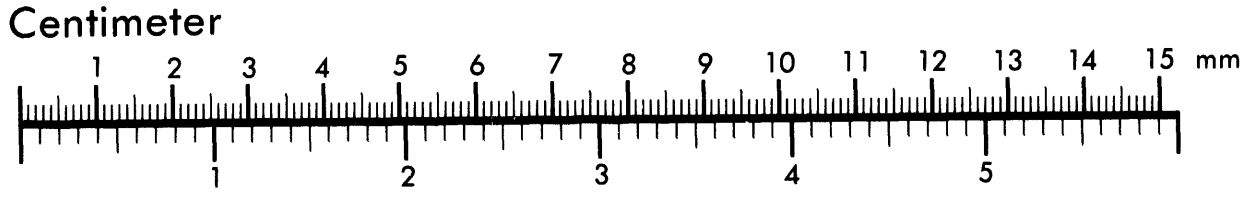

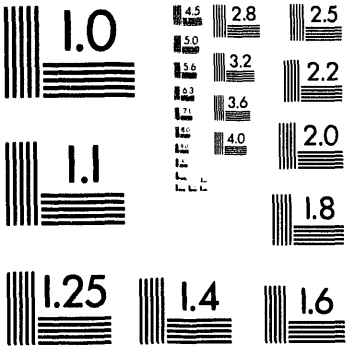

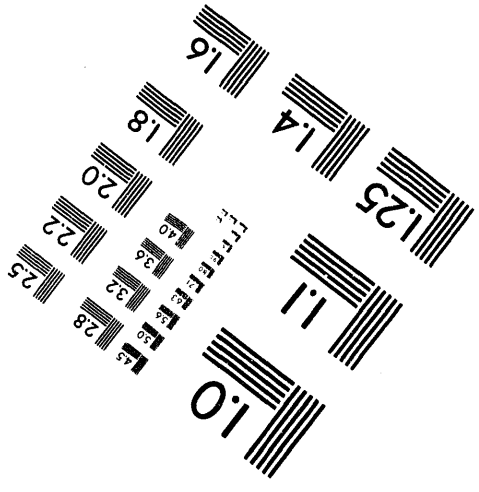

MANUFACTURED TO AIIM STANDARDS
BY APPLIED IMAGE, INC.

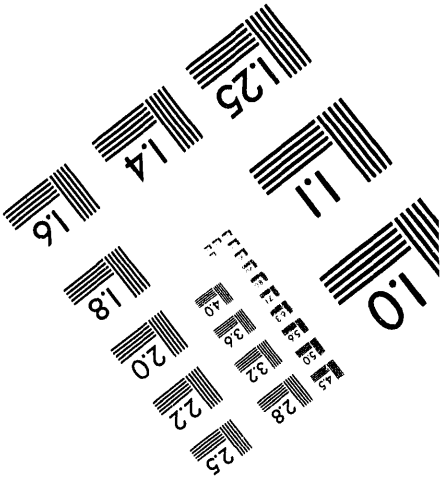

2 of 2

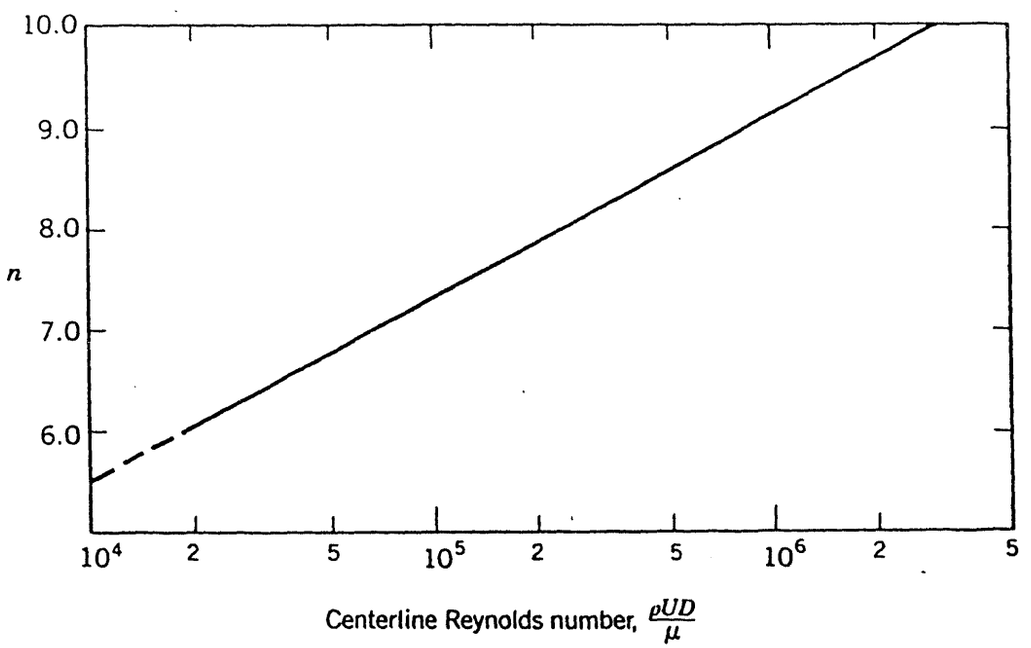

Figure 4.3 Exponent for Power-Law Profile

n. In pure fluid turbulent flow exponent, n, is a function of the Reynold's number. Figure 4.3 (from Hinz, 1975) shows the variation of the exponent, n, in the power law profile with Reynold's number (base on pipe diameter,D, and centerline velocity,V_{max}). In two phase flow, the exponent, n, also varied with the Reynold's number. If the pipe diameter is a constant, the exponent, n, depends on the gas velocity only. The variation of the gas velocity profile with the mean gas velocity is shown in Figure 4.4, Figure 4.5 and Figure 4.6. In Figure 4.4, the solids circulation rate was 11.38 $kg.m^{-2}.s^{-1}$, the probe elevation was 2108 mm above distributor. The local time averaged gas velocity measurements are indicated by (+) at mean velocity $\bar{U}$ = 3.50 m/s and by (▵) at mean velocity $\bar{U}$ = 5.50 m/s respectively. In Figure 4.5, the particle circulation was 14.73 $kg.m^{-2}.s^{-1}$. The probe elevation was 2108 mm above distributor. The local time averaged gas velocity measurements at mean velocity $\bar{U}$ = 3.50 m/s are represented by (+) and at mean velocity $\bar{U}$ = 5.50 m/s by (▵). In Figure 4.6 the particle circulation rate was 20.58 $kg.m^{-2}.s^{-1}$ and the probe elevation was 2743 mm above distributor. The local time averaged gas velocity measurements at mean velocity $\bar{U}$ = 5.5 m/s are plotted by (▵) and at mean velocity $\bar{U}$ = 7.33 m/s are plotted by (+).

From above Figures 4.4, 4.5 and 4.6, it is clear that the gas velocity profile in circulating fluidized bed changes when the mean gas velocity changed. The exponent, n, increases with mean gas velocity and the solids circulation rate is larger, the effect of the mean gas velocity on the gas velocity profile is smaller. And the effect of mean gas velocity on the gas velocity profile weakens

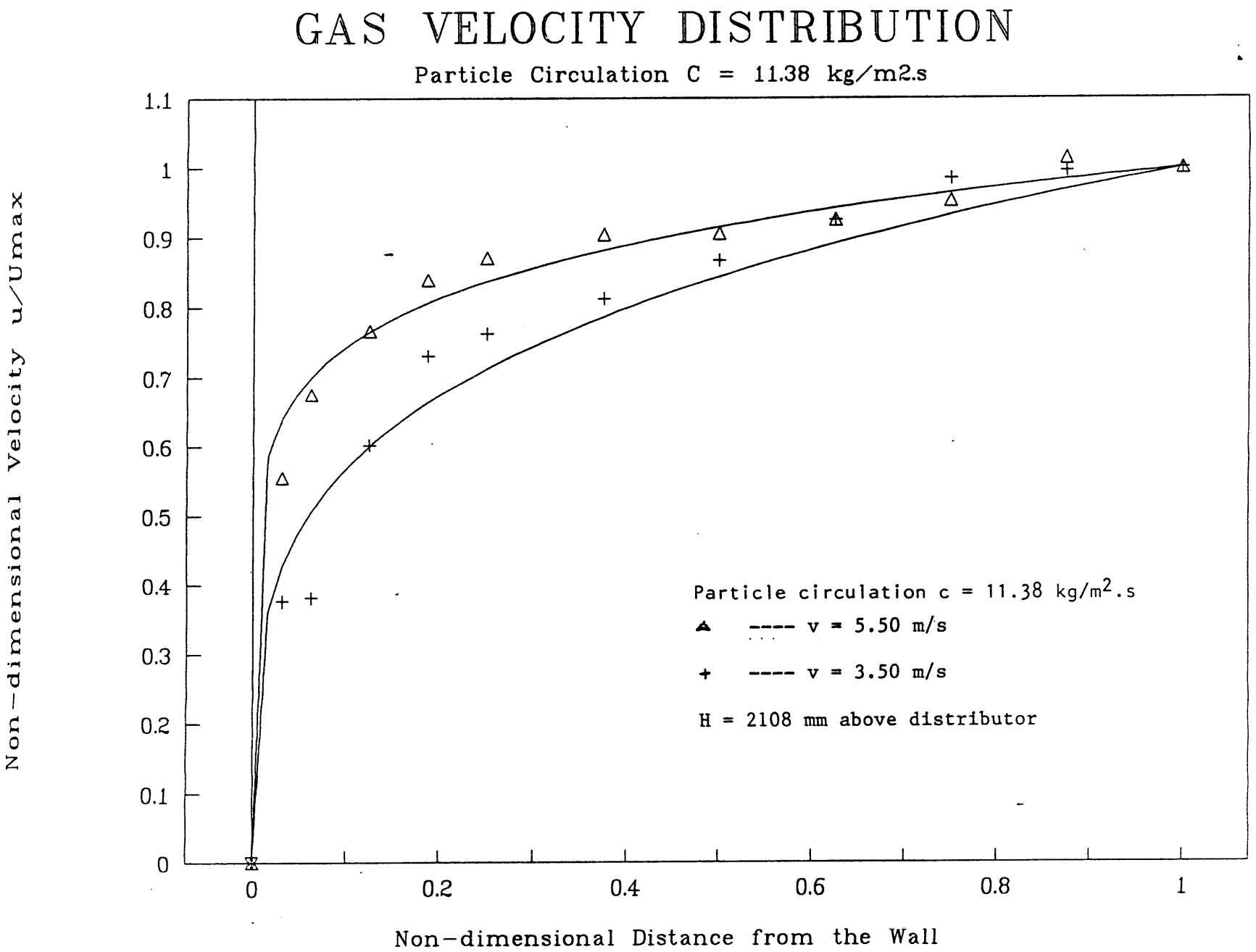

Figure 4.4 Gas Velocity Profile

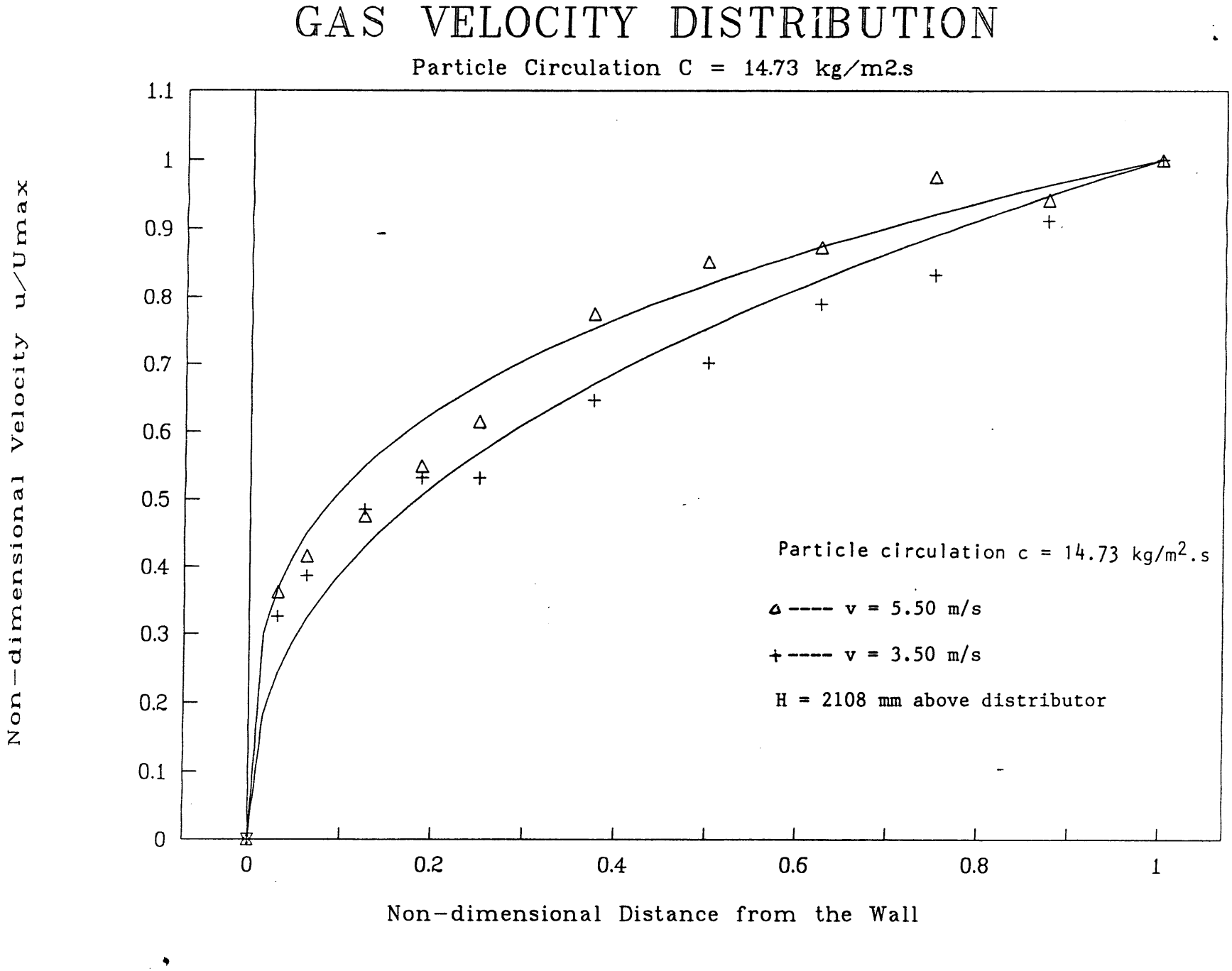

Figure 4.5 Gas velocity Profile

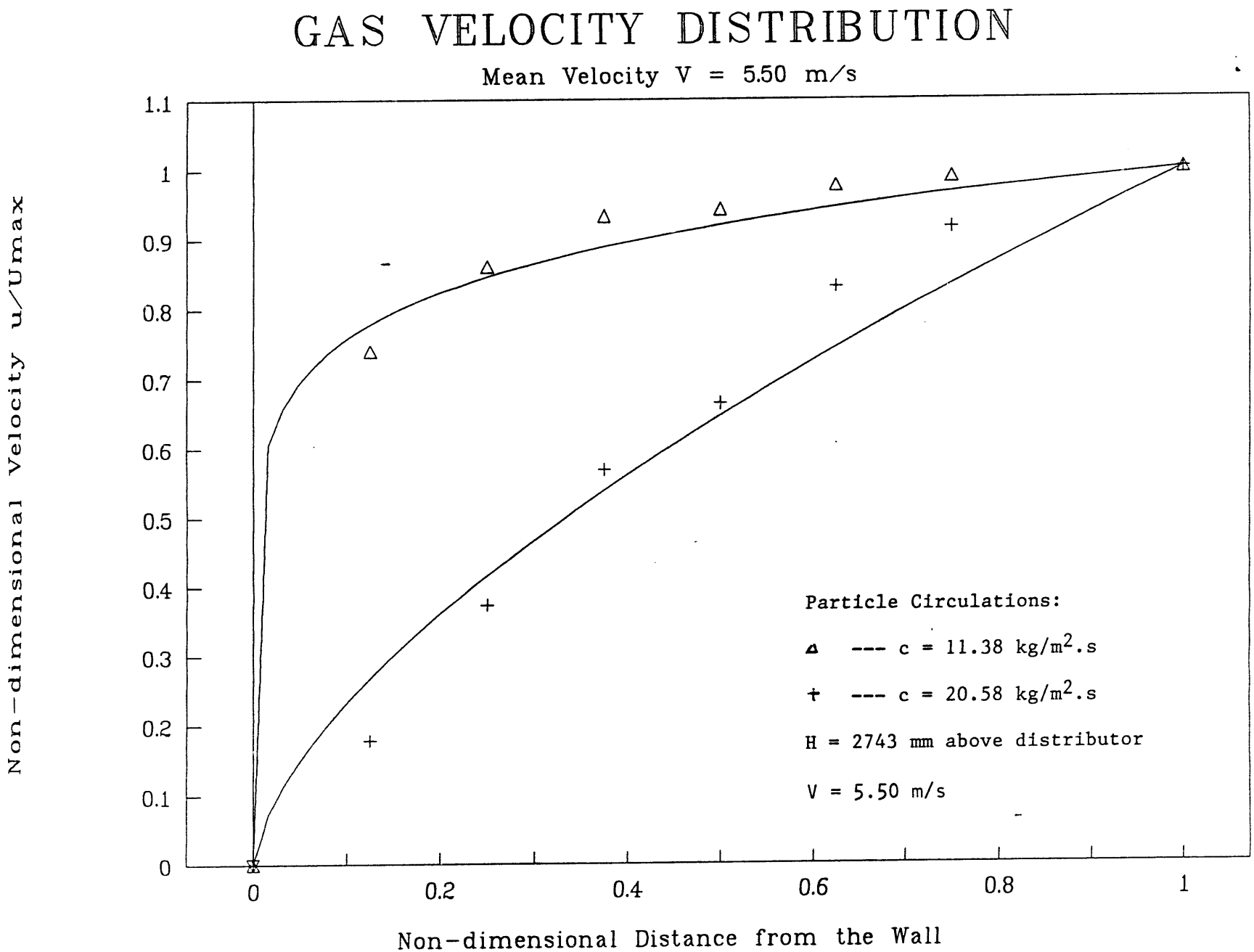

Figure 4.6 Gas velocity Profile

along the elevation of the circulating fluidized bed. This phenomena is apparent from the figures which show that the gas velocity profile in circulating fluidized bed becomes more blunt or "fuller" with the increasing mean gas velocity.

3. Variation of the Gas Velocity Profile with Solids Circulation Rates

In circulating fluidized bed, gas velocity profile is different from pure fluid turbulent flow. It is not only a function of the mean gas velocity but also a function of the solids circulation rate. A core-annular flow structure in circulating fluidized bed formed. The central core region is dominated by a dilute upflowing suspension of solids flowing at higher velocities. the annulus is occupied by a dense, downflowing solids suspension with relative lower velocities. The downflowing solids near the wall influence the gas velocity profile most. It makes the gas velocity profile sharper with increasing solids circulation rate. At a given mean gas velocity, the solids circulation rate determines the flow structure of the annulus flow, the higher the solids circulation rate is, the stronger the annulus flow is. A strong downflowing solids flow reduced the gas velocity very much near the wall of circulating fluidized bed. Figure 4.7, Figure 4.8 and Figure 4.9 show the experimental results of gas velocity profiles at different solids circulation rates. These figures indicated that the solids circulation rate in circulating fluidized bed play a key role on the gas velocity profile.

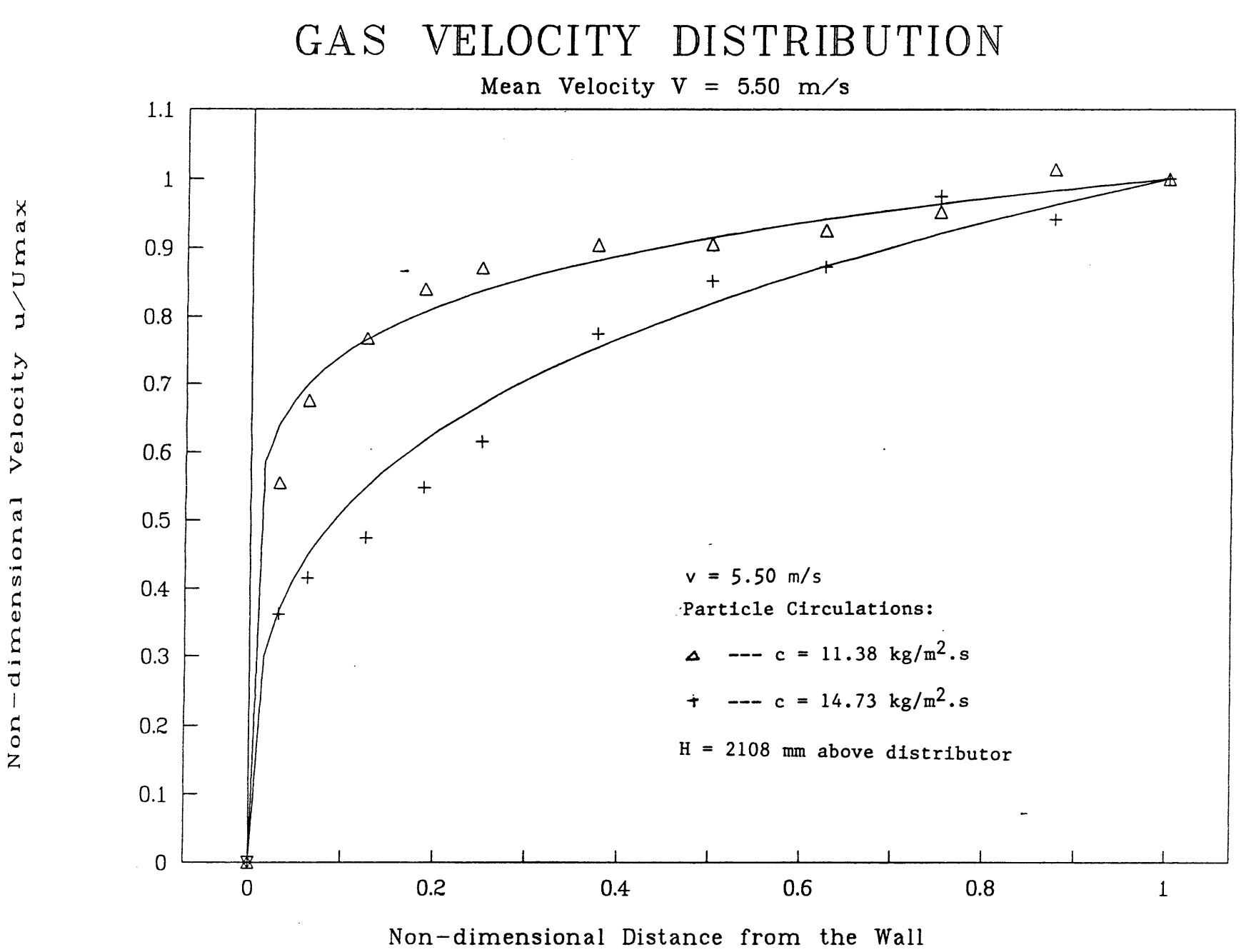

Figure 4.7 Gas velocity Profile

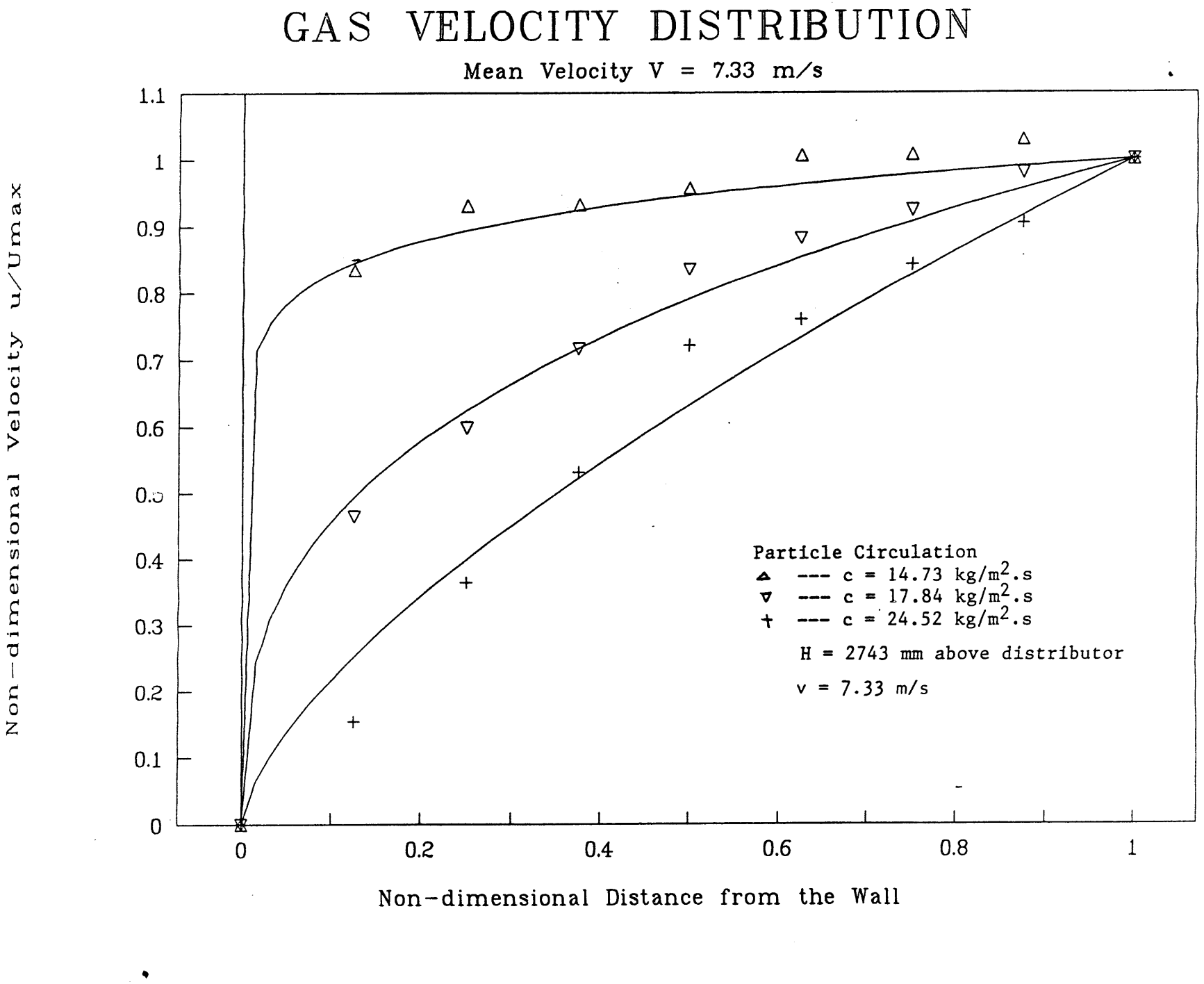

Figure 4.8 Gas velocity Profile

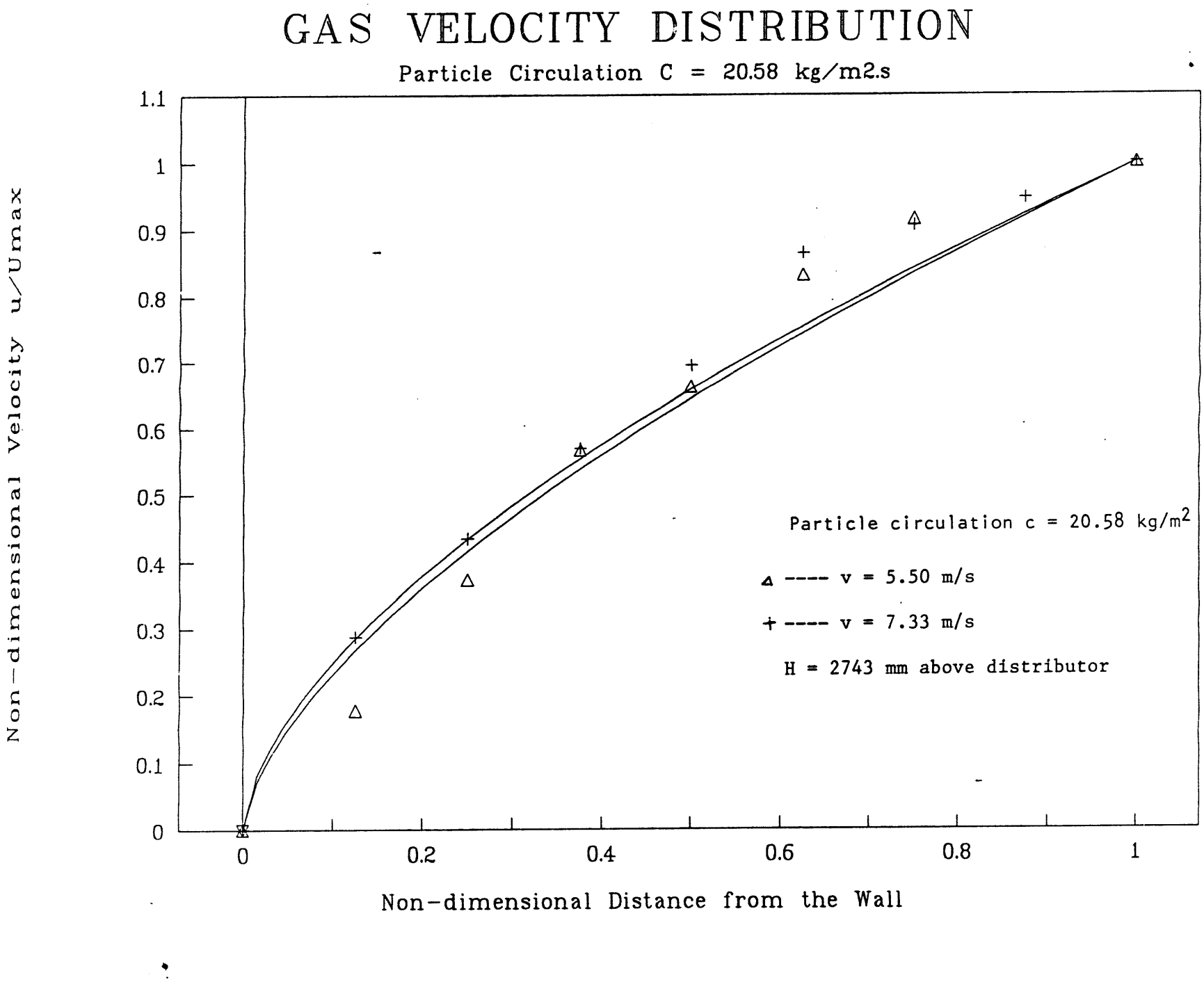

Figure 4.9 Gas velocity Profile

4. Variation of gas velocity profile along with elevation of the riser

The annulus flow in circulating fluidized bed varies along the elevation of the riser. Close to the wall of riser, a larger downflowing solids appear at a lower elevation, to compensate for the increased amount of solids down flow in the annulus near the wall a higher net upflowing solids through the central core region is required. For gas flow, The downflowing solids decrease the gas velocity in annulus region near the wall and gas velocity has to be increased to carry more solids at higher velocity in the central core region. But the elevation effect on the gas velocity profile was not as strong as solids circulation rate and the gas velocity did. Among them the elevation is the weakest factor effecting on the gas velocity profile in circulating fluidized bed. Fig.4.10 shows the measurements of the gas velocity profile at two different elevation, one was at 2108 mm above the distributor and another was 2743 mm above distributor. The solids circulation rate was the same, C = 11.38 $kg.m^{-2}.s^{-1}$, mean gas velocity was 5.5 m/s. From the Figure, the gas velocity profiles at 2743 mm above distributor is more blunt than at 2108 mm above distributor.

The gas velocity profile in circulating fluidized bed depends on the mean gas velocity, the solids circulation rate, the elevation above distributor, and the solids properties. From the experimental data, the power-law gas velocity profile may applied in circulating fluidized bed. The exponent, n, represents the shape of gas velocity profile. As exponent, n, increases, the gas

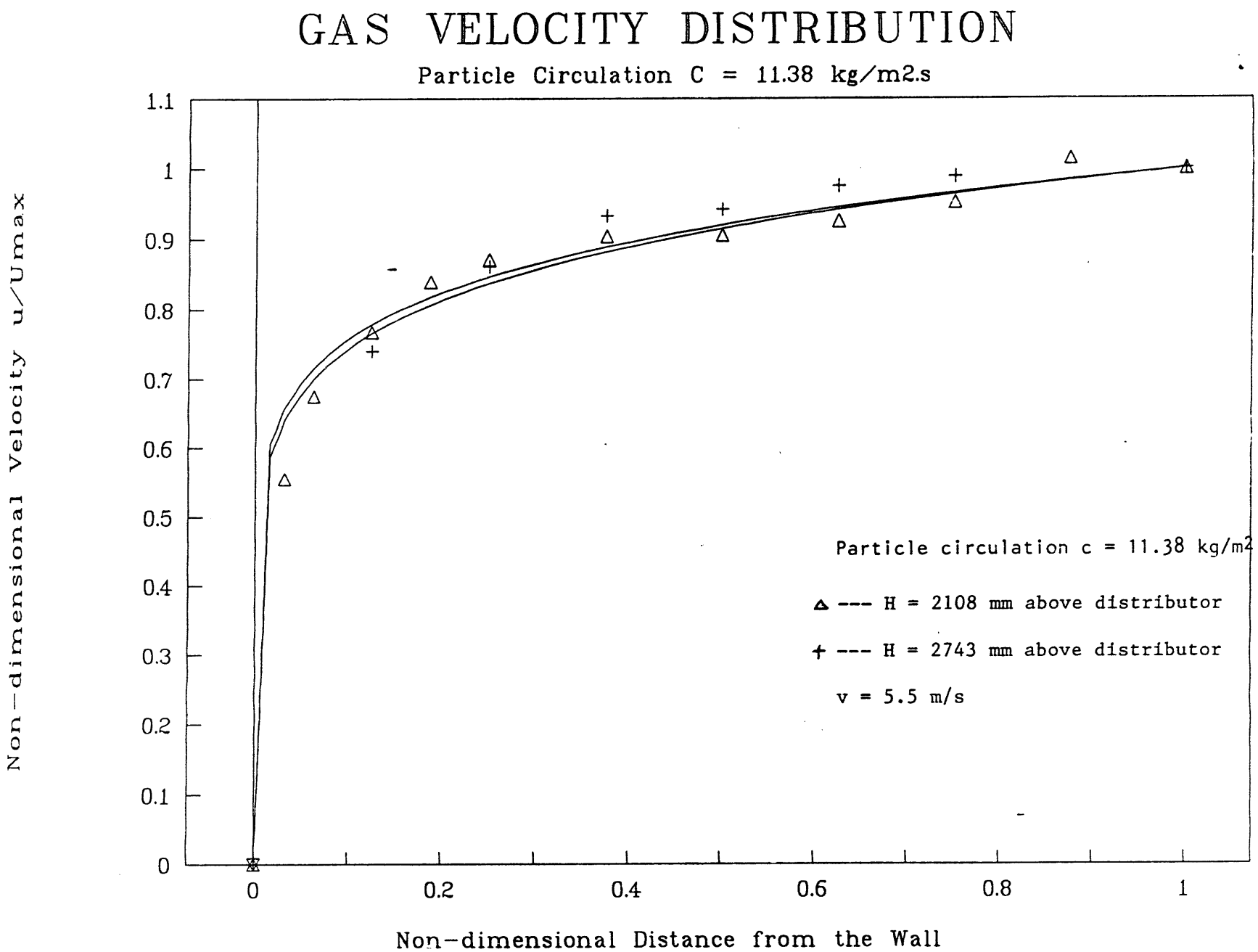

Figure 4.10 Gas velocity Profile
along with Elevation of Riser

velocity profile becomes fuller. Exponent, n, depends on mean gas velocity, solids circulation rates and elevation, solids properties. From experimental data, it is clear that the solids circulation is a key role affecting on the gas velocity profile. The gas velocity profile becomes sharper with a increasing solids circulation rate.

There is a relationship between exponent,n, and the operating parameters, solids properties. Using multivariate regression method, a equation for exponent,n, was obtained

$$n=0.804c^{-2.635}(h/H)^{0.748}Re^{0.742}$$

where h is the probe elevation above distributor, H is the total height of riser, c is the solids circulation rate and Re is Reynold's number based on circulating fluidized bed diameter and mean gas velocity.

Table 4.1 shows the data of experiments and the corresponding exponent, n.

The gas velocity profile is not only a function of Reynolds number, but also a function of solids circulation rate and the properties of the solids in circulating fluidized bed riser. The gas velocity in circulating fluidized bed riser also can be represented approximately by the power law profile. The exponent,n, is dependent on the operating parameters of the circulating fluidized bed, such like mean gas velocity, solids circulation rate and the solid properties. Gas velocity profile in circulating

Table 4.1. Experimental Data and Exponent n

Exp. No.	Exponent n	Mean gas velocity (m/s)	Solids Cir. Rate ($kg.m^{-2}.s^{-1}$)	Elevation (mm)	Diameter of Solids (μm)
1	4.07	3.5	11.38	2108	116
2	2.45	3.5	14.73	2108	116
3	7.77	5.5	11.38	2108	116
4	3.46	5.5	14.73	2108	116
5	1.58	5.5	20.58	2743	116
6	8.29	5.5	11.38	2743	116
7	11	7.33	14.73	2743	116
8	2.94	7.33	17.84	2743	116
9	1.26	7.33	24.52	2743	116

fluidized bed is different from that in pure fluid flow. The mean gas velocity in circulating fluidized bed is not as important as in pure fluid flow on the gas velocity profile. The solids circulation rate play a key role on the gas velocity profile. Gas velocity in the centerline in circulating fluidized bed is much higher than that in pure fluid flow at the same mean gas velocity. Oppositely, the velocity close to the wall in CFB is much less than that in pure fluid flow. The gas velocity profile appears in circulating fluidized bed sharper than that in pure fluid flow at the same Reynold's number.

4.3 Solids Flow through the L-Valve

As shown in the Figure 4.11 solids are being transferred downwards in a standpipe from pressure p_1 to higher pressure p_2. Solids velocities in this figure are denoted by the length of the thick-lined arrows, gas velocities by the length of the dashed arrows, and the relative velocity by the length of the thin-lined arrows. There are two kinds of flow pattern. In case one, Solids are flowing downwards and gas is flowing upwards relative to the standpipe wall. The relative velocity is directed upwards and is equal to the sum of the solids velocity and the gas velocity. In this paper the positive reference direction in determing v_r will be

$$u_r = u_s - (-u_g) = u_s + u_g \qquad (1)$$

For case two, solids are flowing down the standpipe and the gas is always flowing down the standpipe relative to the standpipe wall, but at a velocity less than that of the solids. The relative velocity is also directed upwards and equals to the difference between the solids velocity and the gas velocity

$$u_r = u_s - u_g$$

Gas flowing up relative to the solids causes a frictional pressure drop to be generated. The relationship between pressure drop and the relative velocity is determined by the fluidization curve.

In the standpipe system there are two forms of high bulk density flow, stick-slip flow and aerated flow as shown in Figure 4.12. In this system there are these two forms case (a),(b) and case (c). In case (a) since the solids are flowing upward they must be fluidized, therefore the relative velocity must be sufficient to keep the solids fluidized. The pressure drop in the pipe will slightly exceed the static head of the fluidized solids. If the relative velocity is less than the minimum fluidized velocity, case (b) and (c) will be the stick-slip flow. For stick-slip flow the pressure drop across the pipe given by Wen and Galli(1971).

$$\frac{\Delta P}{L} = \frac{150(1-\epsilon)^2 u_r}{d_v^2 \epsilon^2} + \frac{1.75(1-\epsilon)\rho_g u_r^2}{d_v \epsilon} + (1-\epsilon)(\rho_s - \rho_g)g + \frac{2\rho_g U_{fg}^2}{D} \quad (3)$$

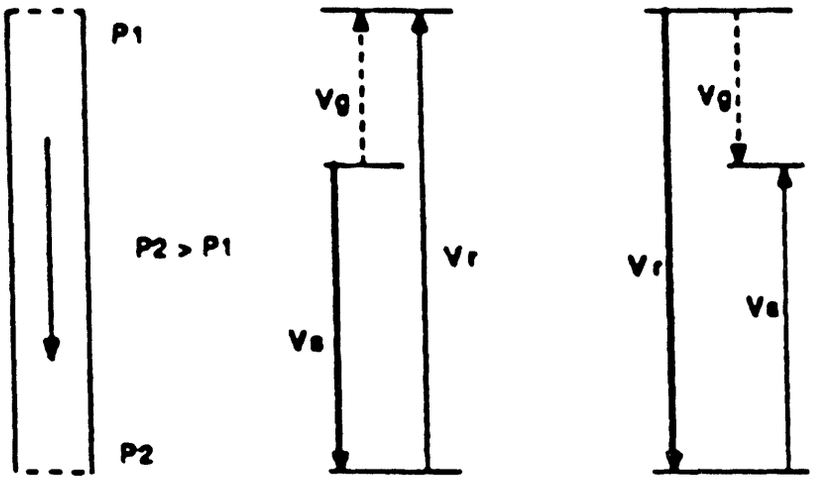

Figure 4.11 Schematic Representation of Gas Flow
Up and Down Relative to the Standpipe
Wall(Geldart,1986)

For case two, solids are flowing down the standpipe and the gas is always flowing down the standpipe relative to the standpipe wall, but at a velocity less than that of the solids. The relative velocity is also directed upwards and equals to the difference between the solids velocity and the gas velocity

$$u_r = u_s - u_g \qquad (2)$$

Gas flowing up relative to the solids causes a frictional pressure drop to be generated. The relationship between pressure drop and the relative velocity is determined by the fluidization curve.

In the standpipe system there are two forms of high bulk density flow, stick-slip flow and aerated flow as shown in Figure 4.12. In this system there are these two forms case (a),(b) and case (c). In case (a) since the solids are flowing upward they must be fluidized, therefore the relative velocity must be sufficient to keep the solids fluidized. The pressure drop in the pipe will slightly exceed the static head of the fluidized solids. If the relative velocity is less than the minimum fluidized velocity, case (b) and (c) will be the stick-slip flow. For stick-slip flow the pressure drop across the pipe given by Wen and Galli(1971).

$$\frac{\Delta P}{L} = \frac{150(1-\epsilon)^2 u_r}{d_v^2 \epsilon^2} + \frac{1.75(1-\epsilon)\rho_g u_r^2}{d_v \epsilon} + (1-\epsilon)(\rho_s - \rho_g) g + \frac{2\rho_g U^2 f_g}{D} \qquad (3)$$

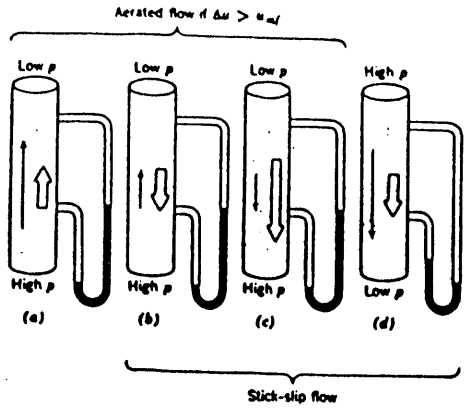

Figure 4.12 Types of Flow Relative Velocity, and Pressure Gradient in Flowing Gas-solids Mixture with High Bulk Density of Solids (Kunii & Levenspiel, 1962)

The first two terms are the pressure drop due to gas-solids friction, the third term is the pressure drop for the gas to support the solids and the fourth is the gas-wall friction loss. For aerated flow, the pressure drop is given by two terms, the static pressure term and the frictional loss term. In case (a) the pressure drop is

$$p_2-p_1=\rho_s(1-\epsilon)(h_1-h_2)g+\rho_g\epsilon(h_1-h_2)g-\Delta p_{fric}$$

In case (b) and (c) the pressure drop is

$$p_2-p_1=\rho_s(1-\epsilon)(h_1-h_2)g+\rho_g\epsilon(h_1-h_2)g+\Delta p_{fric}$$

In any gas-solids flow system a pressure drop "loop" can be defined such that the sum of the pressure drops around the loop will be zero. In any such loop in which a standpipe is a component, the standpipe is usually the dependent part of the loop. That means that the pressure drop across the standpipe will automatically adjust to balance the pressure drop produced by the other pressure drop components in the loop. How is pressure drop adjustment made in the this standpipe?

Figure 3.14 shows the schematic of the L-valve system. The

solids are transferred from the hopper to the riser of the circulating fluidized bed against the pressure difference $p_2 - p_1$. This pressure differential composed of the pressure drop from hopper to the bending of the L-valve P and from point P to the riser of circulating fluidized bed.

$$P_1 - P_2 = (P_1-P_P) + (P_P-P_2)$$

P_1 is the pressure of the hopper, and the P_2 is the pressure in the riser of CFB at the outlet of L-valve. For each term of the right side of above equation, it can be decided by using appropriate method. Before analyzing the pressure drop it is important to realize the flow pattern of solids and gas mixture in each path of the standpipe.

From Figure 4.12, it is impossible that the vertical section of the L-valve operates in the case (a), case (c) and case (d). Vertical section should operate in case (b), The solids are going down while the gas is going up. And it may operate in the stick-slip flow or in the aerated flow dependent on the loop pressure balance.

Horizontal flow is possible only with suspended or fluidized solids, and then only for velocities such that the frictional loss just balances the pressure drop. At a relatively low solids flow rate, all of the solids flowed in a rather narrow region near the top of the pipe. Small ripples seem to travel along the top of the thin solids layer and the lower portion of the solids appears to be

practically stationary. At higher solids velocities, the moving layer of solids increases as the solids velocity increases. When the solids velocity reaches a given value, solids flow appears fluidized state with uniform voidage in whole pipe.

The correlation of Wen and Simmons (19) based on experimental work with narrow cuts of solids from 71 to 755 μm flowing with solids gas ratios of 80 to 780 in horizontal pipe 12.4 and 25.4 mm in diameter interrelated the variables for this kind flow. The velocity of solids is related to that of the gas by the approximate relationship

$$u_0 \approx 2 u_s \tag{7}$$

and the frictional loss $\Delta p_{friction}$ is related to the velocity of solids by

$$\left(\frac{\Delta p_f}{l\rho g}\right)\left(\frac{d_t}{d_p}\right)^{0.25} = 0.537 u_s^{0.45} \tag{8}$$

where Δp_f is the pressure drop across the horizontal pipe, the l is the length of the pipe, ρ is the mean density of the solids, d_t is the diameter of the pipe, d_p is the mean diameter of solids and u_s is the velocity of the solids.

In vertical section of L-valve, the relative velocity is not big enough to reach turbulent flow and only first term on the right

side of equation is kept. The pressure drop in vertical section is

$$p_p - p_1 = \rho_s (1-\epsilon) g L \tag{9}$$

Combining the above two equations:

$$G_s = \rho A u_s = 3.98 A \left(\frac{-(p_2 - p_1) + \rho_s (1-\epsilon) g L}{lg} \right)^{\left(\frac{1}{0.45}\right)} \rho^{(-1.22)} \left(\frac{d_t}{d_p} \right)^{\left(\frac{5}{9}\right)} \tag{10}$$

In a given circulating fluidized bed, p_1 and p_2 are constants and the height and the length of the L-valve are given. There are only four variables. They are the voidage of the vertical section of L-valve, ϵ, the diameter of horizontal section of L-valve, d_t, the mean diameter of solids, d_p, and the mean density of solids in horizontal section of L-valve, ρ. u_s is solids velocity in horizontal section of L-valve. A is the area of the horizontal section of L-valve and the G_s is the mass flowrate

The effects of valve geometry and particle diameters on the performance of the L-valve were investigated. The specific effect of each parameter is discussed individually.

1. <u>The Solids Flowrate Versus Aeration</u>

The test results of aeration on solids flowrate are depicted

in Figure 4.13. Increasing aeration results in an increase in the voidage, ϵ in the vertical section of L-valve and decreasing mean density, ρ in horizontal section of L-valve. Using the following equation

$$G_s=\rho A u_s=3.98A\left(\frac{-(p_2-p_1)+\rho_s(1-\epsilon)gL}{lg}\right)^{\left(\frac{1}{0.45}\right)}\rho^{(-1.22)}\left(\frac{d_t}{d_p}\right)^{\left(\frac{5}{9}\right)} \qquad (10)$$

increasing voidage, ϵ, in vertical section of L-valve will result in decreasing the term, $\rho_s(1-\epsilon)gL$. Hence, the solids velocity is inversely proportional to aeration. When aeration gas flow increases, the mean density of solids in the horizontal section will be reduced because more gas is passed through the horizontal section. This results in an increase in the solids velocity in the horizontal section of L-valve.

When aeration gas is added to the L-valve, solids do not begin to flow till a certain threshold amount of aeration flow is introduced. However, after the threshold aeration is reached, additional gas added to L-valve causes the solids flowrate to increase. However, there is a limiting point in the solids flowrate versus gas flowrate curve for L-valve. The solids flowrate increases as the gas flowrate increases beyond the threshold point. If the gas flowrate increases further the solids flowrate will reach a maximum point and then begin to decrease as shown in Figure 4.13. The solids flowrate passing through vertical section of L-valve is dependent on the area of the pipe, the velocity of the

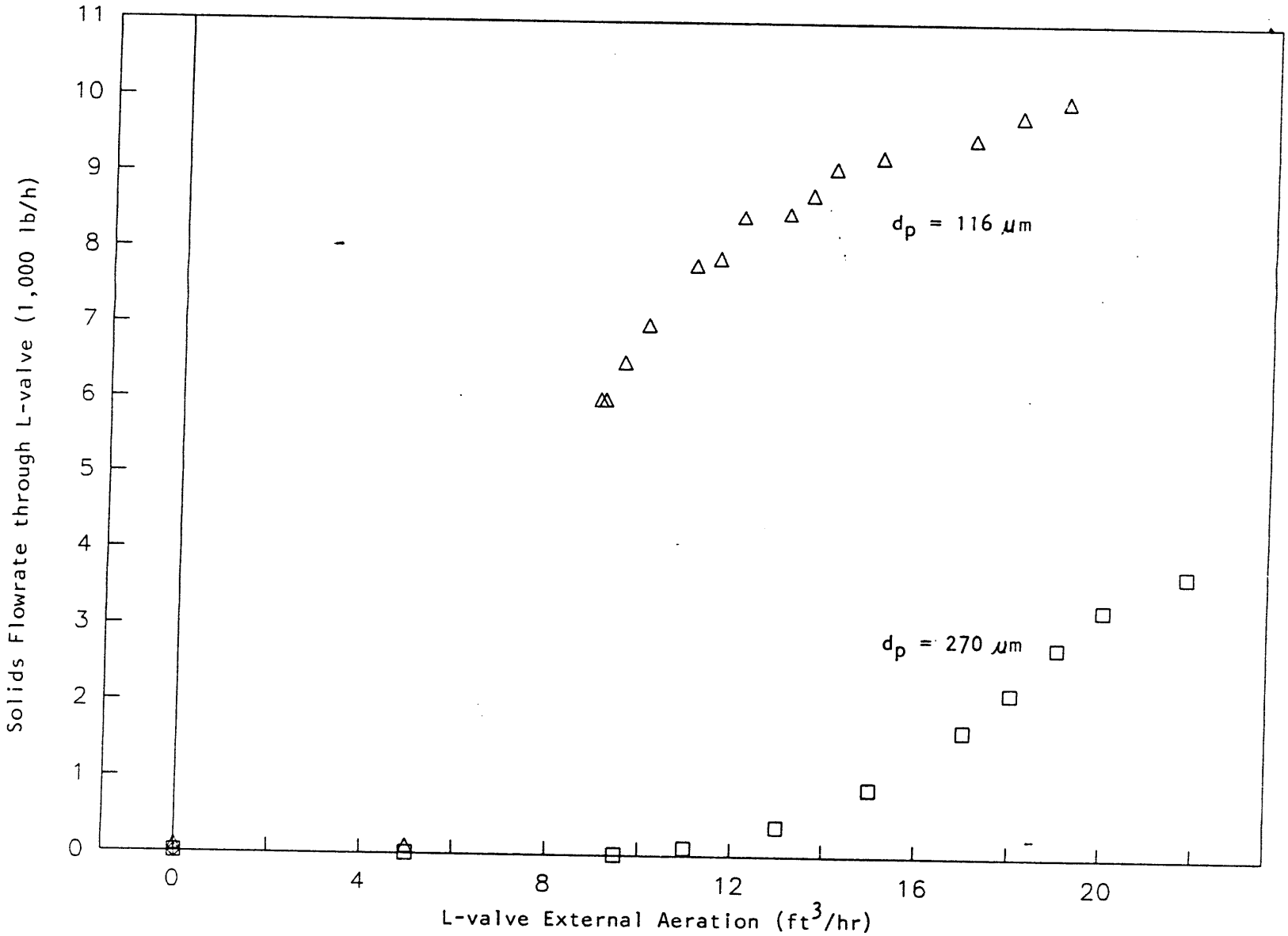

Figure 4.13a Solid Flowrate versus Aeration Rate with Different Solids Using Smaller L-valve

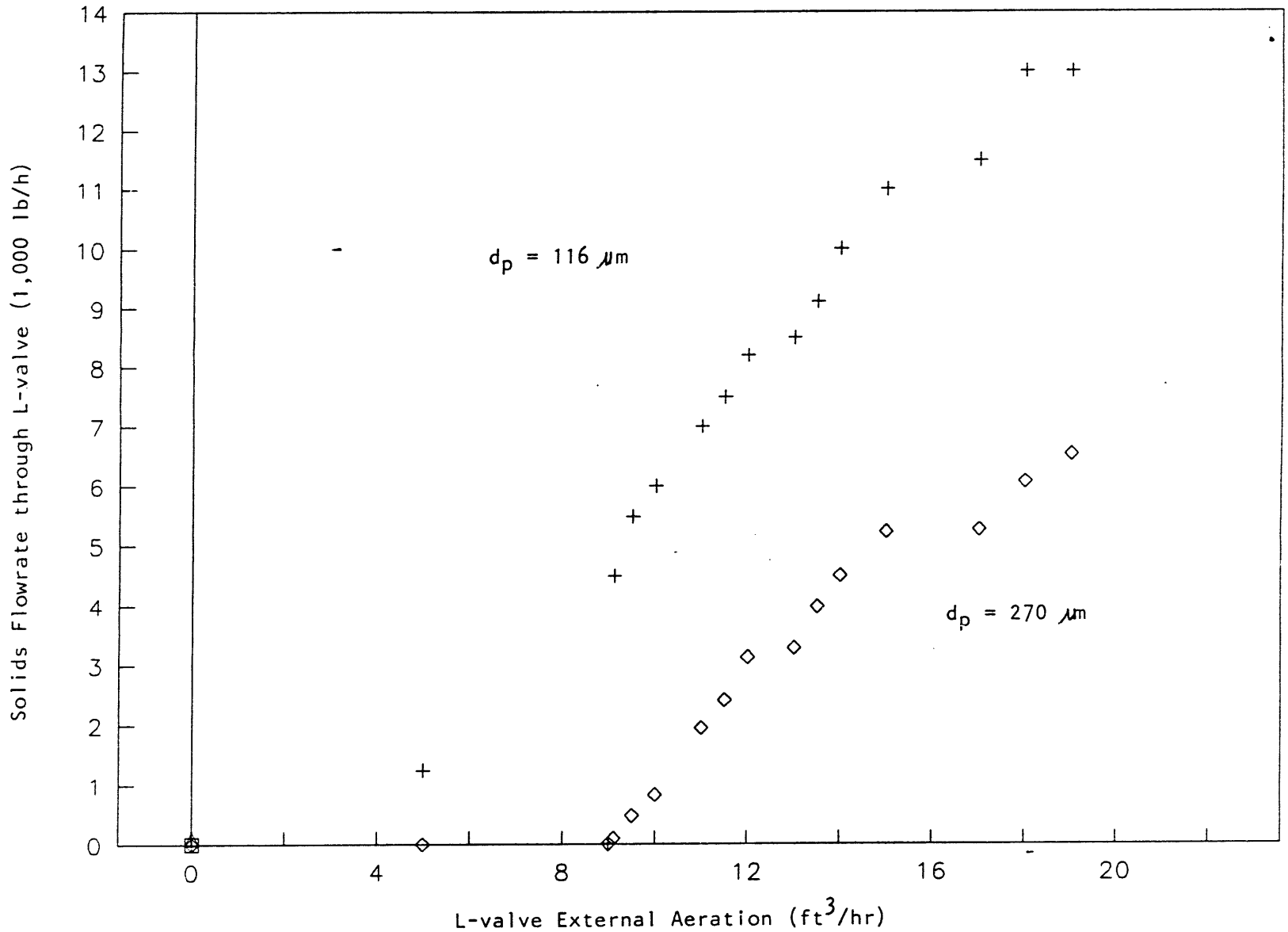

Figure 4.13b Solid Flowrate versus Aeration Rate with Different Solids Using Bigger L-valve

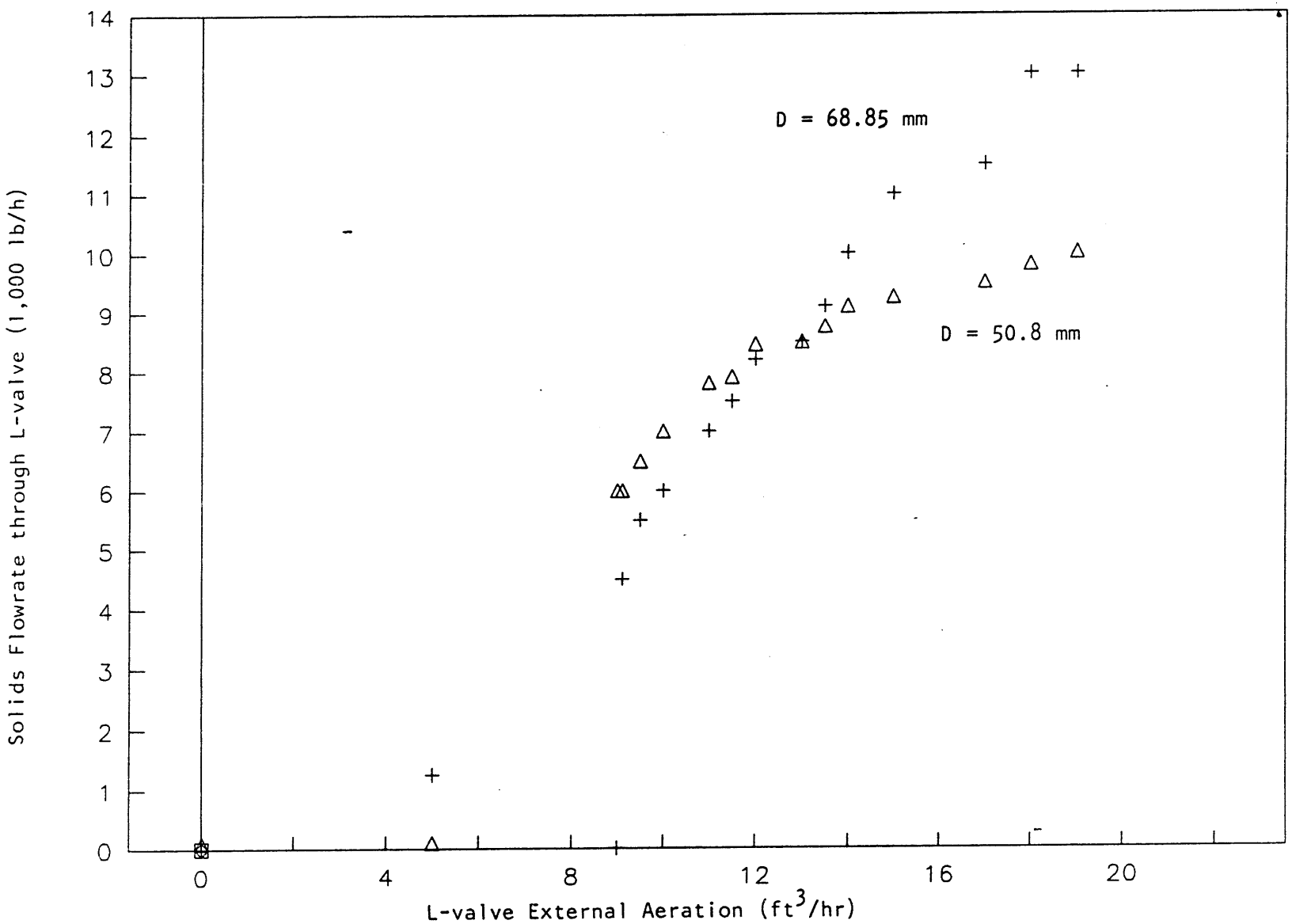

Figure 4.13c Solid Flowrate versus Aeration Rate with Different L-valve Using Smaller Solids

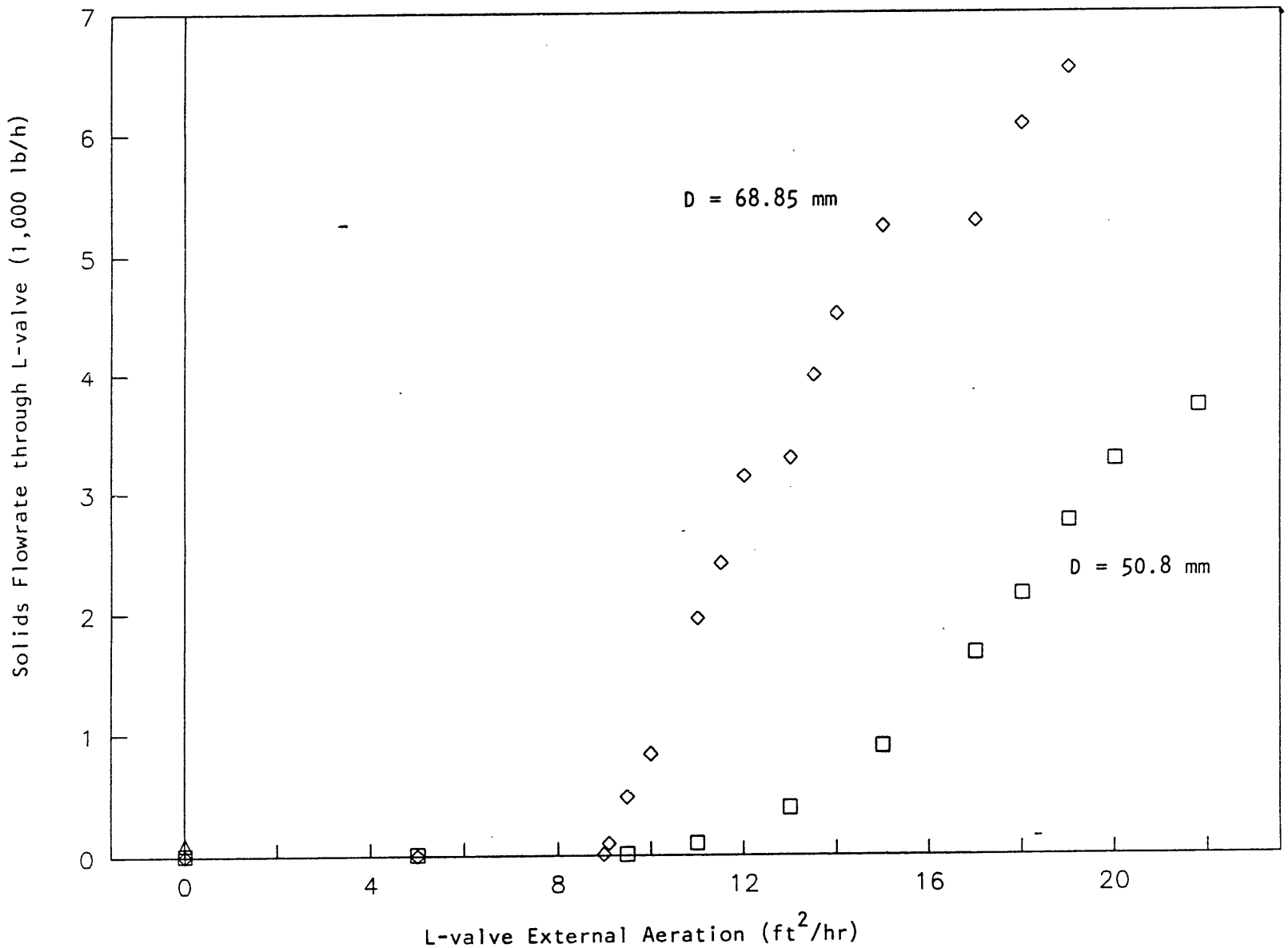

Figure 4.13d Solid Flowrate versus Aeration Rate
with Different L-valve Using Bigger Solids

solids and mean solids density of horizontal section of L-valve. For a given area A, the flowrate of solids is reverse proportional to voidage of vertical section of L-valve and proportional to mean solids density in vertical section of L-valve. Therefore, when the effect of the voidage on the solids flowrate is more dominating than the effect of mean density of solids in the horizontal section of L-valve on the solids flowrate the solids flowrate will decrease as the gas velocity increases. The point at which gas flowrate corresponds to the maximum solids flowrate point is known as the critical point of gas flowrate. On other hand, the gas velocity in the vertical section of L-valve increases up to a point and an increase in the relative velocity between the solids and the gas will reduce the flowrate of the solids moving downwards.

2. The Effect of L-valve Diameter on Solids Flowrate

The effect of L-valve diameter on solids flowrate and L-valve pressure drop was examined. Two L-valve diameters (50.8 mm and 69.8 mm) were studied. The particles used in this test had a mean diameter of 116 μm and 270 μm . A run was made at each combination of L-valve diameter and solids diameter.

A typical plot of L-valve aeration rate (Q_A) versus solids flowrate through L-valve for different L-valve diameter is shown in Figure 4.13c and Figure 4.13d. For both the L-valve diameters tested, solids did not begin to move until an L-valve aeration rate of approximately 4.5 ft^3/hr. The efficiency of the valve increased with increasing diameter. The bigger diameter L-valve can transport more solids at the same aeration rate all the way.

The L-valve pressure drop was also analyzed as a function of diameter of L-valve. The pressure drop of across the L-valve (for different L-valve diameters) against mass flowrate is shown in Figure 4.14. The pressure drop across standpipe (for different L-valve diameters) versus mass flowrate is plotted in Figure 4.15.

Figure 4.14 shows that the pressure drop across the L-valve decreases with increasing L-valve diameter, as expected. Figure 4.15 indicates that the pressure drop across standpipe decreases with increasing diameter of standpipe.

3. The Effect of Particle Size on L-valve

The effect of particle diameter on solids flowrate and L-valve pressure drop was studied. Two particle diameters (116 μm and 270 μm) were studied. The diameters of L-valves used in this test are 50.8 and 68.85 mm.

A typical plot of L-valve aeration rate (Q_A) versus solids flowrate through L-valve for different solids diameter is shown in Figure 4.13a and Figure 4.13b. For all the particle sizes that were studied solids did not flow until a certain threshold value of L-valve aeration rate was reached. For bigger diameter particles, a bigger aeration rate is needed to initiate the solids movement. At a given aeration rate smaller particles move more efficiently in the L-valve. L-valve pressure drop was also investigated as a function of solids diameter. The pressure drop across the L-valve for different particle diameters against mass flowrate is shown in Figure 4.16. The pressure drop across the standpipe (for different solids diameters) versus mass flowrate is shown in Figure 4.17.

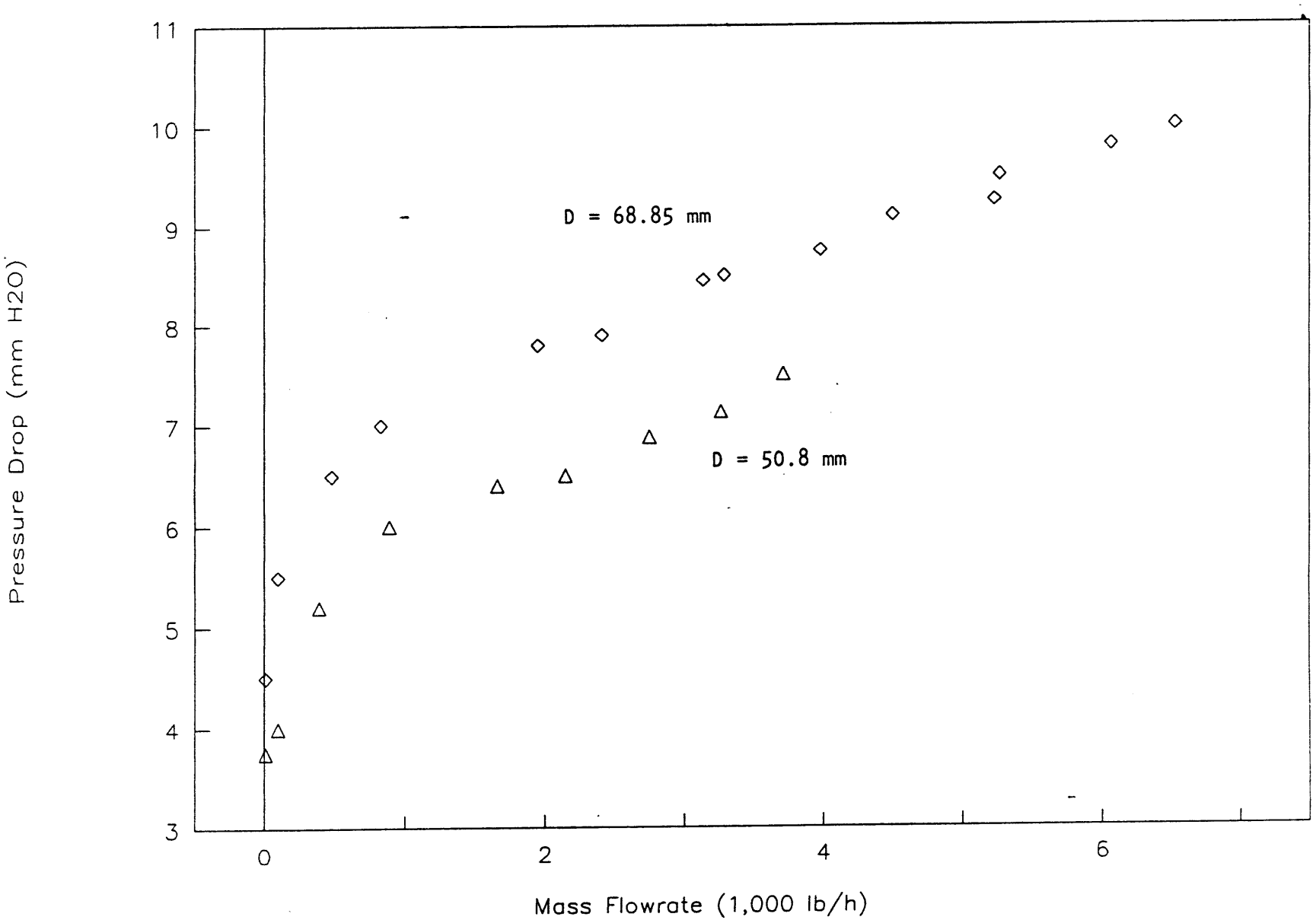

Figure 4.14 Pressure Drop of L-valve versus Aeration Rate at Different Diameter of L-valve

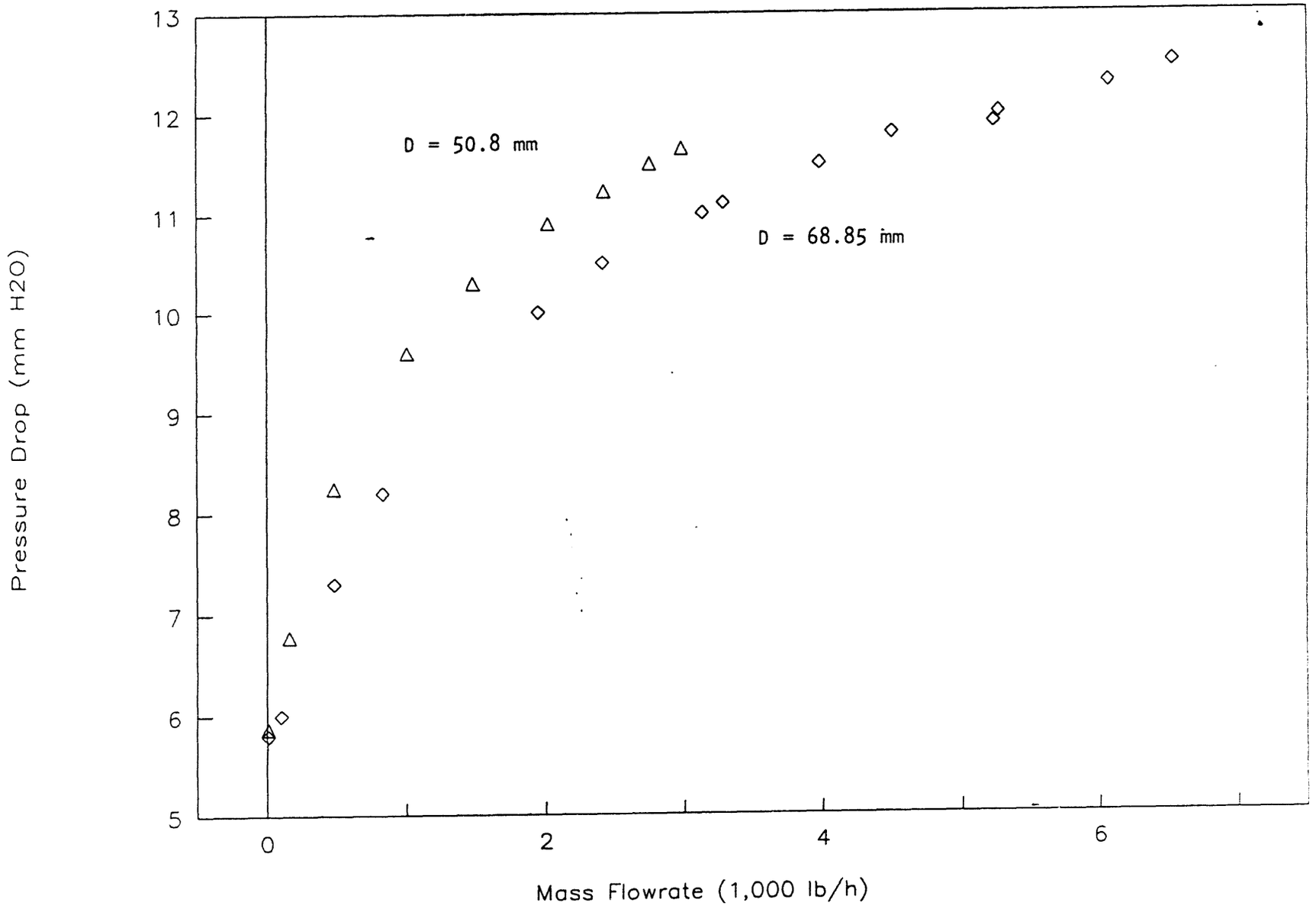

Figure 4.15 Pressure Drop across Standpipe versus Aeration Rate at Different Diameter of L-valve

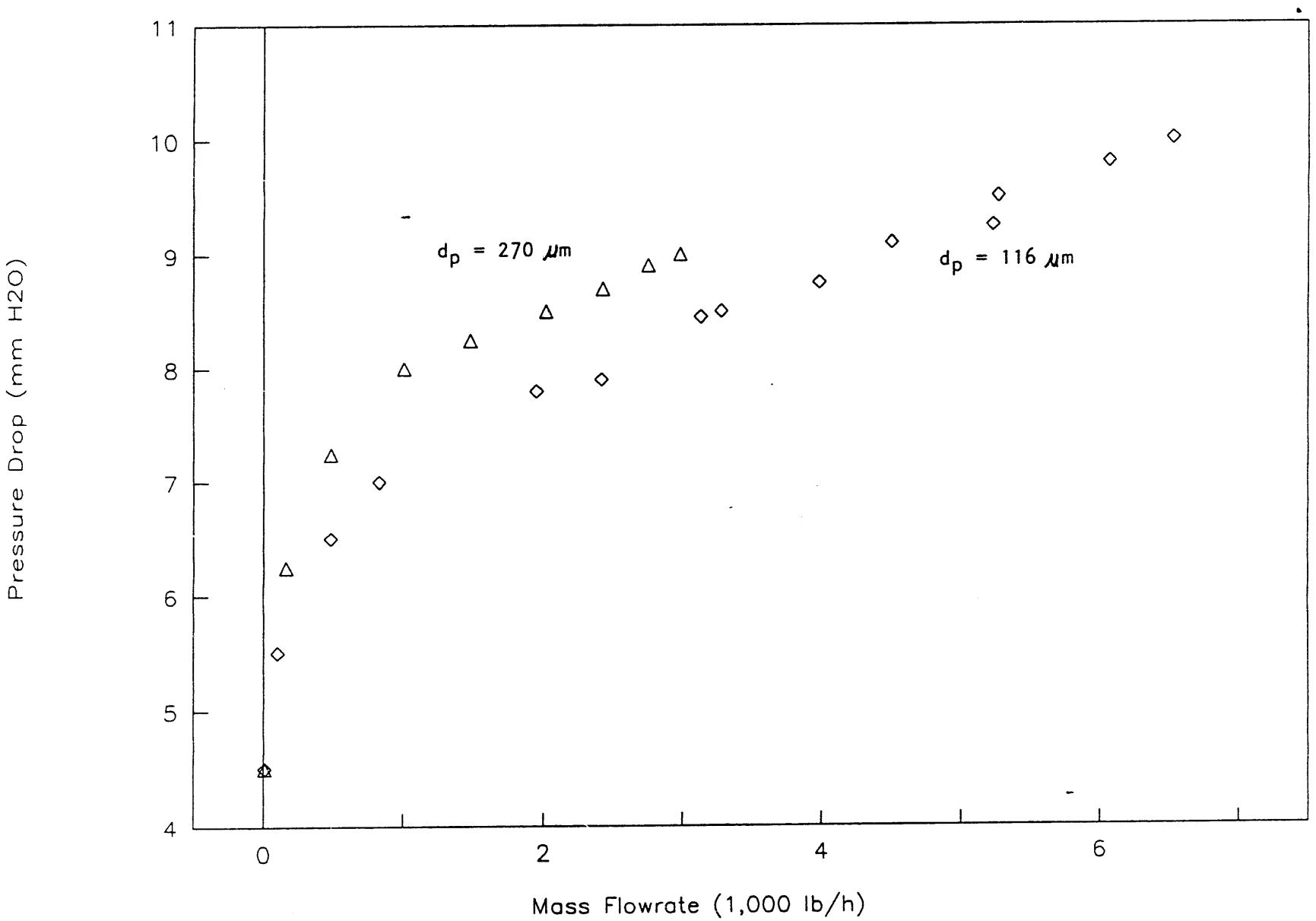

Figure 4.16 Pressure Drop of L-valve versus Aeration Rate at Different Solids Diameter

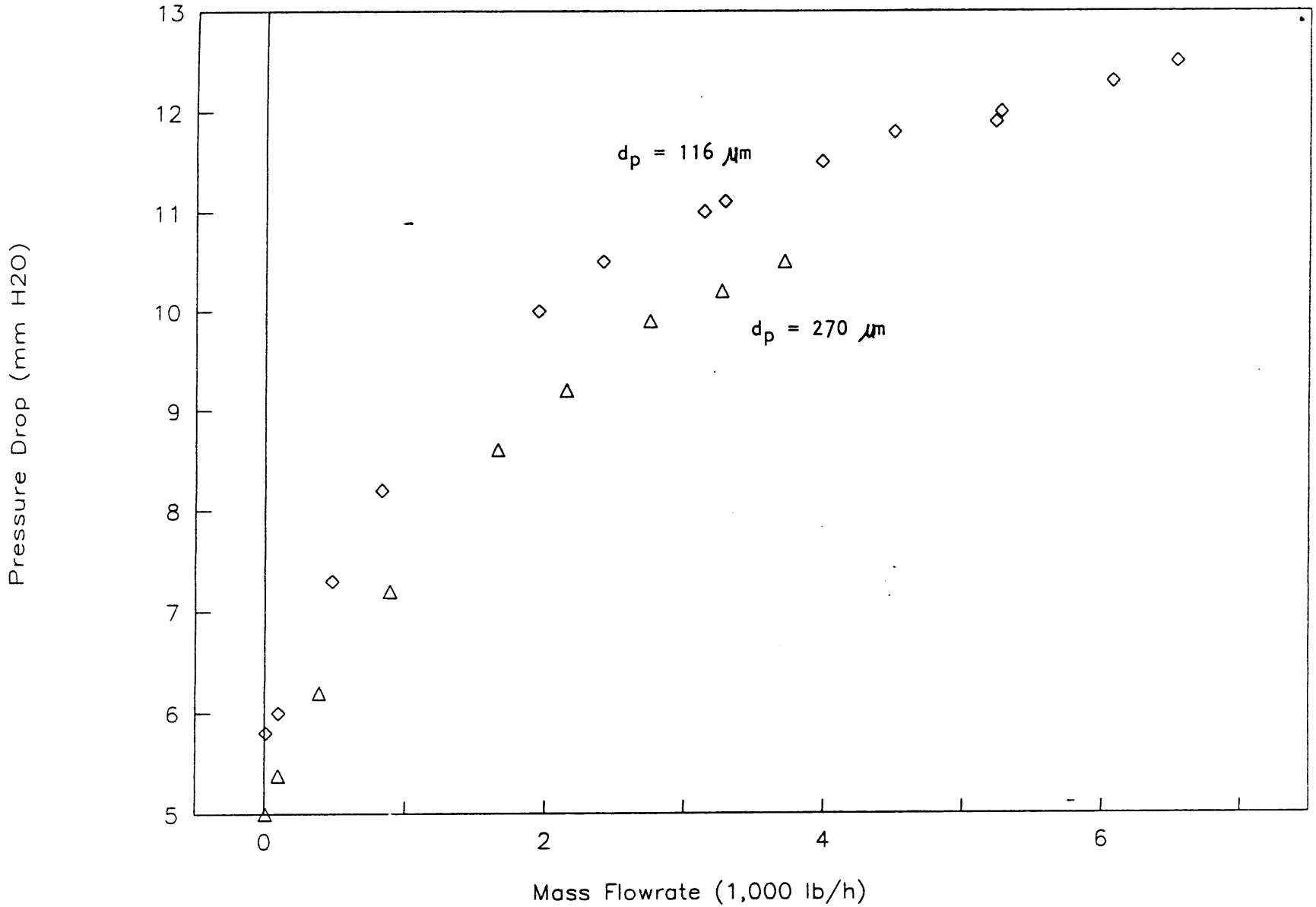

Figure 4.17 Pressure Drop across Standpipe versus Aeration Rate at Different Solids Diameter

Figure 4.16 shows that the pressure drop of L-valve is proportional to the particle diameter. Figure 4.17 suggests that the pressure drop across standpipe decreases with increasing diameter of solids.

In conclusion:

1. The solids flowrate is a function of L-valve geometrical parameters, operating parameter and solids properties.

2. Solids flowrate increases with increasing aeration rate after a value at which solids begin to move.

3. Pressure drop of L-valve increases with increasing solids diameter and decreasing diameter of L-valve.

4. Pressure drop across standpipe increases as the solids diameter and diameter of standpipe decrease.

APPENDIX

This assembly language (PDP-11 MAC) subroutine brings in data from the counter processor.

```
        DRVIN    = 167774
        DRVOUT   = 167772
        ZERO     =      0
        CLDRF    =     40
        GOVAL    =     34
        GOVAL1   =     74
        GOVAL01  =     35
       ;GOVAL03  =     37

LDAFQ::  MOV  #ZERO, @#DRVOUT
         MOV  #CLDRF,@#DRVOUT          ; CLEAR DATA READY FLOP
         MOV  #ZERO, @#DRVOUT

         MOV  (R5)+,R0                 ; GET NUMBER OF ARGUMENTS IN
                                       ; R0

         MOV @(R5)+,R1                 ; GET COUNT,N , IN R1
         MOV  (R5)+,R2                ; GET ADR OF THE FIRST ELEMENT
                                       ; OF ARRAY

                                       ; INTO R2
         MOV  (R5) ,R3                ; GET ADR OF FIRST ELEMENT OF
                                       ; 2ND ARRAY

         MOV #GOVAL,@#DRVOUT          ; ARM LDA COUNTER, SET S1 AND
                                       ; S0, AND
                                       ; MUX ADR TO ZERO

                                       ; VALIDATION ROUTINE
   1$:   MOV @#DRVIN,R4               ; GET LDA DATA INTO R3. BRANCH
         BMI  1$                       ; BACK IF BIT 15 IS SET
         MOV R4, (R2)+                 ; STORE LDA DATA BY R2 AND
                                       ; INCREMENT

                                       ; IF GOVAL01 IS DESABLE, TIME
                                       ; INTERVAL
                                       ; WON'T BE SOTRE
         MOV #GOVAL01,@#DRVOUT         ; SET MUX TO 01 (TIME
                                       ; INTERVAL)
         ;MOV #GOVAL03,@#DRVOUT        ; SET MUX TO 03 (NUMBER OF
                                       ; FRINGES)
         MOV @#DRVIN,(R3)+             ; STORE TIME INTERVAL OR
                                       ; NUMBER OF
                                       ; FRINGES IN R3

         MOV #GOVAL1,@#DRVOUT          ; TOGGLE BIT 5 TO CLEAR THE
                                       ; DATA
         MOV #GOVAL, @#DRVOUT          ; READY FLOP
         DEC R1                        ; DECREMENT THE NUMBER OF
                                       ; SAMPLES
```

```
BNE   1$                        ; BRANCH BACK IF MORE DATA

MOV #ZERO,@#DRVOUT             ; DISARM LDA COUNTER AND CLEAR
                                ; ALL
                                ; OUTPUT BITS

RTS PC

.END
```

This FORTRAN program calculates the statistically reduces the raw data by eliminating all data above or below +/- two standard deviations from the mean. Data is run through the elimination loops three times.

```
C PROGRAM TO ELIMINATE DATA NOT WITHIN THE RANGE OF 2 STANDARD
DEVIATIONS
C THIS PROGRAM WILL RUN THROUGH THIS CALC. TWICE AND STORE DATA IN
FILE\
C TKELLY.DAT
c23456789
      DIMENSION NO(1000),FD(1000),FREQ(1000),VEL(1000),VEL1(1000)
C ASSIGN THE OLD DATA FILE
       TYPE *, 'ENTER THE OUTPUT FILE NAME (OLD DATA FILE)'
       READ(7,100) RESEAR
       OPEN(UNIT=9,NAME=RESEAR,TYPE='OLD')
C ASSIGN THE NEW DATA FILE
100    FORMAT(A10)
       TYPE *, 'ENTER THE INPUT FILE NAME (NEW DATA FILE)'
       READ(7,100) OUTPUT
       OPEN(UNIT=8,NAME=OUTPUT,TYPE='NEW')
C ENTER THE NUMBER OF DATA POINTS
       WRITE(7,*)'ENTER NUMBER OF DATA POINTS'
       READ(7,*)N
       VELSUM=0.0
       SQMN=0.0
C READ DATA FROM FILE AND SUM VELOCITY
       DO 10 I=1,N
      READ(9,1000)NO(I),FD(I),VEL(I)
         VELSUM=VEL(I)+VELSUM
10     CONTINUE
C CALCULATE MEAN VELOCITY
       AVG=VELSUM/FLOAT(N)
       WRITE(7,11) AVG
11     FORMAT(1X,'AVG.VEL.1 IS',1X,E12.4)
C TAKE DIFFERENCE OF VEL(I) AND MEAN, SQUARE DIFFERENCE, SUM RESULT
       DO 20 I=I,N
      SQMN=((VEL(I)-AVG)**2)+SQMN
20     CONTINUE
C CALCULATE STANDARD DEVIATION
       STDDEV=(SQMN/(FLOAT(N)-1))**0.5
       WRITE(7,21) STDDEV
21     FORMAT(1X,'ST.DEV.1 IS ',E12.4)
C CALCULATE LIMITS OF +/- 2*STANDARD DEVIATION
       HIGH=AVG+2*STDDEV
       SLOW=AVG-2*STDDEV
       WRITE(7,22) HIGH
       WRITE(7,24) SLOW
22     FORMAT(1X,'HIGH.1 IS ',E12.4)
24     FORMAT(1X,'LOW.1 IS ',E12.4)
       J=0
       VELSUM=0.0
C ELIMINATE DATA ABOVE AND BELOW AVE +/- 2*STDDEV, STORE REST IN
```

```
NEW ARRAY
      DO 30 I=1,N
     IF (VEL(I) .LE. HIGH .AND. VEL(I) .GE.SLOW) GO TO 25
          GO TO 30
25     J=J+1
       FREQ(J)=FD(I)
       VEL1(J)=VEL(I)
          VELSUM=VEL1(J)+VELSUM
C          WRITE(8,1000) J, FREQ(I), VEL1(I)
30    CONTINUE
C CALCULATE NEW MEAN
      AVG=VELSUM/FLOAT(J)
      WRITE(7,42) J
      WRITE(7,41) AVG
41    FORMAT(1X,'AVG.VEL.2 IS ',E12.4)
42    FORMAT(1X,'N.2 IS ',I3)
      SQMN=0.0
      L=J
C CALCULATE NEW STANDARD DEVIATION
      DO 50 J=1,L
     SQMN=((VEL1(J)-AVG)**2)+SQMN
50    CONTINUE
      STDDEV=(SQMN/(FLOAT(L)-1))**0.5
      WRITE(7,51) STDDEV
51    FORMAT(1X,'STD.DEV.2 IS ',E12.4)
C CALCULATE NEW LIMITS
      HIGH=AVG+2*STDDEV
      WRITE(7,52) HIGH
52    FORMAT(1X,'HIGH.2 IS ',E12.4)
      SLOW=AVG-2*STDDEV
      WRITE(7,53) SLOW
53    FORMAT(1X,'LOW.2 IS ',E12.4)
      K=0
      VELSUM=0.0
C ELIMINATE DATA OUTSIDE LIMITS AND STORE REST IN NEW DATA FILE
      DO 60 J=1,L
     IF (VEL1(J) .LE. HIGH .AND. VEL1(J) .GE. SLOW) GO TO 55
          GO TO 60
55     K=K+1
       WRITE(8,1000) K, FREQ(J), VEL1(J)
          VELSUM=VEL1(J)+VELSUM
60    CONTINUE
      WRITE(7,64) K
      AVG=VELSUM/FLOAT(K)
      WRITE(7,65) AVG
64    FORMAT(1X,'N.3 IS ',I3)
65    FORMAT(1X,'THE FINAL AVERAGE IS ',E12.4)
1000  FORMAT(1X,I3,4X,E12.4,4X,E12.4)
      CLOSE(UNIT=8)
      CLOSE(UNIT=9)
      STOP
      END
```

This FORTRAN program sorts the statistically reduced data in ascending order, counts the frequency of occurance of the velocity data and prepares the data for use in the SAS program to produce velocity histograms.

```
c23456789
      DIMENSION N(1000), F(1000), V(1000),V1(1000),T(1000)
      LOGICAL DONE, FINI
      WRITE(5,10)
10    FORMAT(1X,'ENTER THE NAME OF THE FILE TO BE SORTED')
      READ(5,12) RESEAR
12    FORMAT(A10)
      OPEN(UNIT=15,FILE=RESEAR,STATUS='OLD')
      WRITE(5,15)
15    FORMAT(1X,'ENTER THE NAME OF THE NEW FILE')
      READ(5,16) SFILE
16    FORMAT(A10)
      OPEN(UNIT=14,FILE=SFILE,STATUS='NEW')
      WRITE(5,18)
18    FORMAT(1X,'ENTER THE NUMBER OF DATA POINTS')
      READ(5,*) K
      DO 30 I = 1, K
        READ(15,*) N(I), F(I), V(I)
30    CONTINUE
      PAIRS=K-1
      DONE=.FALSE.
35    IF (.NOT. DONE) THEN
        DONE=.TRUE.
        DO 40 I=1, PAIRS
          IF (V(I) .GT. V(I + 1)) THEN
            TEMP = V(I)
            V(I) = V(I + 1)
            V(I + 1) = TEMP
            DONE=.FALSE.
          END IF
C          WRITE(5,39) I, V(I)
C39        FORMAT(1X,I3,4X,E12.4)
40      CONTINUE
        PAIRS=PAIRS-1
        GO TO 35
      END IF
      L=0
      J=0
      DO 50 I=1,K
        L=L+1
        IF (V(I) .NE. V(I+1)) THEN
         J=J+1
         WRITE(5,95) J, V(I), L, 1
         WRITE(14,95) J, V(I), L, 1
         L=0
95       FORMAT(1X,I3,4X,E12.4,4X,I3,4x,I1)
        END IF
50    CONTINUE
      END
```

```
      DECLARE SUB SCAN CDECL (BYVAL lchan%, SEG sarray%, SEG erstat%)

      DECLARE SUB AOT802 CDECL (BYVAL lchan%, BYVAL brd%, BYVAL chan%, SEG ersta
      DECLARE SUB AOT CDECL (BYVAL lchan%, BYVAL value%, SEG erstat%)
'-------------------------------------------------------------

      DECLARE SUB SET.UP.RTI ()
      DECLARE SUB delay (T AS DOUBLE)
      DECLARE SUB start.clock ()
      DECLARE SUB time.loop ()
      DECLARE SUB TIME.LOOP1 ()
      DECLARE SUB calibration ()
      DECLARE SUB Sampling ()
      DECLARE SUB ADCloop (volt AS SINGLE, cali AS SINGLE, temp AS SINGLE, velo
      DECLARE SUB SETUP.RTI ()



'*************************************************************************
'    Variable declaration AND definition
'*************************************************************************



DIM sarray(0 TO 31) AS INTEGER
DIM erstat AS INTEGER
DIM i AS INTEGER
DIM lchan, board, PCHAN, range, mult, Count, gain AS INTEGER
DIM volt(0 TO 31) AS SINGLE
DIM s, n AS INTEGER
'
'
'
'          setup RTI815 board
'
'
CALL SETUP.RTI
'
'
'
'          start clock
'
'
CALL start.clock
'
'
'         call calibration coefficients
'
'
'
CALL calibration
'
'
'          Set data acquisition frequency and display results

CALL Sampling
'
'
END '
```

```
SUB SETUP.RTI
'*************************************************************************
'  Module         : SET.UP.RTI
'  Description    : module initialize the RTI-815 board
'  Author(s)      :
'
'
'  Modules called:
'              SCAN815      ---- RTI Library routine
'              initialize   ---- RTI Library routine
'              PULSETR815   ---- RTI Library routine
'              PULSE815     ---- RTI Library routine
'
'  Revision History
'
'     Date            Author          Description
'
'
'
'*************************************************************************

DIM erstat AS INTEGER
DIM board  AS INTEGER
DIM freq, freq1 AS INTEGER

'the CONF.DAT is at c:\bc7\bin\
' so enter c:\bc7\bin
SHELL "c:"
SHELL "cd\"
SHELL "cd bc7"
SHELL "cd bin"

'
' Board is set to 1 for RTI-815
'
board = 1
'
' set samplig frequency
'
COLOR 12, 1
CLS
LOCATE 10, 20
INPUT "THE SAMPLING FREQUENCY="; freq
freq1 = 5000 / freq

'
'
'
CALL initialize(erstat)           'initialize RTI variables and timer
IF erstat <> 0 THEN
   PRINT " Initialize Error Code: "; erstat
   STOP
END IF

CALL SCAN815(0, board, 0, 10, 20, 32, 1, erstat)            'lchan = 0
IF erstat <> 0 THEN
   PRINT " Lchan 0 Scan815 Error Code: "; erstat
   PRINT board
   STOP
```

```
END IF

CALL PULSETR815(1, board, 0, 100, freq1, freq1, erstat)        'lchan = 1
IF erstat <> 0 THEN
   PRINT " Pulsetr815 Error Code: "; erstat; " AT 05 CYCLE"
   STOP
END IF


'********** INITIALIZE TIMER FOR ONE-SHOT PULSE (60 MICROSECONDS) **********
CALL PULSE815(3, board, 1, 1, 60, erstat)
IF erstat <> 0 THEN
   PRINT " Error Code: "; erstat
   STOP
END IF
'*******************************************************************************


'********** INITIALIZE TIMER FOR ONE-SHOT PULSE (20 MILLISECONDS) **********
CALL PULSE815(4, board, 1, 1000, 20, erstat)
IF erstat <> 0 THEN
   PRINT " Error Code: "; erstat
   STOP
END IF
'*******************************************************************************


END SUB '
```

```
SUB start.clock
'*************************************************************************
'  Module         : START.CLOCK
'  Description    : This subroutine initialize clock 0 of the 815 board
'                   to count in 1/10 second intervals.  This subroutine
'                   should only be called once.  The 1/10 sec. clock is
'                   actually used by the TIME.LOOP subroutine.
'  Author(s)      :
'
'
'  Modules called:
'                    PULSTART
'
'
'  Revision History
'
'     Date            Author          Description
'
'
'
'*************************************************************************

DIM erstat AS INTEGER

'*************************************************************************
'              no variables are sent or returned however pin 25        *
'              will now count in 1/10 sec. intervals                   *
'*************************************************************************


   CALL PULSTART(1, erstat)
   IF erstat <> 0 THEN
      PRINT " Error Code:"; erstat; " AT 09 CYCLE"
      STOP
   END IF
'
'



'*************************************************************************
'              no variables are sent or returned however pin 26        *
'              will now count in 1/2.5 sec. intervals                   *
'*************************************************************************

'    CALL PULSTART(5, erstat)
'   IF erstat <> 0 THEN
'      PRINT " Error Code:"; erstat; " AT 09 CYCLE"
'      STOP
'   END IF

   END SUB '
```

```
SUB graphic

END SUB
SUB Sampling

DIM volt, cali, temp, num, velo AS SINGLE
'
'
' input the sampling frequency and the number
'
'
COLOR 12, 1
CLS
LOCATE 10, 20
INPUT "THE SAMPLING DATA= "; num
'
'display the time at that the sampling begins
'
'
      COLOR 11, 1
      CLS
      LOCATE 6, 10
      PRINT "The Beginnig Time is   "; TIME$
      COLOR 14, 1
      LOCATE 10, 10
      PRINT "  ADC.CODE     PRESSURE(H20)   TEMPERATURE   "

OPEN "c:\bc7\dat\adc.dat" FOR OUTPUT AS #1

Sampling:
      i = i + 1
      COLOR 10, 1
      LOCATE 8, 10
      PRINT "Now Time is   "; TIME$
      CALL ADCloop(volt, cali, temp, velo)
      PRINT #1, volt, cali

      IF i < num THEN
         GOTO Sampling
      END IF
'
'
'get the mean value of the data
'
'
'
      COLOR 12, 1
      LOCATE 20, 10
      PRINT "Ending Time is  "; TIME$
      temp = temp / num
      velo = velo / num
      LOCATE 14, 20
      PRINT USING "###.######"; velo
      LOCATE 14, 35
      PRINT USING "###.######"; temp
```

```
CLOSE #1

END SUB '
```

```
SUB ADCloop (volt AS SINGLE, cali AS SINGLE, temp AS SINGLE, velo AS SINGLE)
'
' open data file to store adc code
'
DIM sarray(0 TO 31) AS INTEGER
DIM erstat AS INTEGER
'
'
' wait for the  sampling rate pulse
'
CALL time.loop
'
'
      CALL SCAN(0, sarray(0), erstat)
      DO
         CALL check(0, erstat)
      LOOP UNTIL erstat = 117          'loop until all scanarrray is checked
'
'

'      CALL delay(.1)
      volt = 2 * 3.5 / 2048 * sarray(0)
      cali = 2 * 3.5 / 2048 * sarray(1)
      temp = temp + cali
      velo = velo + volt
      COLOR 10, 1
      LOCATE 12, 10
      PRINT USING "######"; sarray(1)
      LOCATE 12, 25
      PRINT USING "###.######"; volt
      LOCATE 12, 40
      PRINT USING "###.######"; cali



END SUB '
```

```
DEFINT A-Z
SUB time.loop

'*************************************************************************
'  Module         : TIME.LOOP
'  Description    : This subroutine controls the 1/10 second timing for
'                   the testing. The clock out that is counting in 1/10
'                   sec. intervals (clock out 0 -- pin #25) is hard wired
'                   to pin 4 which is the DIN 0 bit.  This subroutine
'                   will loop until a rising edge of the clock pulse
'  Author(s)      :
'
'  Modules called:
'
'  Revision History
'
'     Date            Author          Description
'
'
'
'*************************************************************************
   '
   '  address of digital in byte on 815
   '
   CONST dinadr = &H30A

   CONST bitmask = &H1
   '
   '  exit loop when bit goes low
   '
   DO
      STATUS = INP(dinadr) AND bitmask
   LOOP UNTIL STATUS = 0
   '
   '  exit loop when bit goes high
   '
   DO
      STATUS = INP(dinadr) AND bitmask
   LOOP WHILE STATUS = 0

   END SUB '          '
```

```
SUB calibration
END SUB
   SUB delay (delay.time AS DOUBLE)
'*************************************************************************
'  Module         : delay
'  Description    :  THIS SUB DELAYS EXECUTION OF THE PROGRAM FOR
'                    A SPECIFIED TIME INTERVAL
'
'     TIMER = BASIC TIME FUNCTION (NUMBER OF SECONDS SINCE MIDNIGHT
'     DELAY.TIME# = DELTA-TIME TO DELAY PROGRAM EXECUTION
'     FUTURE.TIME# = TIME AT WHICH POINT DELAY IS COMPLETE
'     CURRENT.TIME# = WHAT TIME IS IT NOW?

'  Author(s)      :
'
'
'  Modules called:
'
'
'
'  Revision History
'
'     Date            Author          Description
'
'
'
'*************************************************************************


   '********************** AT WHAT TIME WILL DELAY BE COMPLETE? ***
   '
   FUTURE.TIME# = TIMER + delay.time#
   '
   '*************************************************************

   '********************** CHECK TO SEE IF DELAY IS COMPLETE ******
   DO
      CURRENT.TIME# = TIMER
   LOOP WHILE CURRENT.TIME# <= FUTURE.TIME#
   '*************************************************************

END SUB '
```

BIBLIOGRAPHY

Arena, U., Marzocchella, A., Massimilla, L. and Malandrino, A., (1992), "Hydrodynamics of Circulating Fluidized Beds with Risers of Different Shape and Size", Powder Technology, 70, pp. 237-247.

Bader, R., Findlay, J. and Knowlton, T.M., (1989), "Gas/Solids Flow Patterns in a 30.5cm Diameter Circulating Fluidized Bed", Institute of Gas Technology, Sept. 25, 1989.

Bernard, J.M., Wang, C.P. and Lee, R.M., (1981), "Measurement of Fluid Velocity in the Interior of a Transparent Fluidized Bed with a Laser Doppler Anemometer", AIChE Symp Ser, Vol. 77, No. 205, pp. 37-50.

Berruti, F. and Kalogerakis, N., (1989), "Modelling the Internal Flow Structure of Circulating Fluidized Beds", Can J Chem Eng, Vol. 67, No. 6, pp. 1010-1014.

Birchenough, A. and Mason, J.S., (1976), "Local Particle Velocity Measurements with a Laser Anemometer in an Upward Flowing Gas-Solid Suspension", Powder Tech, Vol. 14, p. 139.

Biswas, J. and Leung, L.S., (1987), "Applicability of Choking Correlations for Fast-Fluid Bed Operation", Powder Tech, Vol. 51, No. 2, pp. 179-180.

Carey, V.P., (1987), "Dependance of Settling Velocity on Particle Concentration in a Fluidized Bed of Spherical Particles", Int J Multiphase Flow, Vol. 13, No. 3, pp. 429-431.

Drahos, J., Cermak, J., Guardani, R. and Schugerl, K., (1988), "Characterization of Flow Regime Transitions in a Circulating Fluidized Bed", Powder Tech, Vol. 56, No. 1, pp. 41-48.

Dry, R.J., (1986), "Radial Concentrating Profile in a Fast-Fluidized Bed", Powder Tech, Vol. 49, No. 1, pp. 37-44.

Dry, R.J., (1987), "Radial Particle Size Segregation in a Fast-Fluidized Bed", Powder Tech, Vol. 52, No. 1, pp. 7-16.

Durrett, R.P., Gould, R.D., Stevenson, W.H., and Thompson, H.D., (1985), "A Correction Lens for Laser Doppler Velocimeter Measurements in a Cylindrical Tube", AIAA J, Vol. 23, No. 9, pp. 1387-1391.

Durrett, R.P., Stevenson, W.H., and Thompson, H.D., (1988), "Radial and Axial Turbulent Flow Measurement with an LDV in an Axisymmetric Sudden Expansion Air Flow", J Fluids Eng, Vol. 110, pp. 367-372.

Durst, F., (1982), "Review-Combined Measurements of Particle Velocities, Size Distributions and Concentrations", Trans ASME, Vol. 104, pp. 284-296.

Durst, F. and Umhauer, H., (1975), "Local Measurements of Particle Velocity, Size Distribution, and Concentration with a Combined Laser Doppler Particle Sizing System", Proc LDA Symp, Copenhagen, p. 430.

Durst, F. and Zare, M., (1975), "Laser Doppler Measurements in Two-Phase Flows", Proc LDA Symp, Copenhagen.

Farmer, W.M., (1972), "Dynamic Particle Size and Number Analysis Using a Laser Doppler Velocity Meter", Applied Optics, Vol. 11, p. 2603.

Fox, C., Molodtsof, Y. and Large, J.F., (1989), "Control Mechanisms of Fluidized Solids Circulation Between Adjacent Vessels", AIChE J, Vol. 35, No. 12, pp. 1933-1941.

Gautam, M., Bocanegra, L., Jurewicz, J.T. and Morris, G. J., (1987), "A Review of LDV Measurements in Gas-Solid Flows", Int'l Symp Multiphase Flows, eds., C.T. Crowe and Z.Q. Fan, Hangzhow, China.

Gautam, M., (1989), "An Experimental Study of the Hydrodynamics Inside Fluidized Bed Bubbles", Ph.D. Dissertation, Dept. of Mech. and Aero. Engg., West Virginia University, Morgantown.

Grace, J.R. and Tuot, J., (1979), "A Theory for Cluster Formation in Vertically Conveyed Suspensions of Intermediate Density", Trans I ChemE, Vol. 57, pp. 49-54.

Guilin, Y., Zhe, H. and Lianzhong, Z., (1984), "Radial Gas Dispersion in a Fast-Fluidized Bed", Fluidization, IV, pp. 145-152.

Hamdullahpur, F., Al Taweel, A.M., Militzer, J. and Kan, M., (1989), "Motion of Hydrodynamic Aggregates", Powder Tech, Vol. 59, pp. 1973-1981.

Hamdullahpur, F., Pegg, M.J., and MacKay, G.D.M., (1987), "A Laser-Fluorescence Technique for Turbulent Two-Phase Flow Measurements", J Multiphase Flow, Vol. 113, No. 3, pp.379-385.

Hartge, E., Li, Y., and Werther, J., (1986) "Analysis of the Local Structure of the Two-Phase Flow in a Fast Fluidized Bed",Circulating Fluidized Bed Technology, Pergammon Press, NY.

Hinze, J.O., (1959), Turbulence, McGraw Hill Book Co., New York.

Hjelmfelt, A.T. Jr. and Mokros, L.F., (1966), "Motion of Discrete Particles in a Turbulent Fluid", App Sci Res, Vol. 16, pp. 149-161.

Homsy, G.M., Jackson, R., and Grace, J.R., (1992), "Report of a Symposium on Mechanics of Fluidized Beds", J. Fluid Mechanics, vol. 236, pp. 477-495.

Horio, M., Ishii, H., Kobukai, Y. and Yamanishi, N., (1989), "Scaling Law for Circulating Fluidized Beds", J Chem Eng Jpn, Vol. 22, No. 6, pp. 587-592.

Jackson, R., (1963), "The Mechanics of Fluidized Beds, Part II", Trans Instn Chem Engrs, Vol. 41, pp. 22-28.

Johnson, L.N., and Leone, F.C., (1964), "Statistics and Experimental Design in Engineering and the Physical Science", Vol. 1, John Wiley & Sons, Inc., N.Y.

Johnston, W., Dybbs, A. and Edwards, R., (1975), "Measurement of Fluid Velocity Inside Porous Media with a Laser Anemometer", The Physics of Fluids, Vol. 18, pp. 913-914.

Jurewicz, J.T., Stock, D.E., Crowe, C.T. and Eschbach, J.E., (1975), "Measurement of Both Gas and Particle Velocities in Turbulent Two Phase Flow", Proc of the Fourth Symposium of Turbulence in Liquids, Rolla, Missouri.

Kale, S.R. and Eaton, J.K., (1985), "An Experimental Investigation of Gas-Particle Flows Through Diffusers in the Freeboard Region of Fluidized Beds", Int'l J of Multiphase Flows, Vol. 11, No. 5, pp. 659-674.

Kato, K., Shibasaki, Tamura, Anta, Wang and Takarada, (1989), "Particle Holdup in a Fast-Fluidized Bed", J Chem Eng Jpn, Vol. 22, No. 2, pp. 130-136.

Kececioglu, I. and Keairns, D.L., (1989), "Computation of Solid Circulation Rates in a Fluidized Bed From Tracer Particle Concentration Distributions", Can J of Chem Eng, Vol. 67, pp. 290-300.

Keefer, D. (1987), "Laser Fluorescence Velocimeter", Applied Optics, Vol. 26, No.1, pp. 91-94.

Kehoe, P.K.W and Davidson, J.F., (1971), "Continuously Slugging Fluidized Beds", Inst Chem Eng Symp Ser, Vol. 33, pp. 97.

Kline, S.J. and McClintok, F.A., (1953), "Describing Uncertainties in Single Sample Experiments", Mech Eng, pp. 3-6.

Knowlton, T., Findlay, J., Sishtla, C. and Chan, I., (1986), "Solids Pressure Reduction Without Lockhoppers: The Restricted Pipe Discharge System", AIChE Symp Ser, Vol. 83, No. 255, pp. 64-73.

Knowlton, T.M., and Hirsan, (1977), "Solids Flow Control Using a NonMechanical L-Valve", Ninth Synthetic Pipeline Gas Symposium, Chicago, Illinois, Oct. 31 - Nov. 2, 1977.

Lai, M.C. and Faeth, G.M., (1987), "A Combined Laser Doppler Anemometer/Laser Induced Fluorescence System for Turbulent Transport Measurements", J Heat Transfer, Vol 109, pp. 254-256.

Lanneau, K.P., (1960), "Gas-Solid Contacting in Fluidized Beds", Trans Inst Chem Engrs, Vol. 38, pp. 25.

Lee, S.L. and Durst, F., (1982), "On the Motion of Particles in Turbulent Duct Flows", Int'l J Multiphase Flow, Vol. 8, No. 2, pp. 125-145.

Lee, S.L. and Srinivasan, J., (1978), "Measurement of Local Size and Velocity Probability Density Distributions in Two-Phase Suspension Flows by Laser Doppler Technique", Int'l J of Multiphase Flow, Vol. 4, pp. 141-155.

Levy, Y. and Lockwood, F.C., (1983), "Velocity Measurements in a Particle Laden Turbulent Free Jet", Combustion and Flame, Vol. 40, pp. 333-339.

Liang, Y., Moy, P.F., Poole, J.A., and Ponte Goncalves, A.M., (1984), "Fluorescence of Rhodamine B on Semiconductor and Insulator Surfaces: Dependence of the Quantum Yield on Surface Coverage", J Phys Chem, Vol. 88, pp. 2451-2455.

Liang, Y. and Ponte Goncalves, A.M., (1985), "Time-Resolved Measurements of the Fluorescence of Rhodamine B on Semiconductor and Glass Surfaces", J Phys Chem, Vol. 89, pp. 3290-3294.

Lourenco, L., Krothapalii, A., Buchlin, J.M., and Riethmuller, M.L., (1986), "Noninvasive Experimental Technique for the Measurement of Unsteady Velocity Fields", AIAA J, Vol. 24, No. 10, pp. 1715-1716.

Maeda, M., Hishida, K. and Furutani, T., (1980), "Velocity Distributions of Air-Solid Suspension in Upward Pipe Flow (Effect of Particles on Air Velocity Distribution), Trans Japan Soc Mech Engrs, 46, p. 2313.

Martin, M.P., Turlier, P., and Bernard, J.R., (1992), "Gas and Solid Behavior in Cracking Circulating Fluidized Beds", Powder Technology, 70, pp. 249-258.

Melling, A. and Whitelaw, J.H., (1973), "Seeding of Gas Flows for Laser Anemometry", DISA Information, 15, p. 5.

Meyers, J.F., (1988), "Laser Velocimeter Data Acquisition and Real Time Processing Using Microcomputer", Int'l Symposium on Application of Laser Anemometry to Fluid Mechanics, Lisbon.

Modaress, D., Wuerer, J. and Elgobashi, S., (1982), Proc AIAA/ASME 3rd Joint Thermophysics, Fluids, Plasma, and Heat Transfer Conf., June 7-11, 1982, St. Louis, Paper AIAA - 82-0964.

Modaress, D. and Tan, H., (1983), "Two-Component LDA Measurement in a Two-Phase Turbulent Jet", AIAA J, 21st Aerospace Science Meeting, Jan. 10-13, Reno, NV.

Mountzaris, T.J. and Jackson, R., (1986), "The Effects of Aeration on the Gravity Flow of Particulate Materials in Vertical Standpipes", AIChE Symp Ser, Vol. 83, No. 255, pp. 10-22.

Neale, G., Epstein, N. and Nader, W., (1972), "Creeping Flow Relative to Permeable Spheres", Chem Eng Sci, Vol. 28, pp. 1865-1874.

Nichols, C.E., (1987), "Preparation of Polystyrene Microspheres for Laser Velocimetery in Wind Tunnels", NASA TM-89163, June 1987.

Patrose, B. and Caram, H.S., (1982), "Optical Fiber Probe Transit Anemometer for Particle Velocity Measurements in Fluidized Beds", AIChE J, Vol. 28, No. 4, pp. 604-609.

Reisfeld, R., Zusman, R., Cohen, Y., and Eyal, M., (1988), "The Spectroscopic Behaviour of Rhodamine 6G in Polar and Non-polar Solvents and in Thin Glass and PMMA Films", Chem Phys Lett, Vol. 147, No. 2.3, pp. 142-147.

Rhodes, M.J. and Geldart, D., (1989), "The Upward Flow of Gas/Solid Suspensions", Chem Eng Res Des, Vol. 67, No. 1, pp. 20-29.

Richardson, J.F. and Zaki, W.M., (1954), "Sedimentation and Fluidization: Part I", Trans Inst Chem Eng, Vol. 32, p. 35.

Salem, T.F., and Gibbs, B.M. (1987), "Solid Circulation Between Fluidized Beds Using Jet Pumps", Powder Tech, Vol. 52, No. 2, pp. 107-116.

Shingles, T. and Silverman, R.W., (1986), "Determination of Standpipe Pressure Profiles and Slide Valve Oriface Discharge Coefficients of Synthol Circulating Fluidized Bed Reactors", Powder Tech, Vol. 47, No. 2, pp. 129-136.

Slack, G.W., (1963), "Sedimentation of Compact Clusters of Uniform Spheres", Nature, Vol. 200, pp. 466-467.

Slack, G.W., Jayaweera, K.O.L.F. and Mason, B.J., (1963), "The Behaviour of Clusters of Spheres Falling in a Viscous Fluid: Part 1", J of Fluid Mech, Vol. 20, pp. 121-128.

Stevenson, W.H. and dos Santos, R., (1977), "Aerosol Sizing by Means of Laser-induced Fluorescence", Appl Phys Lett, Vol. 30, No. 5, pp. 236-237.

Stevenson, W.H., dos Santos, R. and Mettler, S., (1975), "A Laser Velocimeter Utilizing Laser-Induced Fluorescence", App Phys Lett, Vol. 27, No. 7, pp. 395-396.

Subbarao, D., (1986), "Clusters and Lean-Phase Behavior", Powder Tech, Vol. 46, pp. 101-107.

Sutherland, K.S. and Tan, H., (1970), "Sedimentation of a Porous Sphere", Chem Eng Sci, Vol. 25, pp. 1948-1950.

Tchen, C.M., (1947), "Mean Value and Correlation Problems Connected with the Motion of Small Particles Suspended in a Turbulent Fluid", Ph.D. Dissertation, Delft, Martinz Nyhoff, the Hague.

Tsuji, Y. and Morikawa, Y., (1982), "LDV Measurements of an Air-Solid Two-Phase Flow in a Horizontal Pipe", J Fluid Mech, Vol. 120, pp. 385-409.

Van Zoonen, D., (1962), "Measurement of Diffusional Phenomena and Velocity Profiles in a Vertical Riser", Proc Symp Interaction Between Fluid and Particles, Inst Chem Eng, pp. 64-17.

Wang, Z., Bai, D., and Jin, Y., (1992), "Hydrodynamics of Cocurrent Downflow Circulating Fluidized Bed (CDCFB)", Powder Technology, 70, pp. 271-275.

Werther, J., (1991), "Particle Motion and Dispersion of Gas in Circulating Fluidized Beds", Symposium on Mechanics of Fluidized Beds, Stanford University, July 1-4, 1991 (Reported by Homsy et al., 1992).

Wirth, K.E., (1991), "Fluid Mechanics of Circulating Fluidized Beds", Symposium on Mechanics of Fluidized Beds, Stanford University, July 1-4, 1991 (Reported by Homsy et al, 1992).

Yang, W., (1983), "Criteria for Choking in Vertical Pneumatic Conveying Lines", Powder Tech, Vol. 35, pp. 143-150.

Yang, W., (1984), "Mechanistic Models for Transitions Between Regimes of Fluidization", AIChE J, Vol. 30, No. 6, pp. 1025-1027.

Yerushalmi, J. and Cankurt, N.T., (1978), "Gas Backmixing in High Velocity Fluidized Beds", Fluidization, Cambridge Umv. Press, pp. 387-393.

Yerushalmi, J. and Cankurt, N.T., (1979), "Further Studies of the Regimes of Fluidization", Powder Tech, vol. 24, pp. 187-205.

Yianneskis, M., (1987), "Velocity, Particle Sizing and Concentration Measurement Techniques for Multiphase Flow", Powder Tech, Vol. 49, pp. 261-269.

Yianneskis, M. and Whitelaw, J.H., (1984), Proc Symp on Liquid-Solid Flow and Erosion Wear in Industrial Equipment, ASME Fluids Engineering Conference, New Orleans, Feb. 11-17.

Yoshioka, S., Miyamoto, T., Tomura, J., Hirato, M., Kiuchi, N., and Ishiboshi, Y., (1987), "Circulatory Flow of Particles in a 0.96-m-diameter Fluidized Bed", Int Chem Eng, Vol. 27, No. 2, pp. 281-287.

Yousfi, Y. and Gau, G., (1974), "Aerodynamique de L'ecoulement Vertical de Suspensions Concentrees Gaz-Solides - I. Regimes D'ecoulement et Stabilite Aerodynamic", Chem Eng Sci, Vol. 29, p. 139.

Yule, A.J., Chigier, N.A., Atakan, S. and Ungut, A., (1977), "Particle Size and Velocity Measurement by Laser Anemometry", J Energy, Vol. 1, No. 4, pp. 220-228.

DATE

FILMED

9/8/94

END